SAPIENZA
UNIVERSITÀ DI ROMA

Ph.D. Course in Biochemistry

Department of Biochemical Sciences "A. Rossi Fanelli"

XXXII cycle

Characterisation of the key enzymes involved in vitamin B_6 Salvage Pathway in *Escherichia coli* and humans

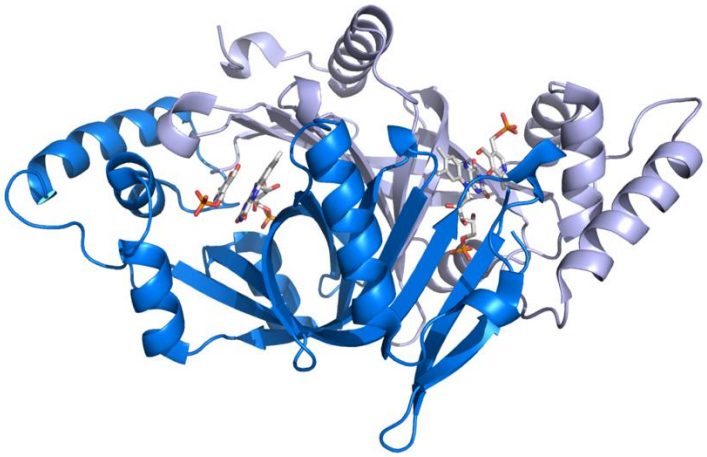

Tutor

Prof. Roberto Contestabile

Coordinator

Prof. Stefano Gianni

Ph.D. Student

Anna Barile

Abstract

The catalytically active form of vitamin B_6, pyridoxal 5'-phosphate (PLP), acts as a coenzyme in a variety of different enzymatic reactions. Organisms which are not able to synthesize PLP *de novo* acquire B_6 vitamers from nutrients and interconvert them through a salvage pathway, which involves pyridoxine 5'-phosphate oxidase (PNPOx) and pyridoxal kinase (PDXK). PNPOx converts pyridoxine 5'-phosphate (PNP) and pyridoxamine 5'-phosphate (PMP) to PLP, using flavinmononucleotide (FMN) as coenzyme. Both *Escherichia coli* and human PNPOx are homodimers and, although these enzymes share only 39% of sequence identity, have very similar structural and functional properties. PNPOx plays a crucial role in the regulation of PLP metabolism. It has been proposed that PLP inhibits the catalytic activity of both *E. coli* and human PNPOx by binding at the active site and acting as a competitive inhibitor. However, PLP can also bind tightly at a secondary site. Our kinetics characterisation suggests that PLP inhibition results from binding of this vitamer at an allosteric site, in both *E. coli* and human enzymes. This interpretation was confirmed by the analysis of mutated forms of *E. coli* PNPOx, in which PLP binding at the active site is impaired. Crystallographic studies carried out by other authors on the *E. coli* PNPOx indicated a possible location of the secondary PLP binding site in two surface pockets of the protein, but site-directed mutants of amino acid residues putatively critical for this interaction showed that this hypothesis is wrong. Molecular docking analyses identified a possible alternative PLP binding site, which is a cleft on the protein surface mainly delimited by arginine residues and located near the subunit interface. Characterisation of mutant forms of this site and crystallographic studies suggested that this might be the allosteric PLP binding site.

Concerning human PNPOx, it is known that missense mutations in the gene encoding this enzyme lead to the onset of a rare neurological disease, the neonatal epileptic encephalopathy (NEE); however, the molecular reason of most PNPOx mutations remains to be established. We expressed PNPOx mutants as recombinant proteins in *E. coli*, purified and characterised them with respect to structural and functional properties, in order to better understand the molecular basis of the disease.

The other key enzyme involved in the salvage pathway is PDXK, which converts pyridoxal (PL), pyridoxamine (PM) and pyridoxine (PN) into PLP, PMP and PNP, respectively. In *Drosophila*, mutations in the *dPdxk* gene encoding PDXK cause chromosome aberrations (CABs) and increase glucose content in larval haemolymph. This observation suggests that PDXK mutations in humans may be involved in diseases such as cancer and diabetes. We analysed the effect of the expression of four PDXK human variants in *Drosophila dPdxk* mutants: three of them (D87H, V128I and H246Q) are listed in databases, and one (A243G) was found in a genetic screening of patients with gestational diabetes. None of the variants was able to completely rescue CABs and glucose content. Our biochemical analysis revealed reduced catalytic activity and different affinity of these variants for PLP precursors. Overall, our findings suggest that, when PLP levels are reduced by the presence of these PDXK variants, cancer and diabetes risk may be increased.

Index

1. Introduction

2. Materials and Methods

4. Discussion

1. Introduction

1.1 Pyridoxal 5′-phosphate: the catalytically active form of vitamin B_6

Vitamin B_6 is water-soluble vitamin essential for normal growth and development. This term denotes all six B_6 vitamers, which share the 2-methyl-3-hydroxypyridine structure; the structural difference between them is due to the substituents on C4 and C5 carbons.[1] The six vitamers are pyridoxine (PN); pyridoxamine (PM), pyridoxal (PL) and their 5′-phosphorylated forms (PNP, PMP and PLP, respectively), which differ in the identity of the chemical group present at the C4 position **(Fig. 1.1)**, and are interconvertible thanks to the action of different enzymes, such as pyridoxal kinase and pyridoxine 5′-phosphate oxidase.[2]

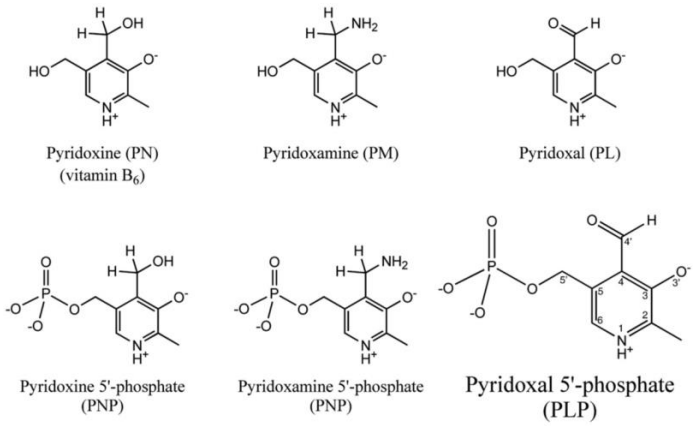

Figure 1.1 *Structure of the B_6 vitamers.* The carbon atoms numbering is shown on the PLP structure.[3]

The catalytically active form of the vitamin, pyridoxal 5′-phosphate (PLP) acts as a cofactor in numerous enzymatic reactions, such as amino acid metabolism and biosynthesis of many neurotransmitters, including dopamine, norepinephrine, histamine, serotonin, and γ-aminobutyric acid.[4] The reactions carried out by PLP-dependent enzymes include the transfer of the amino

group, decarboxylation, interconversion of L- and D-amino acids, and removal or replacement of chemical groups bound at the β- or γ-carbon.[5] In fact, PLP is a very versatile molecule that covalently binds the substrate and then acts as an electrophilic catalyst, thereby stabilizing different types of reaction intermediates.[6] More than 140 enzymatic reactions are PLP-dependent, corresponding to approximately 4% of all classified enzyme activities; about 70 of these occur in humans.[1] Each holo-enzyme contains PLP attached by a Schiff base link to the ε-amino group of a lysine residue at the active site.[7] A classification of PLP-dependent enzymes based on the chemical characteristics of the catalysed reaction was suggested and PLP-dependent enzymes were divided into α, β and γ classes, depending on the carbon atom involved in the transformation.[8] Grishin and collaborators[9] classified PLP-dependent enzymes into five different fold types on the basis of amino acid sequence comparisons, predicted secondary structure elements and available three-dimensional structural information. As mentioned above, PLP participates as a cofactor in numerous enzymatic functions. For example, PLP is very important for the synthesis of neurotransmitters, such as dopamine, γ-aminobutyric acid and adrenaline, acting as a cofactor of enzymes such as decarboxylases.[4] Then, PLP also acts as a cofactor in transamination reactions, fundamental in the amino acids metabolism and, moreover, the keto acids corresponding to some amino acids (such as pyruvate and oxaloacetate, derived from alanine and aspartate amino acid residues, respectively) are important metabolic intermediates.[10] And again, this cofactor participates in the transfer of one-carbon units in the biosynthesis of purines and to glycogenolysis, in which PLP is required for the activity of glycogen phosphorylase.[10] Also in the biosynthesis of heme, PLP is a cofactor of aminolevulinate synthase which catalyses the production of 5-aminolevulinic acid (ALA), the universal precursor of the tetrapyrrole

biosynthesis pathway.[11] In mammals, the condensation of succinyl-CoA with glycine produces this precursor.[10] On the other hand, plants, algae and most bacteria synthesize ALA by two-step transformation: the NADPH-dependent glutamyl-tRNA reductase (HemA) produces the glutamate-1-semialdhyde (GSA), and then, GSA is isomerized to ALA by the PLP-dependent glutamate-1-semialdehyde-2,1-aminomutase (HemL).[11]

Besides the role of PLP as a cofactor, this vitamer can act as reactive oxygen species scavenger in plants, quenching singlet oxygen at rates comparable to vitamins C and E,[12,13] and in *Plasmodium falciparum*.[14] PLP can also modify the expression and action of steroid hormone receptors[15] and may have an effect on the immune function.[16] Moreover, PLP is a transcriptional regulator in Eubacteria[17] and a virulence factor in *Helicobacter pylori*[18] and *Mycobacterium tuberculosis.*[19] Finally, of interest because of its antiepileptic activity,[20] PLP is an antagonist of ATP at P2 purinoceptor7 (P2X7).[21] It has been suggested that when neuroinflammation triggers cellular ATP release, this can lead to epilepsy by activation of P2X7 receptors;[22] and PLP has the potential to block this activation. This could explain the action of PLP on drug-resistant epilepsies, besides the role of this vitamer in the genetic disorders discussed in detail below.[23,24]

1.2 Vitamin B_6 metabolism

The vitamin B_6 is of fundamental importance for all living beings, however, only microorganisms and plants are able to synthesize it *de novo*, using two different biosynthetic routes, the deoxyxylulose 5-phosphate (DXP)-dependent pathway and the DXP-independent pathway. All other organisms

have to acquire vitamers from nutrients and interconvert them in order to match their needs, using a salvage pathway.[25]

1.2.1 Vitamin B_6 *de novo* biosynthesis

As mentioned before, only microorganisms and plants are able to synthesize vitamin B_6 *de novo*. Two independent *de novo* biosynthetic routes are known **(Fig. 1.2)**.[26] The first to be discovered was extensively studied in *Escherichia coli* and for a long time assumed to be ubiquitous, however it has been shown to be restricted to some Eubacteria. This pathway, also called deoxyxylulose 5-phosphate (DXP)-dependent pathway, is articulated in two branches; the first one starts from D-erythrose 4-phosphate, while the second one from pyruvate and glyceraldehyde 3-phosphate. The two branches converge in the last reaction catalysed by PNP synthase (coded by the *pdxJ* gene), forming PNP.[27] In addition to the latter enzyme, other five enzymes are required in this pathway and are encoded by *gapB, pdxB, pdxF, pdxA* and *dxpS* genes. PNP is then oxidized to PLP by PNP oxidase (PNPOx), encoded by the *pdxH* gene.[26] In the second route, the so-called DXP-independent pathway, PLP is directly formed from glutamine, either ribose or ribulose 5-phosphate and either glyceraldehyde 3-phosphate or dihydroxyacetone phosphate by the action of the PLP synthase complex (encoded by the *pdx1* and *pdx2* genes).[28,29] After the second route was serendipitously discovered in fungi, it became clear that it is much more widely distributed than the first one, being found in Archaea, most Eubacteria and plants.[13,30]

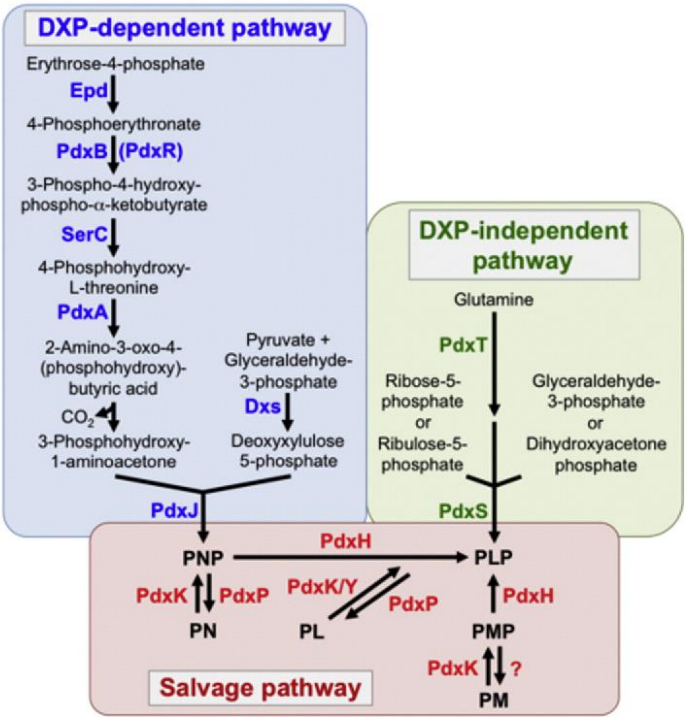

Figure 1.2 *Vitamin B_6 biosynthetic routes*. DXP-dependent pathway: *gapB*, D-erythrose 4-phosphate dehydrogenase; *pdxB*, erythronate-4- phosphate dehydrogenase; *pdxF/serC*, phosphoserine aminotransferase; *pdxA*, 4-hydroxythreonine-4-phosphate dehydrogenase; *dpxS*, 1-deoxy-D-xylulose-5-phosphate synthase; PNP synthase, from *pdxJ* gene. DXP-independent pathway: PLP synthase complex: synthase domain from *pdx1* gene; glutaminase domain from *pdx2* gene. Salvage pathway: PLK, pyridoxal kinase from the *pdxK* gene and pyridoxal kinase 2 from the *pdxY* gene; PNPOx, pyridoxine 5′-phosphate oxidase from the *pdxH* gene.[3]

A further metabolic pathway, that is not only present in microorganisms and plants but also in mammals, is the salvage pathway, in which PLP is recycled from protein turnover or from B_6 vitamers present in foods.[26]

1.2.2 Vitamin B_6 metabolism in humans

The human intestine only absorbs non phosphorylated B_6 vitamers **(Fig. 1.3)**.[31] Therefore, phosphorylated vitamers are first hydrolysed by intestinal phosphatases.[32] Once within the intestine cells, PN and PM can either be converted prior to transport to the liver[33] or once within the liver to pyridoxal phosphate. In the liver (or intestine) PM, PN and PL, are first phosphorylated by the ATP-dependent pyridoxal kinase. The flavinmononucleotide (FMN)-dependent enzyme, pyridoxine 5′-phosphate oxidase (PNPOx) converts the phosphorylated derivative of PM and PN to PLP. Through the "salvage pathway" PLP is formed from the other vitamers taken from the diet or by recycling the cofactor from degraded enzymes[34] **(Fig. 1.2; Fig. 1.3)**. Although PNPOx is mainly expressed in the liver, this enzyme is expressed in all cell types. PLP is exported from the liver bound to albumin.[35] When B_6 vitamers intake exceeds requirements, PLP is dephosphorylated (mainly in the liver) and the resulting PL is oxidized by an aldehyde dehydrogenase or aldehyde oxidase (AOX)[36] to pyridoxic acid prior to excretion in urine. To enter the brain, PLP must dissociate from albumin and be dephosphorylated to PL at the blood-brain barrier (BBB). Dephosphorylation is carried out by tissue non-specific alkaline phosphatase, an enzyme tethered to cell membranes at the BBB by a glycophosphatidylinositol (GPI) anchor. PL crosses the BBB, probably by facilitated diffusion, and is "trapped" as PLP in the brain cells and the choroid plexus by the action of pyridoxal kinase[37] **(Fig. 1.3)**. A similar mechanism occurs in other target cells. Within tissues, PNP or PMP can be converted back to PLP by PNPOx (salvage pathway)[3] **(Fig. 1.2)**.

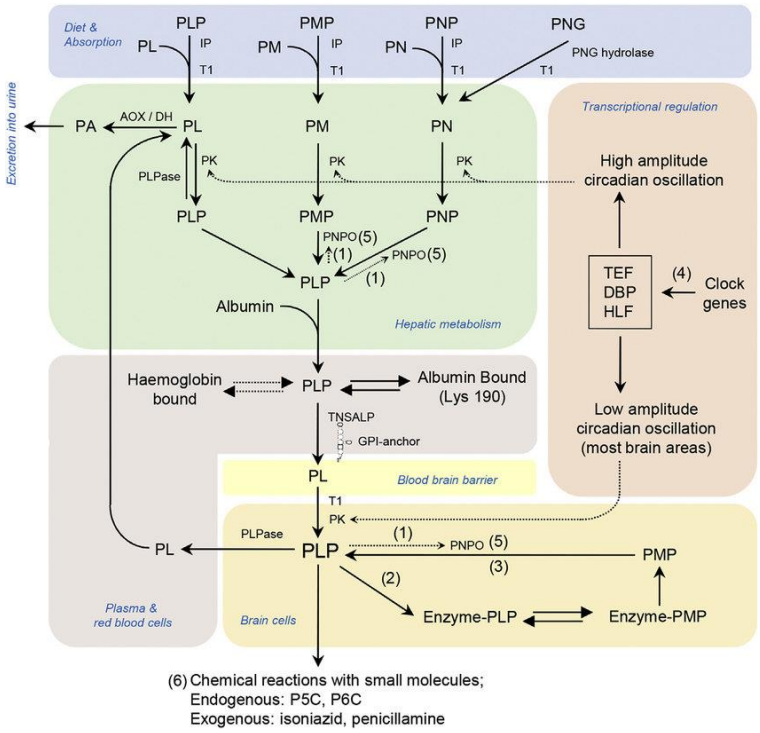

Figure 1.3 *Human PLP synthesis and homeostasis.* AOX/DH, aldehyde oxidase (Mo cofactor)/ β-NAD dehydrogenase; IP, intestinal phosphatases; ; E-PLP, enzyme bound PLP; E-PMP, enzyme-bound PMP; GPI, glycosylphosphatidylinositol anchor; PA, 4-pyridoxic acid; PK, pyridoxal kinase; PL, pyridoxal; PLP, pyridoxal 5′-phosphate; PLPase, pyridoxal-phosphatase; PLPBP/PROSC, pyridoxal 5′-phosphate binding protein; PM, pyridoxamine; PMP, pyridoxamine 5′-phosphate; PN, pyridoxine; PNG, pyridoxine-5′-β-D-glucoside; PNP, pyridoxine 5′-phosphate; PNPO, pyridoxamine 5′-phosphate oxidase; T1, transporter (identity unknown); TNSALP, tissue non-specific alkaline phosphatase. (1) feedback inhibition of PNPOx by PLP; (2) PLP functions as a cofactor; (3) salvage pathway; (4) PLP levels maintained by circadian-clock-controlled transcription factors (DBP, HLF, and TEF) targeting PK; (5) PNPOx mutations cause a B_6-dependent epilepsy; (6) decreasing PLP bioavailability resulting from accumulation of L-Δ^1-pyrroline-5-carboxylic acid (P5C) and Δ^1-piperideine-6-carboxylic acid (P6C).[31]

1.2.3 Key enzymes in pyridoxal 5′-phosphate synthesis

The biosynthetic pathway leading to the formation of PLP is present in bacteria, plants and fungi. Particularly, in *E. coli* metabolism a key enzyme is pyridoxine 5'-phosphate oxidase (PNPOx), which catalyses the last step of vitamin B_6 biosynthesis. However, the oxidation of PNP to PLP is an important step in the recycling of this vitamer in all living beings.[38] PLP can be synthesized by three different enzymes, which are not present in all organisms: pyridoxine 5′-phosphate oxidase (PNPOx); pyridoxal kinase (PDXK), which converts all vitamers into their related phosphorylated derivatives; and pyridoxal synthase, that is not present in γ-proteobacteria and in mammals.[25] In mammals, PLP is recycled from degraded B_6-enzymes and from vitamers acquired from nutrients in the salvage pathway, which essentially involves two ubiquitous enzymes: the ATP-dependent pyridoxal kinase and the FMN-dependent PNPOx.[3] Once it is made, PLP is targeted to apo-B_6 enzymes that are being synthesized in the cell.[39] The mechanism and regulation of the salvage pathway and the mechanism of PLP transfer to PLP-dependent enzymes are poorly understood. Moreover, PDXK and PNPOx play key roles in regulating the level of PLP formation.[3,40]

Pyridoxine 5'-phosphate oxidase

PNPOx is a flavinmononucleotide (FMN)-dependent enzyme that uses molecular oxygen as electron acceptor. This protein is crucial in the PLP salvage pathway; it is responsible for the transfer of a pair of electrons from the C4′ carbon of PNP or PMP to a tightly bound molecule of FMN forming $FMNH_2$. These two electrons are subsequently transferred in a second half-

reaction to molecular oxygen, regenerating FMN and forming H_2O_2.[41] Kinetic studies carried out on rabbit PNPOx have led to the proposal of two possible catalytic mechanisms for oxidizing PNP and PMP to PLP **(Fig. 1.4)**. The first one is a direct hydride transfer from C4′ of the substrate to N5 of FMN, to generate PLP and $FMNH_2$. The second possible mechanism involves the presence of a base at the active site that removes a proton from C4′ of the substrate, which then attacks FMN forming a covalent complex; collapse of this complex would generate PLP and $FMNH_2$ **(Fig. 1.4)**.

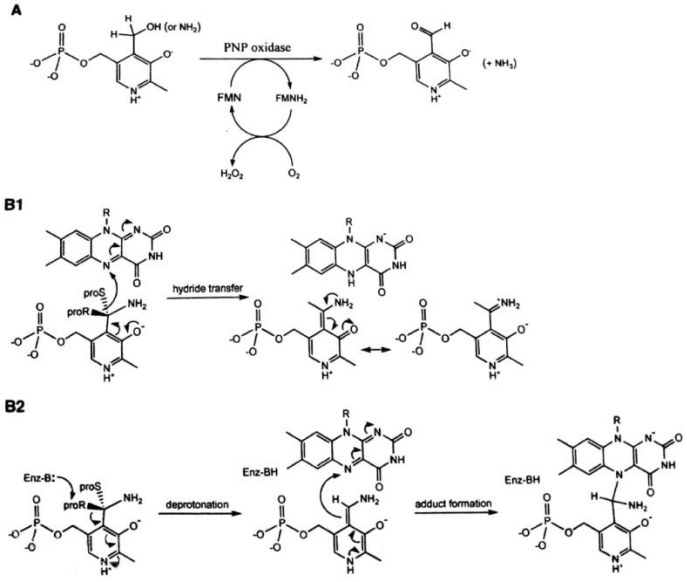

Figure 1.4 *Description of pyridoxine 5′-phosphate oxidase (PNPOx) mechanism.* **A)** Reaction catalysed by PNPOx; **B1)** Direct hydride transfer of C4′ *pro*R hydrogen of PNP (or PMP) substrate to FMN; **B2)** Removal of the *pro*R proton at C4′ of PNP (or PMP) to generate a carbanion.[3]

In either cases, FMN is regenerated by the transfer of the two electrons to oxygen, forming hydrogen peroxide. Experiments performed with site-

directed mutants of the active site and isotope-labelled PMP have shown that the oxidation process involves direct hydride transfer from PNP or PMP to FMN.[3]

Pyridoxal kinase

The other essential enzyme involved in PLP synthesis is pyridoxal kinase, which, in the presence of MgATP, catalyses the addition of a phosphate group to the 5′-alcohol of pyridoxine, pyridoxamine and pyridoxal to form PNP, PMP and PLP, respectively **(Fig. 1.5)**.[3] In this reaction, both substrates are bound to the enzyme forming a ternary complex. The mechanism of phosphorylation has been previously elucidated for the sheep and *E. coli* enzymes and is characterised by a random sequential substrates addition.[42] On the other hand, it has not been reported whether, in human pyridoxal kinase, the ternary complex is formed in an ordered or random sequence.[42]

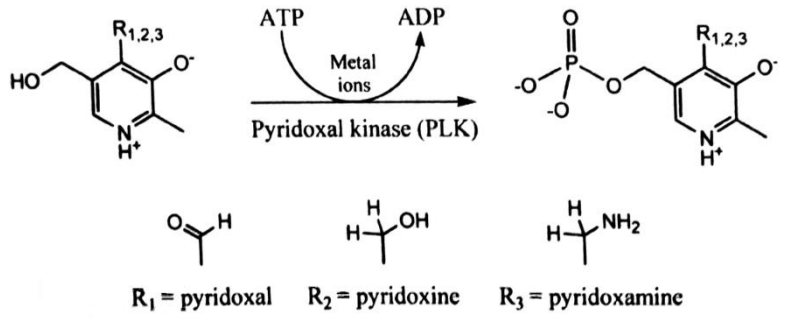

Figure 1.5 *Schematic representation of pyridoxal kinase reaction.*[3]

In pyridoxal kinases, a conserved Asp235 residue is observed that makes a hydrogen-bond interaction with the C5′-OH group of substrates and deprotonates this group, thus resulting in a negatively charged O5′ atom making a direct nucleophilic attack on the ATP γ–phosphate.[43] For the function of many kinases, both monovalent and divalent cations are known to be essential, providing forces for ATP-binding and substrate catalysis.[42] Particularly, in human pyridoxal kinase, the affinity for the ATP and PL substrates increases in presence of K^+ when compared to Na^+, and then, the monovalent metals seem to lower the energetic barriers in the basal and transition state. Moreover, Mg^{2+} and Na^+ cations act in tandem to anchor ATP at the active site, thus suggesting that both monovalent and divalent cations are necessary for the enzymatic function of pyridoxal kinase.[3,42]

1.3 Pyridoxal 5′-phosphate homeostasis

Pyridoxal 5′-phosphate (PLP) is a highly reactive aldehyde, that can react with several nucleophilic compounds in the cell.[31] Intracellular free PLP concentrations are maintained at approximately 1 μM to prevent inappropriate reactions (“aldehyde stress” or “carbonyl stress”); in fact, the very reactive aldehyde group at the C4′ position can easily form aldimines with primary and secondary amines[3] and, moreover, it can react with thiol groups. In humans, toxicity is usually observed when vitamin B_6 uptake exceeds 200 mg/day.[44] Very high doses of supplementation in humans lead to toxicity that presents as sensory neuropathy, whereas low status of this vitamin has been associated with severe malnutrition, venous thromboembolism, many neurological diseases, such as epilepsy, Alzheimer's, Parkinson's and even diabetes and cancer.[45,46] Levels of vitamin

B_6 could also be raised as a result of an environmental insult or genetic defects. Furthermore, the toxicity of PLP has been previously described not only in humans but also in other organisms, such as *Candida utilis*, where PLP can inhibit the enzymatic activity of 6-phosphogluconic dehydrogenase forming a Schiff base with a lysine residue located in the active site of the enzyme.[2,47] Given the toxicity of PLP, different mechanisms are needed in the cells to strictly control the levels of this vitamer.

Several mechanisms are involved in maintaining low concentrations of PLP; at the same time, large amounts of this cofactor are required to saturate the many PLP-dependent enzymes. One regulation mechanism could be the conversion of PL into pyridoxic acid, catalysed by the aldehyde oxidase and the NAD-dependent dehydrogenase enzymes.[36] PL results from the action of phosphatases, which catalyse the removal of phosphate groups. A PLP-specific phosphatase is involved in PLP homeostasis in mammals,[48] and in *E. coli* a specific phosphatase, encoded by the *ybhA* gene, has been identified that maintains PLP homeostasis, reducing PLP toxicity.[2] On the other hand, a candidate for an important missing player in PLP homeostasis is the PLP-binding protein (PLPBP), also called YggS in *E. coli* or PROSC in humans.[31,49] YggS was first identified in *E. coli* as a member of the COG0325 family.[50,51] The aforementioned family shares with alanine racemases and certain decarboxylases a similar folding,[1] and has been shown to bind PLP.[50] In crystal structures of yeast and *E. coli* COG0325 proteins it was observed that, like the N-terminal domain of alanine racemase and ornithine decarboxylase, these proteins fold as TIM barrel, displaying eight β–strands alternate to eight α-helices, and bind PLP in a similar mode.[50] Prunetti and collaborators[49] observed that an *E. coli* K12 Δ*yggS* strain accumulated PNP and that high levels of exogenous PN are toxic to this mutant strain; PLP, PM and PL are not toxic and, the latter vitamer

suppresses the PN toxicity, as also observed expressing the *E. coli yggS* gene in *trans*. The mechanism of this toxicity is unknown, although it was suggested that the high concentration of PNP, perhaps due to the retroactive inhibition of PNPOx by PLP, could inhibit PLP-dependent enzymes, including a particular transaminase involved in the synthesis of branched-chain amino acids.[49] Moreover, in the *ΔglyA ΔyggS* strain was observed a defect in the cell division, probably due to lower levels of D-alanine. Thus, it has been suggested that the phenotypes observed in *E. coli* in the absence of *yggS* are caused by a lower activity of PLP-dependent enzymes.[49] Furthermore, in humans other proteins such as glycogen phosphorylase in muscle,[52] haemoglobin in erythrocytes,[53] and albumin in plasma,[35] can bind PLP and help maintain PLP homeostasis. Interestingly, also the enzymes that produce PLP (PDXK and PNPOx) can bind it tightly.[34,54] Concerning pyridoxal kinase, in *E. coli* it was observed that PLP forms a complex with the enzyme and inactivates it. Interestingly, this complex can be partially reactivated by transferring the tightly bound PLP to apo-B_6 enzymes, which has been suggested to be an important pathway for B_6 enzyme activation.[40] *In vitro* studies suggest that PLP is protected intracellularly by being transferred from these enzymes directly to PLP-dependent enzymes, such as serine hydroxymethyltransferase (SHMT).[39,40,54,55] Safo and collaborators[56] observed that PLP tightly binds at a non-catalytic binding site of PNPOx and remains bound during size exclusion chromatography.[54] Furthermore, the crystal structure of *E. coli* PNPOx, obtained from crystals soaked in a concentrated solution of PLP showed a PLP molecule bound at the protein surface, about 11 Å from the active site.[56] The actual involvement of this surface pocket, which is present as two symmetric sites in the dimeric PNPOx, has never been confirmed experimentally.

1.3.1 Feedback inhibition of pyridoxal 5′-phosphate synthesis

It was previously reported that PLP inhibits both pyridoxal kinase and PNPOx.[57,58] In *Escherichia coli* PNPOx, a competitive PLP product inhibition was observed by Zhao and Winkler, and also substrate inhibition by PNP, but not PMP, was described, that can be reversed by increasing oxygen concentration.[58] PLP product inhibition of *E. coli* PNPOx has been reported to take place with a K_I of 8 μM and attributed to PLP binding at the active site.[58] Also, in previous studies on sheep brain PNPOx, a competitive nature of PLP inhibition with respect to PNP substrate was suggested; the inactivation of the enzyme was apparently due to a modification of a lysine residue, that is located very close to the substrate binding site.[59] Furthermore, steady-state data, obtained from kinetic measurements on rabbit liver PNPOx, indicated that the catalytic mechanism to form the PLP product follows two different kinetic mechanisms depending on the substrate used, with oxygen in both cases functioning as the electron acceptor. Thus, PNP oxidation proceeds via a ping-pong mechanism, while PMP oxidation follows a ternary sequential mechanism.[59] In humans, although the enzyme shares only 39% of sequence identity with *E. coli* PNPOx, a remarkable similarity has been found between the two enzymes in the structure and in the catalytic properties. Particularly, these two enzymes differ in substrate specificity, with the *E. coli* PNPOx displaying a greater preference for PNP; however, in both enzymes PLP acts as product inhibitor.[34] The K_I of PLP for the human enzyme is lower than that of the *E. coli* PNPOx[58] and was estimated to be about 3.2 μM.[34] Since this K_I value is not close enough to that of a putative high affinity binding site, it has been proposed by Musayev and collaborators[34] that PLP inhibits the enzyme by binding at the active site. This product inhibition is probably an important regulatory mechanism of

PLP biosynthesis, however further investigations are required to gain better insight into this mechanism.

Concerning *E. coli* pyridoxal kinase, it has been observed that PLP is a slow tight binding inhibitor of this enzyme.[40] It is known that in *E. coli* two kinases are present, one of which is able to catalyse the phosphorylation of all B_6 vitamers, while the other is specific for PL.[60] In the first pyridoxal kinase, encoded by the *pdxK* gene, the mechanism of PLP inhibition was described in detail, and it is characterised by the formation of a Schiff base between PLP and an active site lysine residue (Lys229). The inactivation is faster when both PLP and MgADP are present compared to when PLP is present alone.[40] The human enzyme is slowly inhibited by PLP[34] and this inhibition is probably due to the formation of a non-covalent enzyme-PLP complex.[43]

1.4 Pyridoxine 5′-phosphate oxidase from *Escherichia coli*

Pyridoxine 5′-phosphate oxidase (PNPOx) is encoded by the *pdxH* gene and has been purified from sheep, rat and pig brain, rabbit liver, and *E. coli* [58,59,61,62] with the most extensive studies being performed on the rabbit liver, sheep brain, and *E. coli* enzymes. In *Escherichia coli*, PNPOx is a relatively abundant enzyme,[58] and there is enough enzyme to serve as a significant reservoir of PLP. It was previously reported that the *pdxH* gene in *E. coli* forms a complex operon with a downstream gene, *tyrS*, which encodes the essential enzyme tyrosyl-tRNA synthetase.[63] The characterisation of *pdxH* mutants revealed several unusual phenotypes, like a block in cell division, excretion of L-glutamate and inhibition of L-isoleucine biosynthesis.[63] Moreover, the absence of growth of *pdxH* mutants aerobically

and anaerobically, also when supplemented with PL, suggested that the PNPOx is not only essentially required for PLP biosynthesis in cells, however, the enzyme could play a role in an alternative pathway.[63] In Eubacteria, PNPOx catalyses the final step of vitamin B_6 metabolism and is a member of the oxidoreductase enzymes, that catalyse a simultaneous oxidation-reduction reaction, where the molecular oxygen is thought to be the sole electron acceptor in the reaction.[25,64] The *E. coli* enzyme is a homodimer, and each monomer counts 218 amino acid residues.[38]

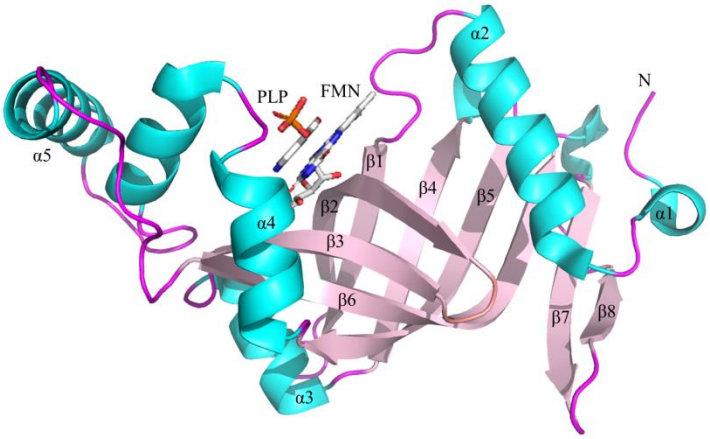

Figure 1.6 *Monomeric structure of E. coli PNPOx*. The eight β-strands are shown in pink, the five α-helices in cyan and loops in magentas; FMN and PLP molecules at the active site are shown as sticks with atom-based colours (PDB code: 1G79[56]).

The folding of each monomer **(Fig. 1.6)** can be described in terms of two domains: the larger domain, which consists of β–strands and two α–helices; and the smaller one, that is formed by the remaining three α–helices and is near the β–barrel core.[38] The binding site of FMN is located in a deep cleft formed by the two subunits and is conserved in the PNPOx structures. In the dimeric structure, two molecules of FMN are bound at the interface and are

also involved in several hydrogen-bond interactions with the protein; particularly, the phosphate group of this cofactor interacts extensively with highly conserved arginine and lysine residues from both subunits of the protein.[38,65] PLP and PNP bind at the *re* face of FMN, with the phosphate group pointing out of the catalytic cavity, in contrast to the FMN phosphate moiety that points downward into the cavity bottom.[56] In previous studies, different crystal structures describing the *E. coli* PNPOx complexed with FMN and PLP were reported.[38,56] The crystal structure of the enzyme without ligands shows an open active site;[65] however, binding of either PNP or PLP elicits a protein conformational change that partially closes the active site.[56] In this close conformation, three conserved residues, Tyr129, Arg133 and Ser137, come closer to PLP phosphate moiety, and together with the Lys72 help the interaction between PLP and FMN, consisting in extensive hydrogen-bonds and van der Waals contacts.[38] All these amino acid residues are highly conserved in most members of the PNPOx family.[65] The invariant Arg197 and His199 residues from the second monomer are situated in front of the pyridine ring of PLP, and make direct hydrogen bond interactions with the carbonyl oxygen on C4′ and the O3′-hydroxyl group of PLP, respectively. Arg197 makes further interactions with the phosphate moiety of PLP.[56] These two residues act as a clamp on PLP sandwiching the pyridine moiety onto the isoalloxazine ring while catalysis takes place.[38] Interestingly, the monoclinic crystal form of the enzyme in complex with PLP showed previously unobserved N-terminal residues that fold over the active site to completely close it and sequester the ligand from the solvent; in fact it has been suggested that the monoclinic crystal structure may represent the catalytic state conformation.[38]

1.4.1 Non-catalytic secondary PLP binding site

It has been previously reported in crystallographic studies carried out in the presence of PLP that there is one molecule of PLP per monomer of PNPOx, and that this PLP is located at the active site, nearby the FMN cofactor. However, soaking crystals with a higher concentration of PLP, the protein structure displayed two molecules of PLP per monomer; one PLP molecule was at the active site, while the second one was located at a non-catalytic PLP binding site[56] **(Fig. 1.7)**. This secondary binding site, was firstly described on the basis of experiments carried out in solution by Yang and Schirch.[54] In this case there were experimentally evidences: for instance, when the *E. coli* PNPOx was incubated with PLP and then passed through a size exclusion chromatography, it retains PLP and shows a normal catalytic activity. Moreover, the spectral property of PLP bound at the apo-PNPOx suggested a non-Schiff base binding (a non-covalent binding of PLP); thus, in both apo- and holo-PNPOx, PLP binds at a non-catalytic site.[54] An unanswered question is the location of the non-catalytic secondary PLP binding site. In the trigonal crystal structure of the *E. coli* enzyme, a second PLP molecule binds to PNPOx at about 11 Å from the active site, prompting speculation that this crystallographic secondary binding site corresponds to the functionally observed secondary PLP binding site (PDB code: 1G79).[56] The plane of the pyridine ring is sandwiched between the side-chains of Phe177 and Lys145 (which also makes a hydrogen bond with the PLP phosphate moiety) and is located close to what seems to be a tunnel that leads to the active site.[38] Adjacent to Phe177, and also guarding the tunnel, is Asn84, which makes a close hydrogen bond to the pyridine nitrogen of PLP **(Fig. 1.7)**. The putative tunnel between the two PLP binding sites is formed almost entirely by one subunit and it is mainly composed by glycine residues

and small side-chains.[56] There are structural water molecules located inside the tunnel. The presence of the side-chains of Asn84, Arg133, Phe177 and Trp178 in the cavity narrows the tunnel. Although the structures show the tunnel to be small for the passage of PLP, the channel could easily open up, since most of the surrounding protein structures are flexible.[56] The possible role of the non-catalytic site in channelling PLP to enzymes that requires it as a cofactor is still an important field of investigations. Binding of PLP at the non-catalytic site of PNPOx might be one method for cells to regulate free PLP concentration *in vivo*.

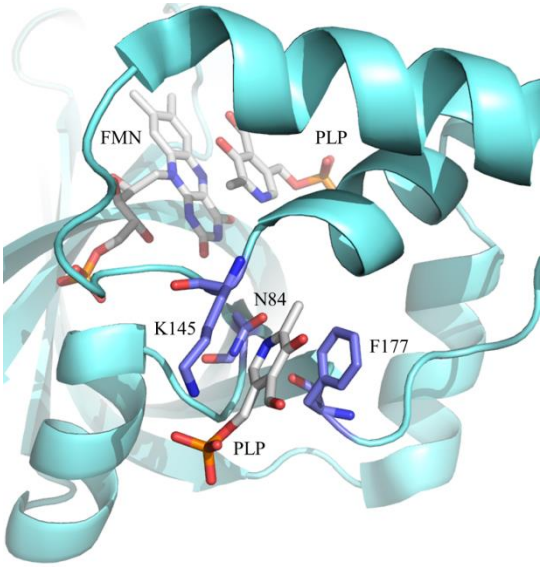

Figure 1.7 *Enlargement showing the non-catalytic secondary PLP binding site*. The protein chain is shown in cyan (PDB code: 1G79[56]). The residues of the putative secondary PLP binding site are shown as sticks, in blue. FMN and both PLP molecules are shown as sticks and coloured by atoms.

1.5 Pyridoxal 5'-phosphate deficiency and related diseases in humans

Because of the essential role of PLP in neurotransmitters metabolism, including dopamine, serotonin, histamine, D-serine, epinephrine and GABA, it is not surprising that inborn errors leading to PLP deficiency result in a pathological phenotype.[66] PLP deficiency occurs through different mechanisms. An example is PNPOx deficiency, caused by inborn defects of the PNPOx enzyme, the neonatal epileptic encephalopathy, a disorder affecting PLP synthesis and recycling. The patients affected by this kind of disease display a particular electroencephalogram pattern and some of them promptly respond to PLP, but not to pyridoxine treatment.[67] Another disorder affecting PLP import into the brain is alkaline phosphatase deficiency, or hypophosphatasia, which is associated with a molecular defect in the gene encoding the tissue non-specific alkaline phosphatase (TNSALP). TNSALP hydrolyses several substances, including inorganic pyrophosphate and PLP. The latter must be dephosphorylated by TNSALP before it can cross the cell membrane.[68,69] Vitamin B_6 deficiency in the brain impairs the synthesis of neurotransmitters, which can cause seizures.[70] Moreover, PLP binding protein (PLPBP) deficiency is a disorder likely due to abnormal intracellular PLP transport, given the fundamental role of this protein in the homeostatic regulation of free PLP levels. The clinical phenotype is similar to that observed in patients with PNPOx deficiency.[31] In other cases, the accumulation of metabolites that inactivate PLP causes the pyridoxine-dependent epilepsy (PDE), that is characterised by ALDH7A1 deficiency (also known as α-aminoadipic semialdehyde dehydrogenase or antiquitin deficiency) or by ALDH4A1 (also known as P5C dehydrogenase) deficiency.[71] ALDH7A1 deficiency results in the build-up of an intermediate with a nucleophilic carbon atom, Δ^1-piperideine 6-carboxylic acid (P6C),

which reacts with PLP thereby inactivating it and resulting in PLP deficiency.[72] Accumulation of Δ^1-pyrroline 5-carboxylic acid (P5C) in ALDH4A1 deficiency has a similar effect in hyperprolinaemia type II.[73] All the deficiencies described above (PNPOx, ALDH7A1, ALDH4A1 and PLPBP), in their most severe forms (neonatal presentations) can have other expected consequences including anaemia, lactic acidosis, and hypoglycaemia.[71] Furthermore, PLP not only acts as a cofactor of numerous enzymatic reactions, but also works as an antioxidant molecule by quenching oxygen reactive species.[13] Several studies suggest that DNA damage is a possible link between metabolism and cancer. In particular, it has been proposed that under metabolic stress conditions or in the case of reduced availability of necessary nutrients some cellular processes such as DNA acetylation/methylation, synthesis of DNA precursors and ROS production can be altered causing DNA damage, which can drive cells toward cancer.[74] Although many studies converge towards a protective role of B_6 in cancer, the molecular mechanisms are not completely understood. PLP, as antioxidant molecule, could play an important role in mediating the cross talk between metabolism and DNA damage, in fact PLP acts against the formation of advanced glycation end products (AGEs), that are genotoxic compounds associated with senescence and diabetes.[75] This relationship between PLP deficiency and diabetes has been previously described,[76–78] but the molecular and cellular mechanisms underlying this relationship have not yet been completely understood. PLP deficiency may impact on diabetes in different ways; for example, Kotake and collaborators[79] previously reported that metabolites produced in the altered tryptophan degradation pathway can interfere with insulin activity, causing insulin resistance. Moreover, given the important role of PLP in controlling the expression of genes involved in adipogenesis and in the metabolic pathway of homocysteine, a deficiency of

this vitamin could cause insulin resistance.[80,81] Rubì and collaborators[78] reported that PLP deficiency may play a role in type I diabetes onset and this is probably due to the function of this vitamer as a cofactor for two enzymes both present in the pancreatic islet: glutamic acid decarboxylase (GAD65), which synthesizes γ–aminobutyric acid (GABA), that, as part of the GABA cycle, may represent means by which the cell can utilize glutamate as a reserve energy source; and L-aminoacid decarboxylase (L-AADC), a key enzyme in dopamine synthesis **(Fig. 1.8)**.[78] Dopamine and serotonin produced by L-AADC could be involved in the regulation of insulin synthesis and secretion, thus, lower levels of dopamine can favour the onset of the type I diabetes.[82] Furthermore, GAD65 can act as autoantigen in pancreatic cells, in fact, it has previously been observed that amino acids 250-273 of this enzyme show sequence similarity with amino acids 28-50 of the coxsackievirus B protein P2-C.[83] It was proposed that, as a result of this molecular mimicry, cross-reactive T-cell proliferation will occur, leading to autoimmune destruction of the B cells.[82] Also, the GAD65 apo- to holo-enzyme change is key for the regulation of this protein. PLP binding domain surrounds the auto-antigenic region described above, thus, a PLP-deficiency results in higher levels of apo-GAD65, which is antigenic and not able to synthesize GABA **(Fig. 1.8)**.[78]

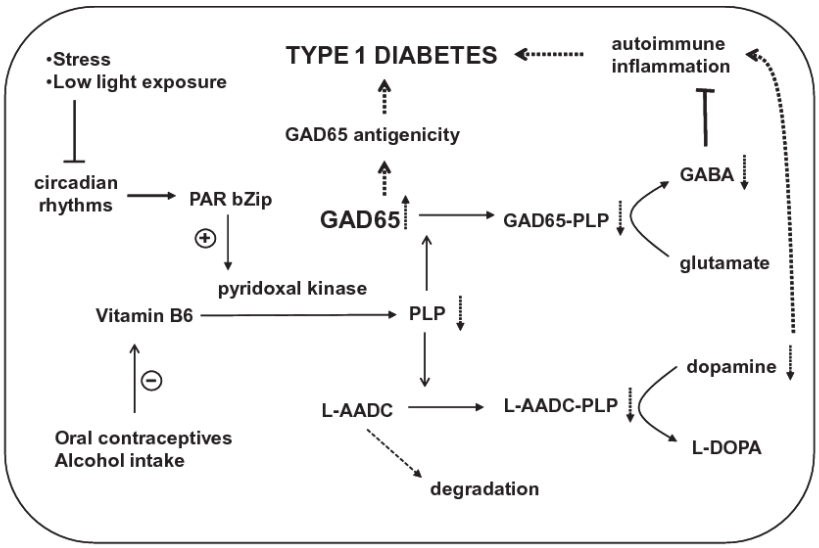

Figure 1.8 *Hypotetical model for PLP deficiency and the onset of type I diabetes*. B6 vitamers are converted into PLP by pyridoxal kinase, whose expression is promoted by the transcription factor PAR bZip. Alteration in circadian cycle, alcohol consumption and use of contraceptives decrease PLP synthesis. GAD65 devoid of PLP does not synthesize GABA. Alteration of L-AADC function lowers dopamine levels. GAD65, glutamic acid decarboxylase; PLP, pyridoxal 5'-phosphate; PAR bZip, transcription factor belonging to proline and acidic amino acid-rich basic leucine zipper transcription factor family; L-AADC, L-aminoacid decarboxylase; L-DOPA, levodopa.[78]

Furthermore, it has been reported that high expression levels of pyridoxal kinase positively correlate with survival of non-small cell lung cancer (NSCLC) patients.[84] In previous studies, mutations in *Drosophila dPdxk* gene caused chromosome aberrations (CABs), that can be rescued by PLP supplementation.[85] The same effect is produced by treating wild type flies with PLP analogues such as 4-deoxypyridoxine (4-DP) or inhibitors of PLP-dependent enzymes like cycloserine and penicyllamine. The alteration of pyridoxal kinase functionality increases the glucose content in larval

haemolymph, and hyperglycaemia and CABs are interconnected by a cause-effect relationship, in which high glucose is largely responsible for CABs.[85]

1.6 Human pyridoxine 5'-phosphate oxidase

As the *E. coli* enzyme, human PNPOx has been crystallized and its structure determined.[34] This protein, in humans, is coded by the *pdxH* gene located on chromosome 17q21.2. As mentioned above, the enzyme has a primary role in the vitamin B_6 salvage pathway and a non-correct functioning of it brings to an abnormal activity of several B_6–dependent enzymes. The three-dimensional fold of the human enzyme is very similar to that of the *E. coli* enzyme. The human and *E. coli* enzymes share 39% sequence identity, but the binding sites for FMN and substrate are highly conserved.[34] As observed with the *E. coli* enzyme, also in this case, thanks to chromatography studies, it has been demonstrated that the human enzyme binds tightly one molecule of pyridoxal 5′-phosphate on each subunit and this tight binding occurs at a non-catalytic binding site.[34] However, unlike the *E. coli* PNPOx,[38,56] no crystallographic data of the secondary PLP binding site in the human enzyme have been reported. In the light of all these considerations, a parallel study of the human and *E. coli* PNPOx would have an extraordinary importance in order to understand more in depth the mechanism of regulation of these enzymes. Human PNPOx is a homodimer and each monomer has a length of 261 amino acids. In crystallographic studies, the first 48 N-terminal residues are not visible in the electron density map because of disorder. The 1.95 Å three-dimensional structure of human PNPOx in the presence of PLP reveals a very similar protein fold to that of *E. coli* [65] (PDB code: 1NRG[34]). The monomer structure of human PNPOx shows the typical two-domain architecture (domain 1 and domain 2), previously observed for *E. coli*. The

larger domain 1 of the *E. coli* enzyme is formed by eight β-strands (β1–β8) and two α-helices (α1 and α2), with the human PNPOx having one additional β-strand, β7′, while the smaller domain 2 of both PNPOx structures is made up of 3 helices (α3, α4 and α5). The β7′ strand and part of the turn and loop regions associated with it are absent in the *E. coli* PNPOx structure because of a 15-residue insertion at residue 238 **(Fig. 1.9)**.[34] The role of these additional structures in human PNPOx might be solely structural, because they have no direct catalytic role and are also not involved in dimer formation. These unique regions are open to the solvent, with the four-amino-acid residue loop that connects the strands β7 to β7′ highly disordered.[34]

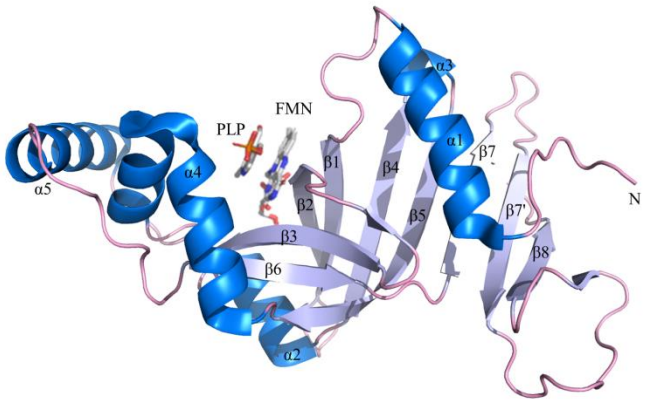

Figure 1.9 *Structure of the human PNPOx monomer*. FMN and PLP molecules are shown as sticks with atom-based colours. The loops are shown in violet; α-helices are shown in blue; β-strands are in light blue. The β7' strand is present only in human PNPOx (PDB code: 1NRG[34]).

One of the most relevant differences in the amino acid sequence between *E. coli* and human PNPOx is that the human enzyme contains six Cys residues, whereas the *E. coli* enzyme contains only a single Cys residue. Unfortunately, only four of the six residues are modelled in the crystal

structure. The other two are located in the missing N-terminal region. Two of the cysteine residues (Cys82 and Cys86, that in the *E. coli* PNPOx correspond to Val54 and Val58, respectively) are located at the dimer interface, each facing its symmetry-related counterpart. The distance from sulfhydryl groups of Cys82 and Cys86 and their related counterpart are 3.6 Å and 4.2 Å, respectively. These distances are significantly longer than an expected disulfide bond, but there is evidence that some disulfide bonds are formed between the monomers. The two remaining cysteine residues, Cys72 and Cys156 (Ala45 and Lys128 in *E. coli* PNPOx, respectively), are located on the surface of the protein and possibly both of them make a disulfide interaction with 2-mercaptoethanol of the buffer used to purify and crystallize the protein.[34]

Other differences between the two structures mainly occur in turns, loops, the N-terminal segment, and the α5 helix. There are two pairs of inter-subunit salt-bridge interactions, including Arg116–Glu143 and Arg181–Asp228 (Arg88-Ile115 and Arg153-Asp200, respectively in *E. coli* PNPOx). The latter is conserved in both PNPOx structures, whereas the former does not occur in the *E. coli* enzyme. In *E. coli*, the Glu143 residue, present in the human enzyme, is replaced by isoleucine, necessitating the rearrangement of Arg116 to make an inter-subunit salt bridge with Glu217 (Glu189 in *E. coli* PNPOx). Interestingly, the latter amino acid residue is strictly conserved in both PNPOx structures, but the salt-bridge interaction between Arg116 and Glu217 is only observed in the *E. coli* structure. Contrarily to the β7 and β8 strands, that are involved in extensive inter-subunit interactions, the new β7′ strand, makes only one weak inter-subunit hydrogen-bond interaction from Met246 to Pro179 (Ser151 in *E. coli* PNPOx).[34] The binding site of FMN is identical to that of the *E. coli* PNPOx structure, with the FMN located in a deep cleft formed by the two subunits with extensive hydrogen-bond

interactions to the protein.[65] These interactions involve both subunits. Most of the salt-bridge and hydrogen-bond interactions between the protein and the FMN are strictly conserved in both PNPOx structures. In particular, these structures have very similar FMN geometry, active-site environment, and bond distances. The bound PLP molecule occupies the same position in the active site and has essentially unaltered conformation in both the human and the *E. coli* PNPOx structures. In addition, the two crystals show similar interactions between the protein and the bound PLP, with almost all of the residues and interactions strictly conserved. The interactions involve both protein subunits; the phosphate moiety of PLP makes salt-bridge and hydrogen-bond interactions with Lys100, Arg161, Tyr157 and Ser165, belonging to a monomer, and Arg225, belonging to the other (Lys72, Arg133, Tyr129, Ser137 and Arg197, respectively in *E. coli* PNPOx).[34] The PLP pyridine ring is stacked parallel against the FMN isoalloxazine ring, with extensive van der Waals contacts between the two. As observed in the *E. coli* structure, C4' of PLP and N5 of FMN are separated by approximately 3.4 Å. The O3′- hydroxyl group of PLP makes a hydrogen-bond interaction with His227 (His199 in *E. coli* PNPOx), whereas the carbonyl oxygen on C4′ makes a water-mediated interaction with Glu77 (Asp49 in *E. coli* PNPOx), and these residues belong to different monomers of the protein. Lastly, the pyridine nitrogen makes a water-mediated hydrogen-bond interaction with Trp206 (Trp178 in *E. coli* PNPOx). The phosphate moiety of PLP is oriented toward the N-terminus of the α4 helix, which further compensates for the PLP negative charge in addition to the salt-bridge interactions. Among the active site residues that make direct or water-mediated contact with the PLP, Glu77 is the only non-conserved residue among the two structures, and it is replaced by Asp49 in *E. coli* PNPOx.[34]

1.6.1 PNPOx mutations and neonatal epileptic encephalopathy

Maintenance of a correct balance among B_6 vitamers inside the cell is of fundamental physiological importance in all organisms, including humans where PLP imbalance causes severe neurological dysfunctions as described above. Among those, of particular significance is the neonatal epileptic encephalopathy (NEE), a severe neurological disorder which usually manifests a few hours after birth, with seizures that can be fatal and do not respond to conventional anticonvulsant treatments. This particular form of epilepsy (an autosomal recessive disorder) is caused by mutations in human PNPOx, that lead to insufficient levels of PLP and a subsequent decreased activity of PLP-dependent enzymes. In one of the first studies about NEE, the authors[86] described a neonate patient whose seizures were not controlled by pyridoxine but were well controlled by PLP. Clayton and collaborators[87] described the same phenomenon in an infant whose levels of B_6 vitamers suggested deficient PLP-dependent enzyme activities: the aromatic amino acid decarboxylase deficiency causes low concentrations of homovanillic acid (HVA) and 5-hydroxyindoleacetic acid (5HIAA) with raised 3-methoxytyrosine and urinary vanillactate. Then, defects in the PLP-dependent pathways for catabolism of threonine and glycine determine an increase in plasma levels of these amino acids.[87] Other patients with similar findings were identified and were shown to have PNPOx mutations leading to reduced enzyme activity.[88] Treatment of PNPOx deficiency was found to be difficult. Reports have emphasized the possibility of normal developmental outcome with early treatment.[89,90] By 2014, it was clear that some patients with PNPOx deficiency respond to treatment with pyridoxine, and treatment with PLP may even aggravate seizures.[90,91] Certain genotypes (R225H/C and D33V) appear more likely to result in seizures responsive to

pyridoxine. Other mutations seem to be associated with infertility, miscarriage, and prematurity. To date, 62 genetically confirmed PNPOx-deficient patients have been reported with 27 different mutations in the gene encoding PNPOx [92–97]Most of them are homozygous missense mutations, but also stop codon suppression, deletions and splice site mutations have been reported in the literature.[40,87,88,90,98–102] So far, the only NEE-related human PNPOx mutations characterised from a functional and structural point of view are R229W,[100] R95C[39] and R116Q.[92] Both R229W and R95C variants resulted to be 350-fold less catalytically efficient than the wild type enzyme and presented a 50-fold and 15-fold reduction in affinity for the FMN cofactor, respectively. The crystal structure of the R229W mutant showed that the mutation prevents the proper binding of the PNP substrate due to the absence of two essential hydrogen bond interactions of His227 and Arg225 with PNP. Moreover, the binding of the FMN cofactor is weakened because of the loss of a hydrogen bond and salt-bridge interactions between FMN and Arg229 and Ser175 residues.[100] Also Arg95 makes salt-bridge and hydrogen interactions with the FMN phosphate and its substitution to Cys95 likely destabilize FMN binding.[39] Recently, the functional effects of the controversial c.347G>A (p.R116Q) mutation of human PNPOx gene have been studied and its pathogenic role in epileptic encephalopathy has been discussed.[92] Patients carrying this mutation present a peculiar clinical feature, namely a later epilepsy onset. *In vitro* biochemical characterisation of the R116Q mutant showed that although the catalytic properties are not drastically changed, the mutation affects the thermal stability of the enzyme. This altered stability of the R116Q enzyme with temperature could be linked to the increased susceptibility to febrile seizures frequently observed in children affected by NEE.[92]

1.7 Human pyridoxal kinase

Human pyridoxal kinase (PDXK) is a member of the ribokinase family and catalyses the ATP-dependent phosphorylation reaction of vitamin B_6. This enzyme is encoded by the highly conserved *pdxK* gene, that is present also in *E. coli*, and in humans is located on the 21q22.3 chromosome.[103] The structures of pyridoxal kinase from sheep brain and *E. coli* were solved in complex with substrates and products.[104,105] Cao and collaborators[103] reported for the first time the crystal structure of human PDXK at 2.8 Å resolution (PDB code: 2F7K), and then, a structure at a better resolution (2.0 Å and 2.2 Å, in absence and in complex with MgATP, respectively; PDB codes: 2YXT and 2YXU) was described by Musayev and collaborators.[42] Human pyridoxal kinase is a homodimer, containing 312 amino acid residues per monomer, related by a non-crystallographic twofold axis in an asymmetric unit and the two monomers interact through hydrogen binding, salt bridges and hydrophobic interactions.[103] Each monomer contains nine α-helices, named α1-9, and 11 β-strands, named β1-11. This structure shows the typical ribokinase superfamily overall folding pattern, with the αβα three-layer sandwich,[106] characterised by a central core of β-strands, surrounded by α-helices **(Fig. 1.10)**.[42] The overall structure is particularly conserved in *E. coli*, sheep brain and human PDXK.[42,103,105] The dimer interface is formed between α1, α9, β1 and β3 from each monomer, and the residues involved in this interaction are substituted by more hydrophobic residues in sheep brain PDXK, thus indicating a stronger hydrophobic interaction between monomers.[103] On the enzyme surface, there is a cavity with negative charge that is favourable for binding the positive charged substrates, such as the pyridine ring of the vitamers and the adenine ring of ATP. ATP interacts with the hydrophobic side chains of Val201, Ile223 and Leu263, and,

interestingly, these data are consistent with the biochemical results obtained for this enzyme. In fact, human PDXK displayed higher affinity for ATP than the sheep brain enzyme, where the aforementioned residues are replaced with less hydrophobic residues (Ala201, Met223 and Met263).[103] Comparison of the structures in absence or in complex with MgATP shows that a loop region between strand β11 and helix α7 (residues 224-228) have rotated away from the active site to allow binding of the ATP. Moreover, the so-called "flap" (residues Gly117-Val128), which is formed by strand β6, Loop I and strand β7, moved closer to the bound ATP, thus suggesting that this flap plays an important role in preventing the unproductive hydrolysis of ATP in the absence of vitamin B_6; in fact, it provides hydrogen-bond interactions to the ATP β- and γ-phosphates.[42,104,105] Metals, both monovalent and divalent cations, are known to be absolute requirements for the function of many kinases, providing driving forces for ATP binding and substrate catalysis.[107] Safo and collaborators[105] observed in previous studies on *E. coli* PDXK that K^+ is the required monovalent cation for the enzyme activity, and in humans, both ATP and PL bind with higher affinity in the presence of K^+.[42] However, Na^+ elicits the maximum enzyme activity, which results to be twofold higher than in the presence of K^+. It is possible that the replacement of K^+ with Na^+ changes the geometry of the active site to a more optimal orientation of catalytic residues, leading to greater enzyme activity in the presence of the latter cation. The Mg^{2+} ion in human PDXK is located between the ATP α- and β-phosphate groups **(Fig. 1.10)**, and this observation is in contrast to the sheep brain PDXK structure, where the ATP phosphate groups interact with a divalent Zn^{2+} cation.[42] In previous studies, it has been reported that even for the mammalian enzymes, ZnATP appears to be a better substrate only when the metal nucleotide concentrations are low, and thus, under physiological conditions, MgATP is the favoured substrate.[108]

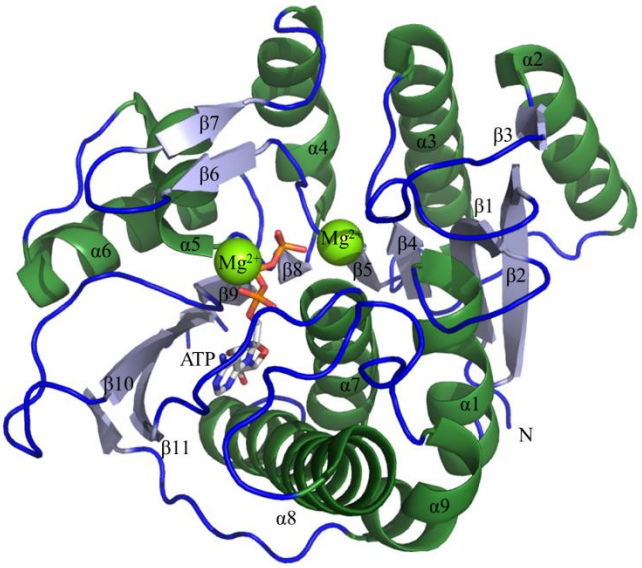

Figure 1.10 *Monomeric structure of human pyridoxal kinase complexed with MgATP*. ATP is shown as sticks with atom-based colours; α-helices are shown in green, β-strands in light blue and loops in blue. Also the Mg^{2+} cations are shown at the active site as spheres (PDB code: 3KEU[42]).

In human pyridoxal kinase, as in the ribokinase superfamily, a conserved amino acid residue (Asp235) of the active site is observed to make a hydrogen-bond interaction with the C5'-OH group of the PL substrate.[43] These data were also confirmed by kinetic studies carried out on two variants of this aspartate residue, D235A and D235N, showing a decrease in catalytic activity and PL affinity, while ATP binding has remained unchanged in both cases.[43] As mentioned above, PDXK is an ATP-dependent kinase and catalyses the conversion of PN, PM and PL to their related phosphorylated derivatives, PNP, PMP and PLP.[109,110] The kinetic constants in the human enzyme are similar for the different vitamers and the estimated parameters are the following: K_M values for PN, PM and PL are 20, 35 and 30 μM, respectively; k_{cat} values are 20, 20 and 45 min^{-1}, respectively; and the K_M values for MgATP, obtained using saturating PN, PM and PL concentrations,

are 210, 330 and 420 μM, respectively.[108] These data confirm the higher affinity of the enzyme for the vitamer than the ATP as observed previously on human PDXK variants of the active site Asp235 residue.[43] PL binding at the active site involves Ser12, Thr47, Asp235, Val19 and Tyr84, that are totally conserved residues, with the exception of Thr47, which is replaced with a proline residue in the *E. coli* structure.[42] The importance of these residues was also highlighted by a work on some pyridoxal kinase inhibitors, such as the ginkgotoxin (4'-O-methylpyridoxine), an analog of vitamin B_6. In fact, Thr47, Tyr84 and Val19 together with Phe43, Val231 and His46 residues are found to make hydrophobic interactions with this inhibitor, that like the PL, entirely places in the PL binding site.[110]

1.7.1 Human pyridoxal kinase in cancer and diabetes

In previous studies, pyridoxal 5'-phosphate has been proposed to influence carcinogenesis through different pathways, including those involved in DNA metabolism, suggesting a protective role of vitamin B_6 against DNA damage.[111] PLP supplementation was inversely correlated with the colorectal cancer risk[112] and the low PLP levels are also correlated to the onset of diabetes.[78] Moreover, an incorrect intake of vitamin B_6 could represent a risk factor for diabetic patients, as it enhances DNA damage. PLP deficiency can result in chromosome aberrations and, thus, it can be related to an increased formation of genotoxic compounds, such as the advanced glycation end products (AGEs).[85] Chromosome aberrations (CABs), such as deletions, duplications, translocations, DNA amplification and formation of aberrant gene fusions can contribute to cancer development.[113] These CABs are mainly generated by unrepaired double strand breaks (DSBs), which can be

induced by external agents (such as chemical mutagens) or by endogenous factors (such as oxidative metabolism).[85] In literature, several works suggested that vitamin B_6 has a protective role against DNA damage and cancer.[114–116] Previously, it has been reported that the mutation *dPdxk1* in the *Drosophila* gene, encoding pyridoxal kinase (*dpdxK*), causes chromosome aberrations. Moreover, the haemolymph of *dPdxk1* larvae contains nearly twice as much glucose as that of the wild type larvae.[85] The hyperglycaemia is interconnected with CABs by a cause-effect relationship, in which high glucose is largely responsible for CABs. High glucose triggers AGEs formation, which through ROS production leads to the formation of chromosome aberrations.[85] Interestingly, this relationship between glucose and CABs, in PLP depleted cells, is evolutionarily conserved as glucose supplementation enhances chromosome damage also in human cells.[46] Furthermore, hyperglycaemia can be considered a cancer risk in diabetic patients by different ways: the excess of glucose can promote cell growth or it can also cause oxidative stress, thus inducing DNA damage.[46] The role of PDXK in chromosome integrity maintenance has also been demonstrated in yeast showing that mutations in the *BUD16* gene, the *pdxK* orthologue, cause gross chromosome rearrangements largely mediated by altered DNA synthesis.[117] A dysfunction of PDXK results in PLP deficiency. It has been reported by Merigliano and collaborators[111] that a decrease in PLP levels strongly impacts on chromosome integrity in both diabetes models, thus suggesting a combined genotoxic effect of low PLP and high glucose levels. The impact of low PLP levels on genome integrity has also been tested on human cells. HeLa cells deprived of PLP by RNA interference directed against the *pdxK* gene showed chromosome aberrations. Moreover, the treatment of HeLa cells with 4-deoxypyridoxine causes chromosome aberrations, confirming the relationship between PLP deficiency and CABs

formation observed in *Drosophila*.[85] These findings suggest that humans carrying mutations in the PDXK encoding gene could have an increased propensity to accumulate chromosome aberrations and a consequent increased risk to develop cancer.

1.8 Aims of the work

Pyridoxal 5'-phosphate (PLP), the catalytically active form of vitamin B_6, is involved in more than 140 enzymatic reactions. This cofactor participates in several metabolic pathways, such as the synthesis of neurotransmitters, the amino acid metabolism, glucose homeostasis and heme metabolism. In different organisms, PLP also performs biological functions other than catalysis, such as those of reactive oxygen species scavenger in plants and transcriptional regulator in Eubacteria. However, only bacteria, fungi and plants are able to synthesize PLP *de novo*, while mammals have to acquire B_6 vitamers from diet and interconvert them using a salvage pathway. This study is focused on two key enzymes of the salvage pathway, pyridoxine 5'-phosphate oxidase (PNPOx) and pyridoxal kinase (PDXK). The work consists of three part: two of them concern the study of *Escherichia coli* and human PNPOx, respectively; the third part concerns the characterisation of human pyridoxal kinase variants.

Part I

Previously, it has been proposed that, in *Escherichia coli*, PNPOx undergoes product inhibition resulting from PLP binding at the active site;[58] however, there are not experimental data supporting the competitive inhibition hypothesis. Moreover, i*n vitro* experiments showed that PLP tightly binds

PNPOx without altering the catalytic activity of the enzyme, thus suggesting that PLP binds at a secondary non-catalytic binding site.[54] Furthermore, previous studies on the crystallographic structure of *E. coli* PNPOx highlighted a secondary PLP binding site, located at a distance from the active site and present in each protein monomer;[56] however, the actual involvement of this surface pocket in PLP binding has never been confirmed experimentally. We decided to clarify these aspects of PNPOx mechanism of regulation, which also concern the role of the enzyme as PLP carrier in the cell and are therefore crucial in *E. coli* PLP metabolism. Thus, in the first part of this work, a complete kinetic characterisation of the PNPOx reaction and an analysis of the inhibition kinetics by PLP were carried out. Then, experiments were performed to localize the actual PLP binding site on the PNPOx structure. Mutant forms of the putative crystallographic PLP binding site and of the active site of the enzyme were produced and characterised with respect the capability to bind and retain PLP and with respect to PLP binding stoichiometry.

Part II

The second part of this work is focused on human PNPOx, which shares only 39% of sequence identity with the *E. coli* enzyme; however, the two proteins share a remarkable similarity in the three-dimensional structure and in the catalytic properties. In fact, also for human PNPOx a competitive product inhibition by PLP has been proposed, and PLP binds tightly at an alternative non-catalytic binding site.[34] Thus, the same characterisation performed for the *E. coli* enzyme was carried out for the human PNPOx, in order to check if the latter enzyme shows a behaviour similar to the *E. coli* enzyme. Furthermore, in humans, a PLP deficiency due to genetic mutations in the PNPOx encoding gene is associated to neonatal epileptic encephalopathy, a

rare genetic disease characterised by early onset and seizures. However, little is known about the structural and functional alterations that such mutations induce in the enzyme. Thus, the characterisation of the catalytic activity and of the FMN binding properties of these mutant forms was performed to gain better insight into the molecular bases of the disease.

Part III

The last part of this work is focused on the characterisation of human PDXK variants present in the population. Growing evidence shows that improper intake of vitamin B_6 and PLP deficiency, resulting from alterations in the *pdxK* gene encoding PDXK, increases cancer risk, particularly in diabetic patients. It has been previously demonstrated that a *Drosophila* mutant model lacking pyridoxal kinase (*dPdxk1*) is characterised by an increased formation of chromosome aberrations (CABs) and advanced glycation end products (AGEs), especially if hyperglycaemia is also present.[85] To check if human PDXK variants can be considered predictive of an increased cancer risk, four human PDXK variants, carrying missense mutations, were expressed into *dPdxk1* mutant flies and the CAB phenotype was analysed in the laboratory of professor Fiammetta Vernì (Department of Biology and Biotechnology "Charles Darwin", Sapienza Università di Roma). Then, the catalytic properties of all PDXK variants were analysed, using the three vitamers pyridoxine, pyridoxamine and pyridoxal, to determine how the mutations of pyridoxal kinase affect the kinetic parameters with different substrates.

2. Materials and Methods

2.1 Materials, bacteria strains, plasmids and growth conditions

Ingredients for bacterial growth and all reagents used for protein purification were from Sigma-Aldrich (St Louis, MO, USA), except DEAE-Sepharose and Phenyl-Sepharose, which were purchased from GE Healthcare (Milwaukee, WI, USA), Ni-NTA agarose was purchased from QIAGEN. Pyridoxine 5'-phosphate was obtained from pyridoxal 5'-phosphate (98% pure; Sigma-Aldrich) according to the method of Kazarinoff and McCormick.[41]

2.1.1 Growth media and supplements

LB broth previously sterilized at 121°C, 3 bars pressure, was used for bacterial growth and isolation. The LB medium used was composed of: 10g/L tryptone, 5g/L yeast extract, 5g/l NaCl. Supplements have been added to growth media: 100 µg/ml ampicillin and 34 µg/ml chloramphenicol; 40 µg/ml kanamycin and 34 µg/ml chloramphenicol; and 40 µg/ml kanamycin, for *Escherichia coli* PNPOx, human PNPOx and human PDXK, respectively. The Minimal Medium M9, used for bacterial cultures of *Escherichia coli* strains, was composed of: 0.6% anhydrous Na_2HPO_4, 0.3% KH_2PO_4, 0.05% NaCl, 0.1% NH_4Cl, 0.4% glucose, 2 mM $MgSO_4$, 0.1 mM $CaCl_2$, and supplemented with 40 µg/ml kanamycin, 100 µM pyridoxal and 100 µM pyridoxine.

2.1.2 Bacteria strains and plasmids

The *E. coli* strain MDS00 (W3110 lacI169 tna^2 sup^0ΔpdxH::Ω(Cm^r)(DE3)), which contains the T7 RNA polymerase gene was used both for the construction of clones and for the protein expression. The mutation ΔpdxH::Ω(Cm^r) has a part of the *pdxH* gene substituted with the cassette for

the chloramphenicol resistance (Cm^r) in order to select the bacteria. In fact this *E. coli* strain does not express the gene for the PNPOx, if it does not have a plasmid with the sequence coding for the enzyme. The strain has the T7 RNA-polymerase gene controlled by the inducible promoter lacI169. The plasmid used for the expression of the gene is a pET 22b(+) (Novagen, USA). An example of this plasmid is shown in **Figure 2.1**.

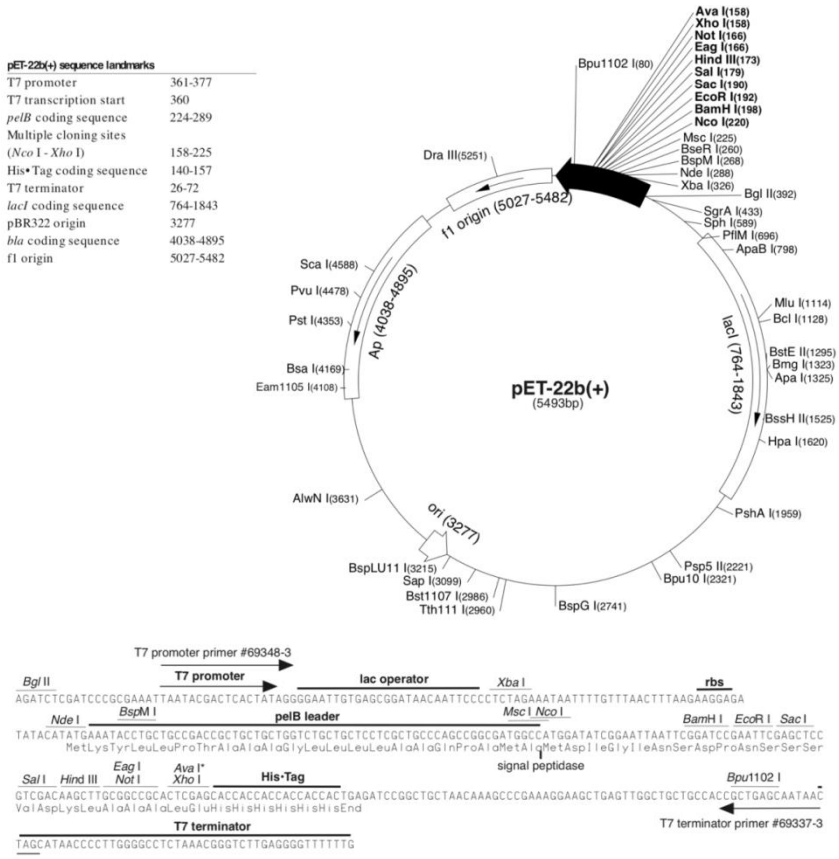

Figure 2.1 *Schematic representation of pET 22b(+) plasmid*. The Multiple Cloning Site, where the gene of interest is inserted, is controlled by the T7 promoter. The plasmid contains also the lac operator (lacO), the gene of the lac repressor (lacI), the gene for the Ampicillin resistance (Amp^r) and the origin of replication in bacteria (ori).

The gene was cloned in the MCS, between *NdeI* and *NcoI*. The expression of the cloned gene is controlled by the T7 promoter, which is recognized by the T7 RNA polymerase (the gene of this polymerase is contained in the bacterial genome). Because the T7 RNA polymerase gene is repressed by the repressor *lacI*, it can be expressed only in presence of an inductor, such as the isopropyl-β-D-1-thiogalactopyranoside (IPTG), which is a molecular mimic of allolactose and triggers transcription of lac operon. Moreover, pET vectors confer antibiotic resistance to the transformed strains. Because of the peculiar characteristics of the MDS00 strain described above, only the PNPOx gene contained in the plasmid is expressed in presence of IPTG.

Competent *E. coli* Rosetta (λDE3) and HMS174 (λDE3) cells (Novagen, USA) were transformed with the pET 28a(+) plasmid (Novagen, USA), in which were cloned the cDNAs codifying for human PNPOx and human PDXK, respectively.[92,108] Rosetta host strains are BL21 derivatives designed to enhance the expression of eukaryotic proteins that contain codons rarely used in *E. coli*. These strains supply tRNAs for AGG, AGA, AUA, CUA, CCC, GGA codons on a compatible chloramphenicol-resistant plasmid. The tRNA genes are driven by their native promoters. DE3 indicates that the host is a lysogen of λDE3, and therefore carries a chromosomal copy of the T7 RNA polymerase gene under control of the *lacUV5* promoter. Such strains are suitable for production of protein from target genes cloned in pET vectors by induction with IPTG. As mentioned above, the plasmid used for the expression was pET 28 a(+) which has a kanamycin cassette (kan^r) for the selection. The human PNPOx gene was cloned in the MCS, between *NdeI* and *XhoI*, as previously described,[34] while the human PDXK gene was cloned between *NdeI* and *EcoRI*.

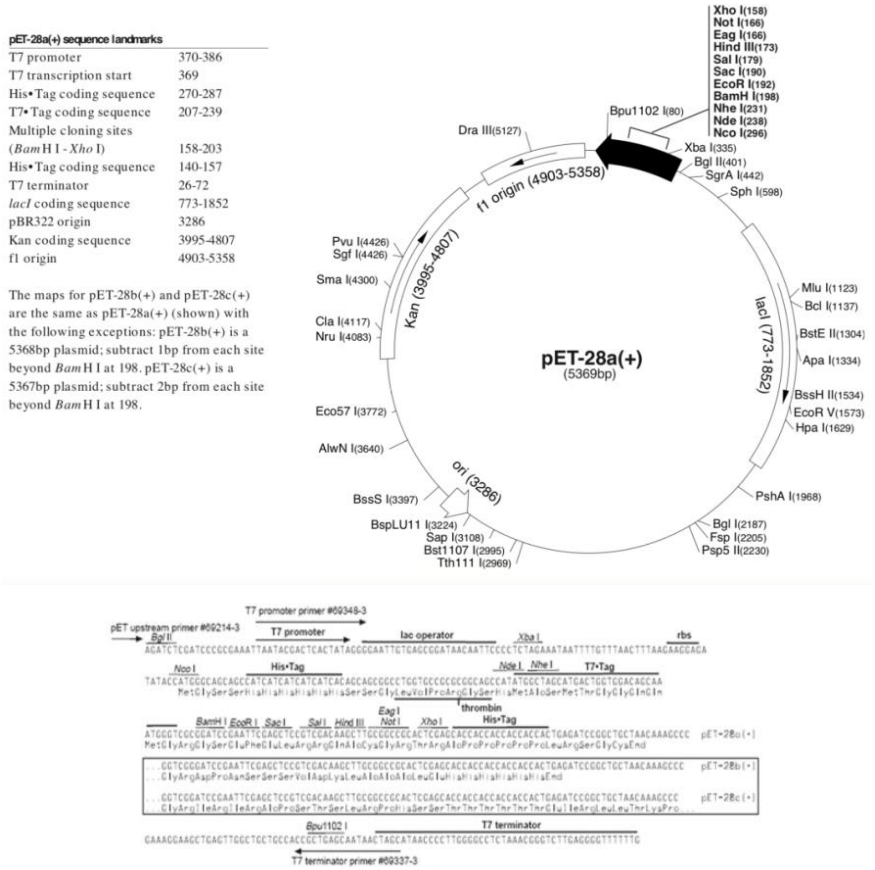

Figure 2.2 *Schematic representation of the pET 28a(+) plasmid*. The Multiple Cloning Site, where the gene of interest is inserted, is controlled by the T7 promoter. The plasmid contains also the lac operator (lacO), the gene of the lac repressor (lacI), the gene for the kanamycin resistance and the origin of replication in bacteria (ori).

2.1.3 Site-directed mutagenesis of PNPOx from *Escherichia coli*

Mutations of the *pdxH* coding region were carried out using the pET22b (+) construct as template and a standard protocol described in the Quick-Change kit from Stratagene (La Jolla, CA). For each mutation, two complementary oligonucleotide primers, synthesized by Metabion International AG (Steinkirchen, Germany), were used. The oligonucleotide sequences are listed

below and the mutated bases are underlined. *E. coli* DH5α cells were used to amplify the mutated plasmids. All mutations were confirmed by sequence analysis of both DNA strands and the only differences with respect to wild-type were those intended. Enzyme expression was performed using the *E. coli* MDS00 strain.[41]

K145A forward, 5'-GCATGGGTTTCGGCGCAGTCCAGTCGC-3'
K145A reverse, 5'-GCGACTGGACTGCGCCGAAACCCATGC-3'
F177A forward, 5'-CCATTGCCGAGCGCTTGGGGCGGTTTTCGC-3'
F177A reverse, 5'-GCGAAAACCGCCCCAAGCGCTCGGCAATGG-3'
N84A forward, 5'-GGTGTTTTACACCGCCCTCGGCAGCCG-3';
N84A reverse, 5'-CGGCTGCCGAGGGCGGTGTAAAACACC-3';
N84W forward, 5'-GGTGTTTTACACCTGGCTCGGCAGCCG-3';
N84W reverse, 5'-CGGCTGCCGAGCCAGGTGTAAAACACC-3'
R23L forward, 5'-CAAAGGCGGGTTACTCCGCCGCGATCTTC-3';
R23L reverse, 5'-GAAGATCGCGGCGGAGTAACCCGCCTTTG-3'
R215L forward, 5'-GTGGAAGATTGATCTTCTTGCACCCTG-3';
R215L reverse, 5'-CAGGGTGCAAGAAGATCAATCTTCCAC-3'
F202M forward, 5'-CCTGCATGACCGCATGTTGTACCAGCGTG-3';
F202M reverse, 5'-CACGCTGGTACAACATGCGGTCATGCAGG-3'
K72I forward, 5'-GCATCGTTTTACTCATACATTACGACGAA-3';
K72I reverse, 5'-TTCGTCGTAATGTATGAGTAAAACGATGC-3'
Y129F forward, 5'-CTCGAAGTGATGAAATTTTTTCATAGCCGCCC-3';
Y129F reverse, 5'-GGGCGGCTATGAAAAAATTTCATCACTTCGAG-3'
R133L forward, 5'-GAAATATTTTCATAGCCTCCCGCGTGATAGC-3';
R133L reverse, 5'-GCTATCACGCGGGAGGCTATGAAAATATTTC-3'
H199A forward, 5'-GAGCATCGCCTGGCTGACCGCTTTTTGTAC-3'
H199A reverse, 5'-GTACAAAAAGCGGTCAGCCAGGCGATGCTC-3'

2.1.4 Site-directed mutagenesis of human PNPOx

The G118R, R141C, R225C, R225H, and R116Q/R225H mutant forms were made on a cDNA coding for human pyridoxine 5'-phosphate oxidase, which had been cloned into the expression vector pET 28a(+). Site-directed mutagenesis was performed by QuickChange methodology (Stratagene, La Jolla, CA, USA). Mutagenic primer sequences, synthesized by Metabion International AG (Steinkirchen, Germany), were as follows:

G118R forward 5'-TCGAGAGTCGAAAAAGAAAAGAGCTGGA-3',
G118R reverse 5'-TCCAGCTCTTTTCTTTTTCGACTCTCGA-3',
R141C forward 5'-CTTAACCGTCAGGTGTGTGTGGAAGGCC-3',
R141C reverse 5'-GGCCTTCCACACACACCTGACGGTTAAG-3',
R225C forward 5'-GGTCAAACCAACTGCCTGCATGACCGG-3',
R225C reverse 5'-CCGGTCATGCAGGCAGTTGGTTTGACC-3',
R225H forward 5'-GGTCAAACCAACCACCTGCATGACCGG-3',
R225H reverse 5'-CCGGTCATGCAGGTGGTTGGTTTGACC-3',

with the underlined nucleotides generating the mutation. For the double mutant R116Q/R225H, the mutagenic primers R225H forward and R225H reverse were used on the pET28-PNPOx construct expressing the R116Q mutation.[92]

Concerning the X262Q mutation, where the stop codon was replaced with a glutamate residue resulting in a 28-amino acids longer protein, seven PCR reactions were performed in a row using the SimpliAmp™ Thermal Cycler (Thermo Fisher Scientific, Waltham, MA, USA). Seven different oligonucleotides have been synthesized, which have the 3'-end part of the sequence that overlaps with the primers of the previous reaction. Each reaction adds four new codons to the sequence, coding for four new amino

acid residues. In the first two primers there is a mutation that replaces the stop codon with glutamate. The standard T7 primer was used as forward primer. The reverse primers used are labelled from 1 to 7 and reported below, and the mutated nucleotides and the new stop codon are underlined.

X262Q_1 5'-AGGTCCCAGAGCTGAGGTGCAAGTCTCTCATAG-3';
X262Q_2 5'-CACTCTGGGCCAGCAGGTCCCAGAAGCTGAGGT-3';
X262Q_3 5'-ACCTAGCCCTAGCTCCACTCTGGGCCAGCAGGT-3';
X262Q_4 5'-ACACCCTCTCTTGACACCTAGCCCTAGCTCCAC-3';
X262Q_5 5'-CTGGGTCCCAATCCCACACCCTCTCTTGACACC-3';
X262Q_6 5'-CTTAGAAAGAAGGGCCTGGGTCCCAATCCCACA-3';
X262Q_7 5'-CCTTCGAATTCTTAGAAAGAAGGGCCTGGGTC-3'.

The last oligonucleotide adds also to the sequence two restriction sites, GAATTC and TCCGAA, for *EcoRI* and *XbaI*, respectively.
All mutations were confirmed by sequence analysis of the constructs. Plasmids were purified using a NucleoSpin Plasmid EasyPure kit (Macherey-Nagel, Germany).

2.1.5 Site-directed mutagenesis of human PDXK

D87H, V128I, H246Q and A243G PDXK variants were generated by introducing mutations (by PCR based site-directed mutagenesis, Quick-Change II XL Site-Directed Mutagenesis Kit, Agilent, Santa Clara, CA, USA) into the wild type HA-tagged PDXK gene. Primers used are listed below.

D87H forward 5'-GCCAGGAACGACTTGTGCCTCGTATAACCTGTG-3'
D87H reverse 5'-CACAGGTTATACGAGGCACAAGTCGTTCCTGGC-3'

V128I forward 5’-GCGAAGGCTCGATGTACATCCCGGAGGACC-3’
V128I reverse 5’-GGTCCTCCGGGATGTACATCGAGCCTTCGC-3’
H246Q forward 5’-GTTATTGGGGTGCTTCTGTGTCCACGCCAGG-3’
H246Q reverse 5’-CCTGGCGTGGACACAGAAGCACCCCAATAAC-3’
A234G forward 5’-CTTGTGTGTCCACCCCAGGAGCATGGC-3’
A243G reverse 5’-GCCATGCTCCTGGGGTGGACACACAAG-3’

2.2 Methods used in the studies on *Escherichia coli* and human PNPOx

2.2.1 Expression and purification of *E. coli* PNPOx

E. coli wild type and mutant PNPO forms were expressed using a pET 22b(+) construct containing the *pdxH* gene, transformed into *E. coli* MDS00 strain cells lacking *pdxH*.[41,62] Apo-PNPOx was obtained by chromatographic separation[62] (briefly described below).

An overnight culture (20 ml) of *E. coli* MDS00 transformed with plasmid pET 22b(+)-PNPOx was used to inoculate 4 L of LB broth, and the growth medium was supplemented with ampicillin (100 µg/ml) and chloramphenicol (34 µg/ml) in order to allow the selection of the resistant strains. Bacteria were allowed to grow for approximately 5h, at 37 °C (until OD_{600} of ~0.5 was reached), then the growing temperature was lowered to 28 °C and the expression of PNPOx induced with 0.1 mM IPTG. Cells were harvested at 6000 g for 30 min and suspended in a 50 mM potassium-phosphate (KPi) buffer, pH 7.3, containing 2 mM EDTA, 5 mg/L of lysozyme, FMN and one SIGMAFAST™ protease inhibitor cocktail tablet (Sigma-Aldrich, Saint Louis, MO, USA). The cell lysis was carried out by sonication on ice (3 min using a 70% amplitude for 20 s pulses alternate to 20 s intervals). The lysate was precipitated with ammonium sulfate (AS) at 25% and centrifuged for 30

min at 6000 g. The supernatant was precipitated again at 55% AS. This was followed by a further centrifugation. The pellet was dissolved in 100 mM KPi buffer, pH 7.0, containing 0.2 mM EDTA and 5 mM 2-mercaptoethanol and loaded on a Bio-Gel P6DG column (Sigma-Aldrich, St. Louis, MO, USA). The same buffer was used to elute the protein and to separate the protein extract from other cellular components such as carbohydrates, lipids and the exceeding FMN not complexed with the enzyme. The eluted protein was loaded on a CM Sephadex C-25 column (Sigma-Aldrich, St. Louis, MO, USA), pre-equilibrated with 20 mM KPi buffer, pH 6.8, containing 0.2 mM EDTA and 5 mM 2-mercaptoethanol. The protein was eluted with a linear gradient from 20 mM KPi buffer, pH 6.8, containing 0.2 mM EDTA and 5 mM 2-mercaptoethanol to 100 mM KPi buffer, pH 7.0, containing 0.2 mM EDTA, 5 mM 2-mercaptoethanol and 400 mM NaCl. The fractions containing the protein were selected using spectrophotometric and SDS-PAGE analyses and collected. The protein was dialyzed overnight against 50 mM Na-HEPES buffer, pH 7.6, containing 150 mM NaCl.

2.2.2 Expression and purification of human PNPOx

The cDNA coding for the hypothetical human PNPO (NCBI nucleotide database entry AK001397) was inserted into the pET 28a(+) expression vector. The pET 28a(+)-human PNPOx construct was used to transform the *E. coli* Rosetta (λDE3) cells (Novagen, USA). The pET 28a(+) vector adds 20 residues to the N-terminus of human PNPOx, including a sequence of six His residues for binding to a Ni-NTA column.

The growth medium used for these experiments, such as the plasmid DNA purification and the bacteria transformation procedures, were the same previously described for *E. coli* PNPOx. The only difference occurs for the

antibiotics used, which were kanamycin (40 µg/ml) and chloramphenicol (34 µg/ml).

Cells were harvested and suspended in 50 mM Tris-HCl buffer, pH 7.6, containing 300 mM NaCl. The cell lysis procedure and the ammonium sulfate precipitation were the same as for the *E. coli* PNPOx. The pellet was suspended in 20 mM KPi buffer, pH 7.8, containing 150 mM NaCl and dialyzed overnight against the same buffer. The protein solution was then centrifuged at 12000 g for 30 min. The supernatant was directly loaded onto a 5 ml HisTrap column (GE Healthcare Life Sciences, Milwaukee, WI, USA) which has been previously equilibrated with the suspension buffer. The loaded column was washed with 20 mM KPi, pH 7.8, buffer containing 150 mM NaCl and 10 mM imidazole, in order to tale out different macromolecules such as lipids and carbohydrates. The protein was eluted with a 50 ml gradient of imidazole (from 10 mM to 300 mM) in the suspension buffer. The fractions containing the protein were selected using spectrophotometric and SDS-PAGE analyses. The collected fractions were dialyzed overnight in 20 mM KPi buffer, pH 7.8, containing 150 mM NaCl and 5 mM 2-mercaptoethanol, in order to take out the imidazole.

To optimize the purification of the dimeric form of human PNPOx, a further size exclusion chromatography was carried out using the HiLoad 16/600 Superdex 200 pg column (GE Healthcare Bio-Sciences, Pittsburgh, PA, USA). The column was equilibrated with 20 mM KPi buffer, pH 7.5, containing 150 mM NaCl and 5 mM 2-mercaptoethanol. The sample (5 ml volume) was centrifuged at 12000 g for 30 min, and then loaded on the column. The flow rate of the elution was 1 ml/min. Only the fractions corresponding to the elution of 62 KDa, which is the molecular weight of the functional dimer, were collected.

Preparation of apo-PNPOx

The apo-enzyme forms were prepared at low pH through phenyl sepharose chromatographic step, as previously described.[62] The pH of the sample was lowered by adding 100 mM KPi buffer, pH 5.0, containing 5 mM 2-mercaptoethanol and 0.2 mM EDTA. The solution was brought to 20% saturation of ammonium sulfate and loaded onto a phenyl Sepharose column (GE Healthcare Life Sciences, Milwaukee, WI, USA), pre-equilibrated with 20% ammonium sulfate in 100 mM KPi buffer, pH 5.0. The protein sample was loaded onto the column and washed with the equilibrating buffer continuously until the absorbance at 450 nm of FMN was below 0.05 in the eluate. The column was then washed with 10 ml of 0.1 M sodium phosphate (NaPi) buffer, pH 7.6, containing 5 mM dithiothreitol and 0.2 mM EDTA. The apo-PNPOx was eluted by washing the column with 20 mM KPi buffer, pH 7.2, containing 2-mercaptoethanol and EDTA, as above, and 15 % propylene glycol.

2.2.3 Determination of concentration and purity of PNPOx

The collected fractions were analyzed using a Hewlett-Packard 8453 diode-array spectrophotometer (Agilent Technologies, Santa Clara, CA, USA) and the SDS-PAGE run in order to determine the concentration and the purity rate of the fractions, respectively.

Polyacrylamide gel electrophoresis was used to separate the proteins and verify the purity rate of the fractions collected after the chromatography. Before the loading on the SDS-PAGE gel (Bio-Rad, Hercules, CA, USA), the protein sample was mixed with the loading buffer and boiled at 100 °C for 5 min in order to completely denature the proteins. At the end of the electrophoretic separation, all the proteins can be analyzed by Quick Coomassie staining (Bio-Rad, Hercules, CA, USA).

The protein subunit concentration of both apo-PNPOx and holo-PNPOx was generally calculated using the theoretical molar extinction coefficients at 278 nm of 71200 M^{-1} cm^{-1} and 76760 M^{-1} cm^{-1} for *E. coli* and human enzymes, respectively (calculated with the Expasy PROTPARAM tool, Switzerland). However, using the method developed by di Salvo and collaborators,[62] protein subunit concentration was evaluated taking into account the contribution of FMN to the absorbance at 278 nm. According to the Lambert-Beer Law, $A = \varepsilon cl$, where A is the solution absorbance at a certain wavelength λ, ε is the molar extinction coefficient of a substance at λ; c is the concentration of the solution, and l is the pathlength, the concentration of FMN was evaluated using a molar extinction coefficient at 445 nm of 12400 M^{-1} cm^{-1}. The contribution of FMN at 278 nm was measured using a molar extinction coefficient of 23400 M^{-1} cm^{-1}, and then, the protein subunit concentration was estimated using the theoretical molar extinction coefficients at 278 nm of the apo-forms of *E. coli* and human PNPOx, 47760 M^{-1} cm^{-1} and 53360 M^{-1} cm^{-1} [(34)], respectively.

2.2.4 Differential Scanning Fluorimetry (DSF) assays

DSF assays were performed using a Real Time PCR Instrument (CFX Connect Real Time PCR system, Bio-Rad, Hercules, CA, USA). In a typical experiment, 2 μM of the protein in 50 mM Na-HEPES buffer, pH 7.6, containing 150 mM NaCl, was mixed with Sypro Orange (5x, Thermo Scientific, Waltham, MA, USA) and various ligands (total volume of 25 μl) in a 96-well PCR plate. Fluorescence was measured from 25 °C to 95 °C in 0.4 °C/30 s steps.[118] The excitation fluorescence was set at 450-490 nm and the emission fluorescence was recorded between 560 nm and 580 nm. All samples were run in triplicate. Denaturation profiles were analysed using the Graph Pad software (San Diego, CA, USA) after removal of points

representing quenching of the fluorescent signal due to post-peak aggregation of protein-dye complexes. All curves were normalised and fitted to a sigmoidal equation to obtain the melting temperatures (T_m). Alternatively, the melting temperatures were obtained by plotting the first derivative of the fluorescence emission as a function of temperature (-dF/dT) by using the Bio-Rad CFX manager software (Hercules, CA, USA).

2.2.5 Kinetic studies

Kinetic measurements were performed using a Hewlett-Packard 8453 diode-array spectrophotometer (Agilent Technologies, Santa Clara, CA), using a 1-cm pathlength cuvette, at 37°C in 50 mM Na-HEPES buffer at pH 7.6. Reactions were started by the addition of the enzyme to buffer containing PNP and kept under constant stirring by a magnetic bar, to ensure a rapid mixing. Kinetic traces were exactly the same when the order of addition of reaction components was inverted by adding PNP last. The protein concentration used for the wild type *E. coli* and human PNPOx was 0.5 µM, while 1 µM protein subunit concentration was used for the R225H PNPOx. PNP concentration was varied from 1.5 to 100 µM, and PLP from 0.2 to 16 µM. Product formation was followed at 388 nm, where PLP absorbs maximally with a molar absorbance coefficient of 5330 $M^{-1}cm^{-1}$, as calculated from standard PLP solutions, whose concentration was determined in 0.1 M NaOH.[119] Activity assays were also carried out in 50 mM TRIS-HCl pH 7.6. In this case, an extinction coefficient of 4253 M^{-1} cm^{-1} at 414 nm was calculated for PLP.

2.2.6 Stopped-flow experiments on *Escherichia coli* PNPOx

The PLP dissociation constant was also determined by stopped-flow spectroscopy. Kinetic binding experiments were carried out on a thermostated SX-17 stopped-flow instrument (Applied Photophysics, Leatherhead, UK) with high fluorescence sensitivity and low inner-filtering, in 50 mM Na-HEPES buffer at pH 7.2, at 25 °C. Protein-bound FMN was excited at 445 nm and total fluorescence emission was collected by using a 510-nm cut-off glass filter. In these experiments PNPOx was mixed in the stopped-flow apparatus with solutions of increasing PLP concentrations from 8 to 40 μM before mixing. Since fluorescence changes were very small, the enzyme concentration was increased to 20 μM (before mixing), and several traces (from 8 to 16) at each PLP concentration were acquired and averaged to increase the signal-to-noise ratio.

2.2.7 Measurement of PLP content of the PNPOx-PLP complex

Retention of PLP by *E. coli* PNPOx was analysed by measuring the PLP content of the protein after incubation with PLP and chromatographic separation. Wild type and PNPOx mutant forms (100 μM) were mixed with 100 μM PLP and incubated at 30 °C for half an hour. Unbound PLP was separated from the protein on a Superdex 200 10/300 GL size exclusion chromatography column (GE Healthcare Bio-Sciences, Pittsburgh, PA, USA), using a FPLC system. The column was equilibrated with 50 mM Na-HEPES buffer, pH 7.5.

After chromatography, the PLP content of fractions containing PNPOx was measured using apo-*E. coli* serine hydroxymethyltransferase (apo-SHMT) as PLP acceptor. The protein eluted from the Superdex 200 10/300 GL column was treated with 0.6 M KOH and 25% v/v $HClO_4$, to release PLP complexed with PNPOx. Then, aliquots of these samples were added to apo-SHMT.

SHMT activity, due to reconstituted holo-SHMT, was measured in 50 mM Na-HEPES buffer, pH 7.5, containing 200 μM DTT and 100 μM EDTA at 30 °C, using methylene-tetrahydrofolate dehydrogenase as coupled enzyme, with L-serine, nicotinamide adenine dinucleotide phosphate ($NADP^+$) and tetrahydrofolate as substrates. The initial velocity of the SHMT reaction was determined over the first 45 s at 340 nm, using an extinction coefficient of 7200 M^{-1} cm^{-1}.[54]

2.2.8 Determination of the dissociation constants of FMN and PLP binding equilibria

The dissociation constants for FMN binding to wild type and mutant enzymes were analysed taking advantage of FMN fluorescence quenching observed upon binding of this cofactor to apo-PNPOx.[100] Fluorescence emission measurements were carried out at 25 °C, in 50 mM Na-HEPES buffer at pH 7.6, with a FluoroMax-3 Jobin Yvon Horiba spectrofluorometer (Kisshoin, Japan), using a 1-cm pathlength quartz cuvette. Fluorescence emission spectra were recorded from 470 nm to 570 nm upon excitation of FMN at 450 nm. Excitation and emission slits were set at 2 nm and 4 nm, respectively. Increasing concentrations of the apo-enzyme (from 30 nM to 1 μM, and from 100 nM to 3 μM, for *E. coli* and human PNPOx, respectively) and a fixed FMN concentration (50 nM) were used. Dissociation constants were calculated from saturation curves obtained measuring FMN fluorescence emission intensity as a function of increasing protein concentration. Data between 520 nm and 530 nm were averaged and analysed according to a modified version of **Eq. 8**.

As described above for the analysis of the FMN binding equilibrium, a similar experiment was carried out to estimate the dissociation constant of PLP. Analyses took advantage of FMN fluorescence quenching observed

upon binding of PLP to PNPOx. All analysed PNPOx forms were used at a fixed final subunit concentration of 0.1 μM, while adding increasing concentrations of PLP (from 0.1 to 6 μM). Excitation and emission slits were set at 3 nm and 5 nm, respectively. Dissociation constants were calculated from saturation curves obtained measuring FMN fluorescence emission intensity as a function of increasing PLP concentration and analysed using a quadratic equation (**Eq. 8**). Titration experiments carried out to determine the stoichiometry of PLP binding to PNPOx were performed using the same method with excitation and emission slits set at 1 and 3 nm, respectively. PLP binding to apo-PNPOx was analysed taking advantage of protein intrinsic fluorescence quenching observed upon binding of PLP to apo-PNPOx. Increasing concentrations of PLP (from 0.1 μM to 6 μM) and a fixed apo-enzyme concentration (0.1 μM) were used. The excitation wavelength was set at 280 nm and fluorescence emission spectra were recorded from 300 nm to 450 nm, with excitation and emission slits set at 3 nm and 5 nm, respectively. Fluorescence emission values between 335 nm and 345 were averaged and analysed according to a modified version of **Eq. 8**.

2.2.9 Data analysis

Data were analysed using the software Prism (GraphPad Software Inc., San Diego, CA, USA) or Matlab (Mathworks, USA). Kinetics of PLP formation from PNP obtained in HEPES buffer were analysed with an empirical equation describing an exponential process followed by a linear phase:

$$y = \alpha_E(1 - e^{-k_E t}) + k_L t \qquad \text{(Eq.1)}$$

The α_E term is the amplitude of the exponential phase, and the k_E and the k_L terms are the rate constants of the exponential process and the linear phase,

respectively. Steady-state kinetic parameters (k_{CAT} and K_D) in HEPES buffer were determined by nonlinear least squares fitting of initial velocity data to the quadratic equation Eq. 2, in which v_i is the initial velocity of the reaction, V_{MAX} is the maximum velocity of the reaction, [PNP] is the total substrate concentration, $[E_0]$ is the total enzyme concentration and K_D is the dissociation constant of the substrate binding equilibrium $E + PNP \leftrightharpoons E \cdot PNP$ that, assuming a rapid establishment of the equilibrium, is equivalent to K_D.

$$v_i = \frac{[PNP] + E_0 + K_D - \sqrt{-(K_D + [PNP] + E_0)^2 + 4\,([PNP] + K_D) - 4\,E_0\,[PNP]}}{2\,E_0}\,V_{MAX}$$

(Eq. 2)

Kinetic parameters of the quadruple mutant in TRIS buffer were obtained by fitting initial velocity data as a function of substrate concentration using the Michaelis-Menten equation.

Apparent k_{CAT} and apparent K_D values obtained from PLP inhibition studies were fitted to Eq. 3 and Eq.4, respectively, in which K_{Is} is the inhibition constant of PLP, when it binds to the substrate-bound enzyme, and k_{CAT} is the catalytic constant. K_D and K_{Dp} are the dissociation constants of the substrate, obtained for the free or the product-bound enzymes, respectively, as shown in Scheme 1A. Since Scheme 1A comprises a thermodynamic cycle, K_I (the inhibition constant of PLP bound to the free enzyme) was determined through Eq. 5, which is based on the principle of detailed balance.

$$k_{CAT}^{app} = \frac{K_{Is}}{K_{Is}+[PLP]}\,k_{CAT} \qquad \text{(Eq. 3)}$$

$$K_D^{app} = \frac{K_D\, K_{Is} + K_{Dp}[PLP]}{K_{Is} + [PLP]} \quad \text{(Eq. 4)}$$

$$K_I = \frac{K_D\, K_{Is}}{K_{Dp}} \quad \text{(Eq. 5)}$$

In the stopped-flow experiments the PLP and PNPOx concentrations were comparable, thus pseudo-first order conditions could not be met. Under these conditions the data obtained from stopped-flow experiments were fitted to:

$$y = \alpha_F \frac{1 - e^{-k_F t}}{1 + \omega\, e^{-k_F t}} + \alpha_S\, e^{-k_S t} + \alpha_B \quad \text{(Eq. 6)}$$

which was tailored to account for the observed biphasic time courses, and where the α's and k's are the amplitudes and observed rate constants, respectively, of the fast (F) and slow (S) phases, and α_B is the equilibrium baseline fluorescence. The first term of Eq. 6 represents the time course of a second-order reaction under non-pseudo first order conditions.[120] k_F is given by Eq. 7, which describes the dependence of the observed rate constant on PLP concentration, and ω is a dimensionless parameter (with values $-1 < \omega < 0$) measuring the deviation of the system from pseudo-first order conditions;[120] k_{ON} and k_{OFF} are the second order binding and first order dissociation rate constants, respectively. The second term of Eq. 6 accounts for the decay of the PNPOx-PLP complex as discussed in the Results section (Scheme 2).

$$k_F = \sqrt{k_{ON}^2 (E_0 - [PLP])^2 + k_{OFF}^2 + 2k_{ON}^2 k_{OFF}^2 (E_0 + [PLP])}$$

(Eq. 7)

Fluorescence data obtained in PLP binding equilibrium experiments were analysed according to the quadratic Eq. 8,[121,122] in which F_{rel} is the measured relative fluorescence, F_0 is the fluorescence measured in the absence of ligand, F_{inf} is fluorescence at infinite ligand concentration, $[E_0]$ is the total enzyme subunit concentration, $[P_0]$ is the total PLP concentration and K_I is the dissociation constant of the equilibrium $E + P \leftrightharpoons E \cdot P$.

$$F_{rel} = F_0 + \left(F_{inf} - F_0\right) \times \frac{[P_0]+[E_0]+K_I-\sqrt{-(K_I+[P_0]+[E_0])^2+4\,([P_0]+K_I)-4\,[E_0\,][P_0]}}{2\,E_0}$$

(Eq. 8)

2.3 Methods for the studies on *human* PDXK variants

2.3.1 Expression and purification

Variant PDXK genes were cloned into the pET 28a (+) expression vector and this was transformed into *E. coli* HMS174 (λDE3) pLysS competent cells for protein expression. The selection of the resistant strains was allowed by the addition of kanamycin (40μg/ml) to the growth medium. Purification of proteins was carried out as previously described.[108] Thanks to the addition of the His6-tag on the N-term of human pyridoxal kinase, this protein can be purified by immobilized metal affinity chromatography on a nickel-nitrilotriacetic acid (Ni-NTA) column. The column was equilibrated with 50 mM KPi buffer, pH 7.5, and the dialysed protein, after centrifugation at 12000 g for 30 min, was loaded on the column. Before eluting the protein, the column was washed with the equilibrating buffer, containing 150 mM NaCl. The protein was eluted with a linear gradient of imidazole, from 10 to

200mM, in the same buffer, and the fractions were run on SDS-PAGE gel to confirm the presence of the recombinant protein. The collected fractions were dialysed overnight in 100 mM Na-BES buffer, pH 7.3, containing 150 mM NaCl. The protein concentration was measured using a theoretical molar extinction coefficient of 30888 M^{-1} cm^{-1}, calculated with the Expasy PROTPARAM tool, (Switzerland).

2.3.2 Differential Scanning Fluorimetry (DSF) assays

DSF assays were performed on Real Time PCR Instrument (CFX Connect Real Time PCR system, Bio-Rad, Hercules, CA, USA). The experiment was carried out using 2 μM of the protein in 50 mM Na-BES buffer, pH 7.3, containing 150 mM NaCl. The protein was mixed with Sypro Orange (5x, Thermo Scientific, Waltham, MA, USA), using a total volume of 25 μl in a 96-well PCR plate. Fluorescence was measured from 25 °C to 95 °C in 0.4 °C/30 s steps.[118] The excitation fluorescence was set at 450-490 nm and the emission fluorescence was recorded between 560 nm and 580 nm. All samples were run in triplicate. Denaturation profiles were analysed using Graph Pad software (San Diego, CA, USA) after removal of points representing quenching of the fluorescent signal due to post-peak aggregation of protein-dye complexes. All curves were normalised and fitted to sigmoidal equation to obtain the melting temperatures (T_m). Alternatively, the melting temperatures were obtained by plotting the first derivative of the fluorescence emission as a function of temperature (-dF/dT) by using the Bio-Rad CFX manager software (Hercules, CA, USA).

2.3.3 Kinetic studies

Enzyme activity was assayed with PL and ATP (sodium salt) as substrates, using 1 µM enzyme, and were performed in a 1 cm thermostated cuvette in 100 mM Na-BES buffer, pH 7.3, containing 100 mM $MgCl_2$, at 37 °C. The conversion of PL into PLP was followed at 388 nm as previously described,[108] in an Agilent 8454 UV/Vis diode array spectrophotometer (Agilent Technologies, Santa Clara, CA, USA). An extinction coefficient of 4900 $M^{-1}cm^{-1}$ was used to calculate the concentration of the PLP product. Enzyme activity with PN and PM as substrates was measured in a spectrophotometric coupled assay, in which the phosphorylated products generated by PDXK were converted into PLP by *E. coli* PNPOx. The assay was carried out in the same conditions described above, with either 0.1 µM PDXK and 1 µM PNPOx (when using PN) or 0.05 µM PDXK and 5 µM PNPOx (when using PM). For each PDXK variant form, two series of initial velocity measurements were carried out, varying the concentration of one substrate while keeping the concentration of the other fixed and saturating. The obtained saturation curves were fitted to the Michaelis-Menten equation, using the software PRISM (GraphPad, La Jolla, CA, USA), obtaining estimates of the kinetic parameters.

3. Results

Part I

Studies on E. coli PNPOx

3.1 Regulation and PLP binding properties of pyridoxine 5'-phosphate oxidase from *Escherichia coli*

The first part of this work is focused on the regulation and PLP binding properties of pyridoxine 5'-phosphate oxidase (PNPOx) from *E. coli,* that catalyses the last step of the so-called deoxyxylulose 5-phosphate-dependent pathway,[26] and plays a pivotal role in controlling intracellular homeostasis and bioavailability of pyridoxal 5'-phosphate (PLP). PLP product inhibition of PNPOx has been reported[58] and attributed to PLP binding at the active site; however, data supporting this hypothesis have not been presented. Moreover, PLP has been proposed to bind with high affinity also at a secondary tight binding site, spatially distinct from the active site. This tightly bound PLP is protected by the solvent and, thus it is readily transferred to the apo-PLP-dependent enzymes.[54] For these reasons, we decided to perform a complete kinetic characterisation of the wild type PNPOx to better understand the nature of product inhibition and the location of the PLP binding site.

3.1.1 Effect of pyridoxal supplementation on *E. coli* PNPOx knock-out strain

It has been previously reported that an *E. coli* Δ*pdxH* strain (lacking PNPOx) grows slower than the wild type strain on minimal medium supplemented with PL.[63] This is unexpected, since PL should sustain a normal cell growth when it is converted into PLP by the two kinases (PdxK/Y). Another *E. coli* mutant strain was analysed, that lacks the pyridoxine 5'-phosphate synthase and, thus, is unable to synthesize PLP (Δ*pdxJ*). The growth rates of wild type and mutant *E. coli* strains (Δ*pdxJ* and Δ*pdxH*) were measured in minimal M9

medium. The Δ*pdxJ* strain grew very slowly, whereas the Δ*pdxH* strain did not grow at all. In M9 medium supplemented with PN (100 μM) or PL (100 μM), the Δ*pdxJ* strain recovered the wild type phenotype **(Fig. 3.1)**. On the other hand, the Δ*pdxH* strain did not grow in M9 supplemented with PN **(Fig. 3.1 A)**, whereas, if PL was added to the medium, the mutant strain slowly grew; however, the growth curve was substantially different from that of the wild type strain **(Fig. 3.1 B)**.

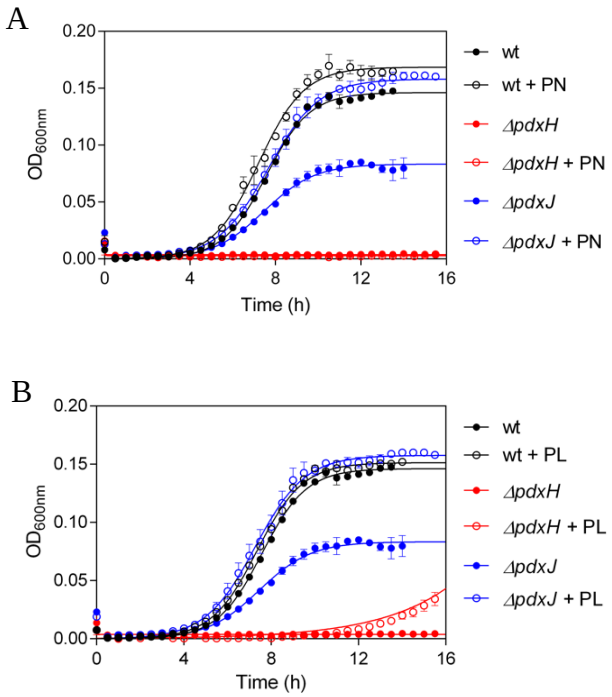

Figure 3.1 *Growth curves of wild type and mutant E. coli strains in minimal M9 medium.* **A)** Growth curves in M9 supplemented with 100 μM pyridoxine (PN) and **B)** with 100 μM pyridoxal (PL). Reported values are the mean ± standard error of three independent measurements.

These results suggest that PNPOx has a cellular function that goes beyond its catalytic role. This function may actually be related to its capability to bind PLP at the secondary tight binding site.

3.1.2 Kinetic studies on the wild type enzyme

Kinetics of pyridoxal 5'-phosphate formation from pyridoxine 5'-phosphate

PNPOx is able to use both PNP and PMP as substrates; however, the *E. coli* enzyme, contrarily to its mammalian counterpart that shows similar catalytic efficiency with both substrates,[34] oxidises PNP with a catalytic efficiency that, at pH 7.6 (which is the internal pH of *E. coli* cells[123]), is about 50-fold higher.[58] The PNP oxidation catalysed by *E.coli* PNPOx is the last step of PLP *de novo* biosynthesis. In our experiments, we used PNP as substrate, while oxygen concentration corresponded to that present in aqueous solutions exposed to air, thus it was approximately 7 mg/L (0.2 mM). Since K_M for O_2 is around the same value,[124] we expect *E. coli* PNPOx to be half-saturated by O_2 in our reaction conditions. The catalytic activity of PNPOx is usually measured in TRIS buffer to avoid accumulation of PLP in the solvent and the consequent product inhibition,[125] since PLP forms a Schiff base with TRIS and is sequestered from solvent. When PNPOx activity measurements were carried out in a different buffer (50 mM Na-HEPES pH 7.6), in which free PLP is allowed to accumulate in the solvent, we observed complex kinetics that could not be explained by a simple competitive product inhibition. In HEPES buffer, after mixing substrate and enzyme, a deceleration phase in which the initial velocity of the reaction decreases was observed. This is followed by a slow and constant rate of PLP formation **(Fig. 3.2)**. This behaviour is evident from the first derivative of the kinetic trace, showing

that the reaction rate decreases exponentially with a half-time of about 40 s **(Fig. 3.2, inset)**. In contrast, in TRIS buffer, the reaction rate decreased almost linearly with time. The entire time course of PLP formation observed in TRIS buffer could be fitted to a closed form of the time-integrated Michaelis-Menten equation,[126] showing that the substrate depletion causes the decrease of the reaction rate.

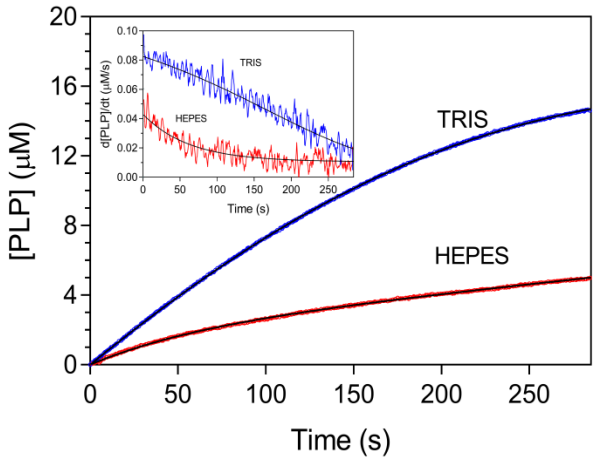

Figure 3.2 *Kinetics of PNP oxidation to PLP in TRIS and HEPES buffers*. Comparison of kinetics obtained with 0.5 μM enzyme (protein subunit concentration) and 15 μM PNP, carried out in 50 mM TRIS-HCl and 50 mM Na-HEPES buffers at pH 7.6. The kinetics trace obtained in TRIS buffer was fitted to a closed form of the time-integrated Michaelis-Menten equation,[126] while the time course of the reaction carried out in HEPES buffer was fitted to **Eq. 1** (continuous black lines through the experimental traces). The inset shows the first derivative of experimental and theoretical traces.

The fitting procedure of the kinetics obtained in HEPES buffer failed. In this case, the time course of the reaction may be described as an exponential process followed by a linear phase, and data were fitted to an empirical equation describing this behaviour **(Eq. 1)**, where the α_E term is the

amplitude of the exponential phase, and the k_E and the k_L terms are the rate constants of the exponential process and the linear phase, respectively.

$$y = \alpha_E(1 - e^{-k_E t}) + k_L t \qquad \textbf{(Eq.1)}$$

To estimate the PLP concentration formed in the initial deceleration phase, different substrate concentrations were used **(Fig. 3.3 A).** This analysis showed that the amplitude of the exponential phase increases hyperbolically with substrate, reaching a maximum value of 1.7 ± 0.2 μM **(Fig. 3.3 A, inset)**. This concentration of PLP is definitely higher with respect to the enzyme concentration used in the experiments (0.5 μM). On the other hand, when the enzyme concentration was varied at fixed and saturating substrate concentration (15 μM), the amount of PLP produced in the exponential process increased proportionally **(Fig. 3.3 B, inset)**.

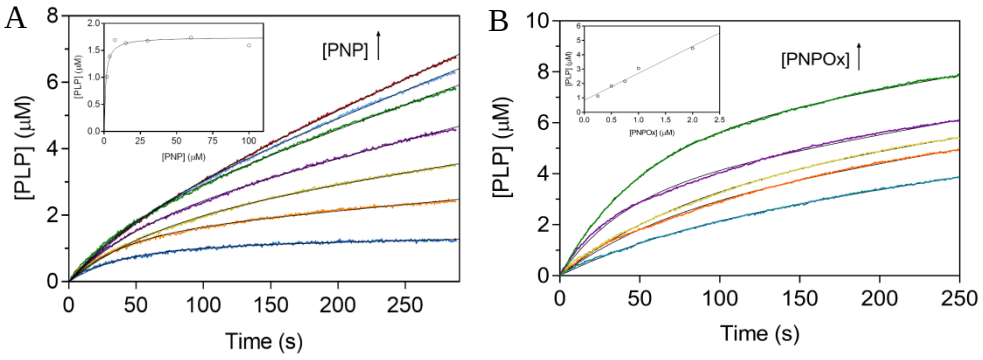

Figure 3.3 *Analysis of reactions catalysed by PNPOx in HEPES buffer*. **A)** A fixed concentration of enzyme (0.5 μM) was mixed with buffer containing different PNP concentrations (1.88, 3.75, 7.5, 15, 30, 60 and 100 μM). Starting reactions by the addition of substrate as last component yielded identical kinetics. All kinetics were fitted to **Eq. 1** (see materials and methods for details). The inset shows the concentration of PLP formed in the deceleration phase as a function of substrate concentration. **B)** Increasing enzyme concentration (0.25, 0.5, 0.75, 1 and 2 μM), while keeping PNP concentration fixed (15 μM),

proportionally increased the amount of PLP produced in the deceleration phase, as shown in the inset and determined from fitting of kinetics to **Eq. 1**.

The initial velocity of the reactions obtained at different PNP concentrations was measured by linear fitting of the first 25 s of the kinetic traces. **Figure 3.4** shows the saturation behaviour of the initial velocity. Because of the low turnover number of the reaction catalysed by PNPOx (about 0.3 s^{-1}),[62] a relatively high enzyme concentration (0.5 μM) was used with respect to substrate, which was varied between 1.9 and 100 μM. These conditions are not compatible with classical Michaelis-Menten kinetics, in which the enzyme concentration is much lower than substrate concentration. Therefore, the initial rate was analysed as a function of PNP concentration using a quadratic equation **(Eq. 2)**, which accounts for the decrease of free substrate concentration due to the formation of the enzyme-substrate complex.

$$v_i = \frac{[PNP] + E_0 + K_D - \sqrt{-(K_D + [PNP] + E_0)^2 + 4\,([PNP] + K_D) - 4\,E_0\,[PNP]}}{2\,E_0}\,V_{MAX}$$

(Eq. 2)

Kinetic parameters obtained from the analysis were k_{cat} = 0.28 ± 0.01 s^{-1} and K_D = 1.6 ± 0.4 μM. These observations indicate that during turnover a species is produced which slows down the velocity of the reaction, and must arise from the accumulation of PLP in solution.

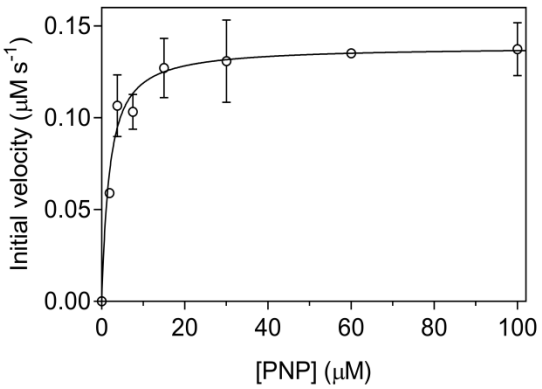

Figure 3.4 *Analysis of initial velocity of the reaction in HEPES buffer*. The saturation curve obtained by plotting the initial velocity of the reaction as a function of substrate concentration was analysed using quadratic **Eq. 2**, obtaining the kinetic parameters reported in the text. Error bars correspond to s.e.m. of the initial velocity values estimated as explained in the text.

In order to analyse the effect of PLP on reaction kinetics, increasing concentrations of exogenous PLP were added to the reaction mixture, while enzyme and substrate concentrations were maintained constant. Interestingly, PLP has the effect to progressively reduce the amplitude of the deceleration phase **(Fig. 3.5)**; above 4 μM PLP concentration, the deceleration phase is not visible.

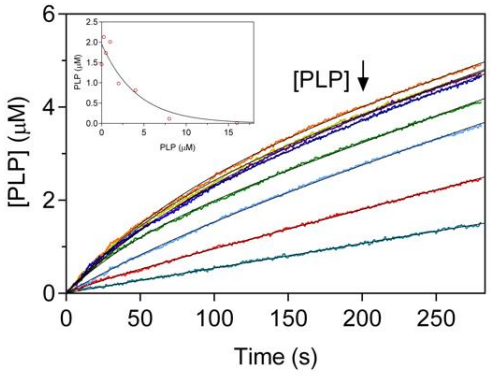

Figure 3.5 *Effect of PLP on reaction kinetics*. Kinetics obtained by the addition of increasing concentrations of exogenous PLP (0, 0.25, 0.5, 1, 2, 4, 8 and 16 μM) to reactions containing 0.5 μM enzyme and 15 μM PNP.

These observations demonstrate that the deceleration observed in HEPES buffer is a consequence of PLP accumulation in the solvent and of its binding to PNPOx. When PMP was used as substrate in HEPES buffer, the rate of PLP formation was extremely slow, making difficult the observation of the deceleration phase, if present. With *E. coli* PNPOx in TRIS buffer, other authors observed PNP substrate inhibition,[58] which we could not detect even at very high PNP concentration (up to 1 mM; **Fig. 3.6**). This difference may be attributed to the higher pH (8.5) used in the previous experiments.

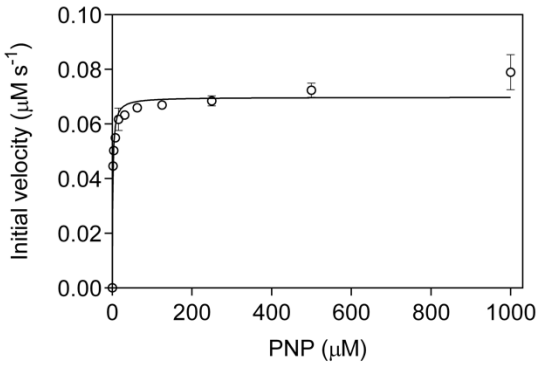

Figure 3.6 *Dependence of the initial velocity of the reaction on PNP concentration in TRIS buffer*. The saturation curve obtained by plotting the initial velocity of the reaction as a function of substrate concentration was analysed using quadratic **Eq. 2**. Error bars correspond to s.e.m. of the initial velocity values. It is clear that, even at very high PNP concentration, no substrate inhibition is observed.

Mechanism of PLP product inhibition

The deceleration phase observed in PNP oxidation kinetics results from PLP inhibition, however, it is not compatible with a competitive product inhibition. Previously, the inhibition by PLP had been reported in sheep brain and *E.coli* PNPOx, with an apparent inhibition constant of 2 μM [59] and 8 μM[58], respectively. In both cases, a competitive product inhibition has been proposed in which PLP binds at the active site. In order to clarify the mechanism of PLP inhibition, a complete inhibition kinetic characterisation was carried out in HEPES buffer. Progress time curves obtained at different PNP and PLP concentrations were analysed to measure the initial velocity of the reaction, and under all conditions the initial velocities showed a saturation behaviour **(Fig. 3.7 A)**. Analysis of saturation curves, obtained at increasing

PLP concentration, using the quadratic **Eq. 2** shows that PLP affects both apparent k_{cat} and K_D **(Fig. 3.7 B)**.

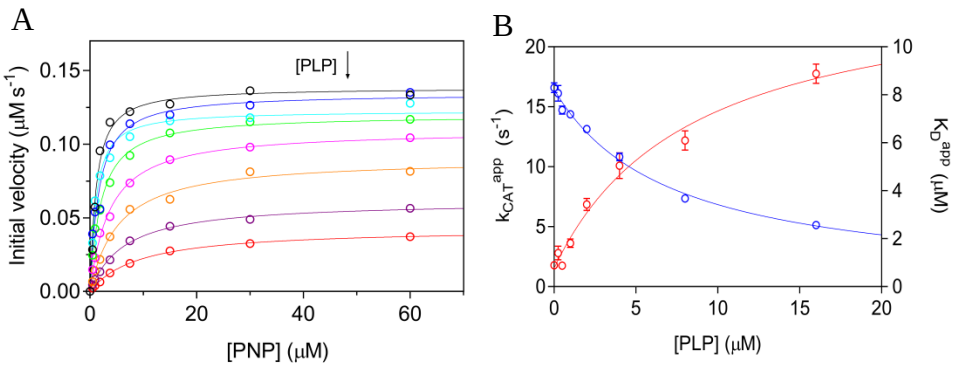

Figure 3.7 *Characterisation of PLP inhibition*. **A)** The initial velocity of the reaction was measured with 0.5 μM enzyme (protein subunit concentration), varying PNP concentration while keeping exogenous PLP fixed and at different concentrations (0, 0.25, 0.5, 1, 2, 4, 8 and 16 μM). The resulting saturation curves were fitted to **Eq. 2**, obtaining estimates of apparent k_{cat} and K_D. **B)** Fitting of apparent k_{cat} (blue symbols) and K_D (red symbols) as a function of PLP concentration, using **Eqs. 3, 4 and 5** gave estimates of dissociation and inhibition constants. Error bars correspond to s.e.m. of parameter values.

This behaviour is indicative of a mixed-type inhibition **(Scheme 1 A)**, in which the inhibitor (PLP in this case) binds to both free and substrate-bound enzymes. The apparent k_{cat} and K_D constants depend hyperbolically on PLP concentration as shown in **Fig 3.7 B.** Fitting of data in **Figure 3.7 B** to the equations reported below allows the estimation of all dissociation and inhibition constants (K_D, K_{Dp}, K_I and K_{Is}), reported in **Table 1** (for details, see description of **Eqs. 3, 4 and 5** in the materials and methods section).

$$k_{CAT}^{app} = \frac{K_{Is}}{K_{Is}+[PLP]} k_{CAT} \qquad \textbf{(Eq. 3)}$$

$$K_D^{app} = \frac{K_D\, K_{Is} + K_{Dp}[PLP]}{K_{Is} + [PLP]} \qquad \textbf{(Eq. 4)}$$

$$K_I = \frac{K_D\, K_{Is}}{K_{Dp}} \qquad \textbf{(Eq. 5)}$$

The two inhibition constants (K_I and K_{Is}) were obtained for binding of PLP to the free and the substrate-bound enzymes, respectively. The k_{CAT} is the catalytic constant of the enzyme. The dissociation constants K_D and K_{Dp} represent the substrate dissociation rate, observed for the free or the PLP product-bound enzymes, respectively. All constants are shown in **Scheme 1A**.

A

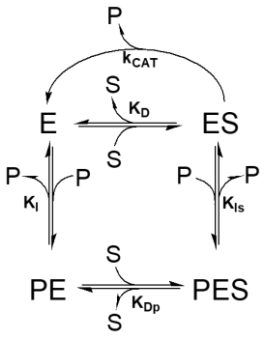

B

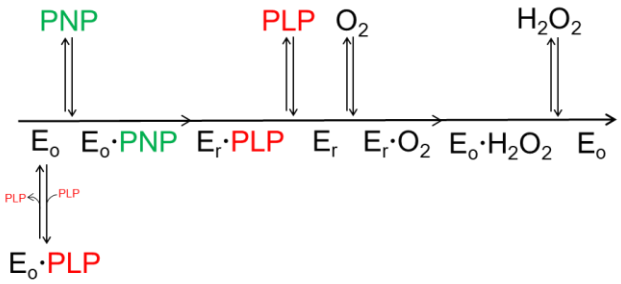

Scheme 1 A) Steady-state kinetics scheme of a mixed-type inhibition system in which the enzyme (E) is able to bind both the PNP substrate (S) and the PLP product (P) at the same time. Only the ES species is catalytically active and able to convert the substrate into the product **B)** Ping-pong kinetic mechanism of the reaction catalysed by PNPOx, in which E_o

and E_r are the oxidized and the reduced forms of the enzyme, respectively. E_o is also able to bind PLP, forming a dead-end product.

A double reciprocal plot of initial velocity data confirms the mixed-type inhibition by PLP **(Fig. 3.8 A)**. According to the previous analysis secondary plots of K_D /V_{max} and 1/V_{max} as a function of PLP concentration **(Fig. 3.8 B, C)** gives inhibition constants of 0.59 ± 0.07 μM and 7.13 ± 0.52 μM for PLP binding to free and substrate-bound enzyme, respectively. The value of k_{cat} in the absence of PLP (0.27 ± 0.01 s^{-1}) is also similar to that estimated for the first deceleration phase from fitting of initial velocities **(Table 1)**.

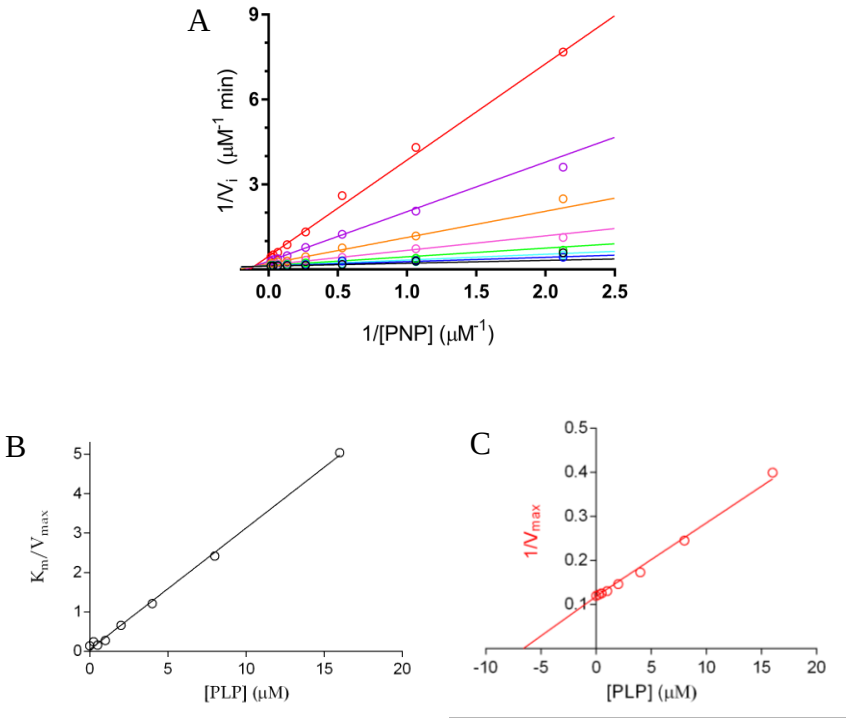

Figure 3.8 *Characterisation of PLP inhibition*. **A)** Plot of the reciprocals initial velocities ($1/V_i$) on the concentration of the substrate (1/[PNP]) and **B, C)** the secondary plot of $1/V_{max}$ and K_D/V_{max} as a function of PLP concentration confirm the mixed-type inhibition by PLP.

	Parameter	Wild type
Kinetics of PNP oxidation	[a]k_{cat} (s^{-1})	0.3[(62)]
	[a]K_D (μM)	2[(62)]
	[b]k_{cat} (s^{-1})	0.28 ± 0.01
	[b]K_D (μM)	1.6 ± 0.4
Inhibition kinetics	[c]k_{cat} (s^{-1})	0.27 ± 0.01
	[c]K_D (μM)	0.90 ±0.55
	[c]K_{Dp} (μM)	12.85 ±1.68
	[c]K_I (μM)	0.59 ± 0.07
	[c]K_{Is} (μM)	7.13 ± 0.52

Table 1 *Parameters obtained from kinetic measurements on wild type E. coli PNPOx*. [a]Determined in TRIS buffer. [b]Determined in HEPES buffer from fitting of initial velocity. [c]Determined from PLP inhibition kinetics.

Stopped-flow kinetics

The PNPOx-PLP binding reaction was also studied by stopped-flow spectroscopy to estimate the kinetic on- and off-rate constants **(Fig. 3.9)** and took advantage of the increase in FMN fluorescence observed upon addition of different PLP concentrations to an enzyme solution. In these experiments, 20 μM PNPOx (protein subunit concentration) was mixed in the stopped-flow apparatus with increasing PLP concentrations (from 2 to 34 μM before mixing), at 25 °C. All kinetic traces were biphasic with a fast phase

characterised by increasing fluorescence and a slow phase with decreasing fluorescence intensity **(Fig. 3.9 A)**. The observed time courses were fitted to **Eq. 6** and are consistent with a two-step mechanism shown in **Scheme 2**, in which a second-order reaction determining an increase of fluorescence is followed by a first-order process converting the enzyme-PLP complex to a E-PLP* species with decreased fluorescence. In the **Eq. 6** reported below, the α's and k's are the amplitudes and observed rate constants, respectively, of the fast (F) and slow (S) phases, and α_B term is the equilibrium baseline fluorescence. k_F term is given by **Eq. 7** (reported below), which describes the dependence of the observed rate constant on PLP concentration, k_{ON} and k_{OFF} are the second order binding and first order dissociation rate constants, respectively. The ω parameter measures the deviation of the system from pseudo-first order conditions[120] (for more details see materials and methods section).

$$y = \alpha_F \frac{1-e^{-k_F t}}{1+\omega\, e^{-k_F t}} + \alpha_S\, e^{-k_S t} + \alpha_B \qquad \textbf{(Eq. 6)}$$

$$k_F = \sqrt{k_{ON}^2(E_0 - [PLP])^2 + k_{OFF}^2 + 2k_{ON}^2 k_{OFF}^2(E_0 + [PLP])} \qquad \textbf{(Eq. 7)}$$

$$\text{E + PLP} \underset{k_{OFF}}{\overset{k_{ON}}{\rightleftharpoons}} \text{E-PLP} \underset{k_{-C}}{\overset{k_C}{\rightleftharpoons}} \text{E-PLP*}$$

Scheme 2 *Kinetic mechanism of PLP binding to PNPOx*.

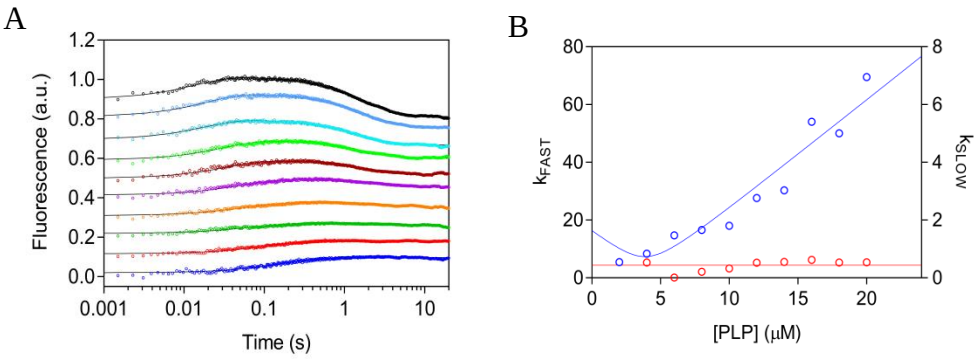

Figure 3.9 *PLP binding measured by stopped-flow spectroscopy*. 20 μM PNPOx was 1:1 mixed in the stopped-flow apparatus with PLP (8, 12, 16, 20, 24, 28, 32, 36 and 40 μM) in Na-HEPES buffer at 25 °C. **A)** For a better view, the time courses of the reactions were separated on the Y-axes by adding an increasing value and are shown on a log(time) scale. Traces were fitted to **Eq. 6** (solid lines). **B)** Dependence of k_{FAST} (blue symbols) and k_{SLOW} (red symbols) on PLP concentration; k_{FAST} was fitted to **Eq. 7** and k_{SLOW} to a line with slope = 0 (solid lines).

Consistently, the fast phase depended on PLP concentration, whereas the slow phase was independent of PLP concentration **(Fig. 3.9 B)**. Fitting of data to **Eq. 7** yielded the following parameters: k_{ON} = 11.35 ± 1.27 μM^{-1} s^{-1}; k_{OFF} = 3.24 ± 2.24 s^{-1}, and thus a dissociation constant k_{OFF} / k_{ON} = 0.28 ± 0.19 μM, which in **Scheme 1 A** is referred to as K_I, and represents binding of PLP to free enzyme. Since the slow phase was clearly independent of PLP concentration with an average value of k_{SLOW} = 0.73 ± 0.12 s^{-1}, this phase may be related to a process taking place within the PNPOx-PLP complex. Given that the absorption spectrum of the PNPOx-PLP complex excludes the formation of a Schiff base (based on the absence of the characteristic 420 nm peak[54]), it may be proposed that the slow phase is due to a rearrangement of

PLP within the PNPOx binding pocket or to a protein conformational change which affects the FMN microenvironment.

3.1.3 Analysis of PLP binding equilibrium

PLP binding to PNPOx was characterised using spectrofluorimetric measurements and taking advantage of the increase in FMN fluorescence observed upon addition of PLP to an enzyme solution **(Fig. 3.10)**. Emission spectra (from 470 nm to 570 nm) in the presence of different PLP concentrations were measured at 25 °C, in 50 mM Na-HEPES buffer pH 7.6, upon excitation at 450 nm. The average relative fluorescence emission between 520 nm and 530 nm as a function of total PLP concentration was analysed with the **Eq. 8**, using the protein subunit concentration as fixed parameter.

$$F_{rel} = F_0 + \left(F_{inf} - F_0\right) \times \frac{[P_0]+[E_0]+K_I-\sqrt{-(K_I+[P_0]+[E_0])^2+4\,([P_0]+K_I)-4\,[E_0\,][P_0]}}{2\,E_0}$$

(Eq. 8)

Interestingly, the K_D of the wild type enzyme (0.15 ± 0.04 μM) is comparable to the K_I for PLP binding to the free enzyme determined by inhibition kinetics and rapid kinetics measurements, and is referred to as K_I in **Scheme 1 A**. Moreover, the titration of more concentrated wild type PNPOx solutions (1, 2 and 4 μM) with PLP, using the same fluorimetric method, allowed determination of the stoichiometry of PLP binding to the enzyme, which, in contrast with previous observations,[54] was of one PLP molecule per PNPOx dimer **(Fig. 3.10, inset)**.

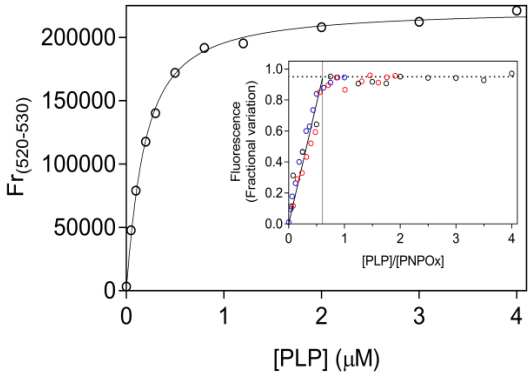

Figure 3.10 *Analysis of PLP binding equilibrium of the wild type PNPOx.* The figure shows the PLP binding curve obtained with 100 nM PNPOx (protein subunit concentration). The inset shows the binding stoichiometry analysis obtained with three different and much higher protein subunit concentrations (1 μM, black symbols; 2 μM, red symbols; and 4 μM, blue symbols). Fluorescence change, expressed as fractional variation as a function of the $[PLP_{tot}]$/[protein] ratio, is linear as shown by the thick continuous line, up to the stoichiometry point corresponding to the crossing with the horizontal dotted line. The vertical thin line through the stoichiometry point indicates that about one PLP molecule binds per enzyme dimer.

3.1.4 Retention of PLP by PNPOx and activity of the PLP-PNPOx complex

It is known by previous experiments that *E. coli* PNPOx binds PLP so tightly that, when incubated with it and then passed through a desalting column, it retains PLP with a 1:1 ratio (100% with respect to protein subunits), and maintains 85% catalytic activity.[54] We have repeated this experiment with wild type PNPOx. The enzyme at 100 μM concentration was incubated with an equimolar amount of PLP and then passed through a size exclusion chromatography column (Superdex 200 10/300 GL column) using an FPLC system, obtaining a good separation between unbound PLP and protein. The

stoichiometric binding of PLP to the protein was calculated using a coupled assay with the apo-*E. coli* serine hydroxymethyltransferase (apo-SHMT), as previously described.[54] The experiment was carried out in triplicate and the stoichiometric binding of PLP with respect to the protein subunit was estimated to be approximately 66 ± 26 %. Furthermore, the catalytic activity of the wild type PNPOx-PLP complex, obtained from chromatography, was measured. When the kinetics of PLP formation, using a final enzyme concentration of 0.5 µM, were performed in HEPES buffer, we could not observe any difference in the obtained kinetics, as reported in previous experiments carried out in TRIS buffer.[54] Also a control enzyme sample that was not incubated with PLP was analysed. However, with 8 µM enzyme, kinetic profiles were very different: the PNPOx-PLP complex gave slower kinetics that lacked the first deceleration phase **(Fig. 3.11)**.

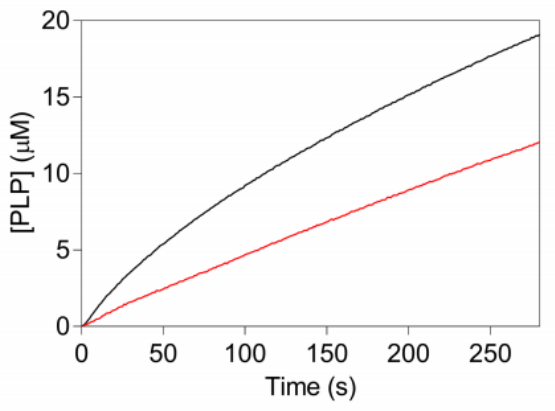

Figure 3.11 *Kinetics of PNP oxidation to PLP in HEPES buffer catalysed by wild type PNPOx with tightly bound PLP*. Reactions were carried out as explained in **Fig. 3.2** and started by diluting enzyme samples, either the PNPOx-PLP complex obtained after incubation with PLP and size exclusion chromatography (red trace) or an untreated control sample (black trace) in 50 mM Na-HEPES buffer pH 7.6 containing PNP, obtaining 8 µM enzyme and 240 µM substrate final concentration.

3.2 Location of the PLP binding site

From the kinetic characterisation of the wild type PNPOx, it has been demonstrated that enzyme inhibition occurs with the binding of PLP at an allosteric site. The inhibition constant of the enzyme, in absence of PNP substrate, obtained from kinetic experiments suggest that the allosteric site is a binding site with higher affinity for PLP than the active site, as also confirmed by the equilibrium measurements and rapid equilibrium kinetics. Thus, in order to identify where the allosteric site is located, several mutant forms of PNPOx were produced, expressed and purified. Then, all mutant enzymes were characterised with respect to their ability to bind PLP.

3.2.1 Characterisation of the potential PLP binding site identified through crystallographic studies

In literature, it is already known that PLP binds at a secondary high affinity binding site both in *E. coli* and in human enzyme.[34,54] In *E. coli*, crystallographic data suggest a location of this PLP binding site on the protein surface, however, the actual involvement of the residues, identified to interact with PLP in this crystal structure, has not yet been confirmed experimentally. Crystallographic data suggested three amino acid residues as responsible for PLP binding at the tight binding site[56] **(Fig. 1.7)**: Asn84, Lys145 and Phe177. On the basis of this information, a double (K145A/F177A) and two triple (N84A/K145A/F177A and N84W/K145A/F177A) mutants were produced, purified and characterised, to verify the actual involvement of these residues in PLP binding.

Differential scanning fluorimetry analysis

In order to check whether the introduced mutations alter the overall stability of PNPOx, differential scanning fluorimetry (DSF) measurements were carried out. DSF can be a useful and rapid method to characterise proteins, and also to identify potential protein ligands. In this method, proteins are incubated with a fluorescent dye, which alters its fluorescence upon binding to the hydrophobic regions of the proteins.[118] Sypro Orange (Thermo Scientific) was used as fluorescent dye. After incubation, the protein-dye sample was heated, and the fluorescence monitored as the heat rises (see materials and method). The unfolding of the protein, and exposure of hydrophobic parts of the protein, gives rise to a characteristic pattern in the fluorescence as a function of temperature.[118] All *E. coli* PNPOx mutant forms (2 μM) were analysed in 50 mM Na-HEPES buffer, pH 7.6, containing 150 mM NaCl,. All curves were normalised and fitted to the Boltzmann equation to obtain the melting temperatures (T_m). All PNPOx mutants of the crystallographic site showed a lower T_m than the wild type enzyme (53.1 ± 0.3 °C), thus resulting less stable **(Fig. 3.12)**. Values of T_m obtained for the K145A/F177A, N84A/K145A/F177A and N84W/K145A/F177A are the following: 48.5 ± 0.2 °C, 47.2 ± 0.1 °C and 47.8 ± 0.1 °C, respectively.

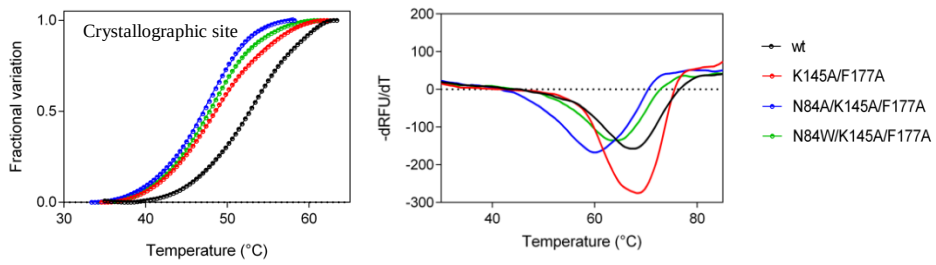

Figure 3.12 *Differential scanning fluorimetry measurements on crystallographic site mutants of E. coli PNPOx.* The fluorescence change is illustrated in the figures on the left,

and is expressed as fractional variation as a function of temperature. Graphs on the right show the first derivative of fluorescence emission (–dRFU/dT) as a function of temperature. Thermal denaturation data were fitted to the Boltzmann equation to obtain the melting temperatures,[118] reported in the text. The curves are the result of three independent experiments but, to better understand the data, the standard error bars were not reported in the graph.

Kinetic studies on crystallographic site mutants of PNPOx

Catalytic activity measurements of crystallographic site mutant forms of *E. coli* PNPOx were carried out in 50 mM TRIS-HCl buffer, pH 7.6, at 37 °C, and the formation of the characteristic TRIS-PLP aldimine product was followed at 414 nm, with a molar extinction coefficient of 4253 cm^{-1} M^{-1}. Kinetic constant measurements were obtained with a fixed concentration of the enzyme (typically, 0.5 μM) and increasing substrate (PNP) concentrations (from 1.9 to 100 μM). Although the crystallographic site mutants are less stable than the wild type **(Fig. 3.12)**, their catalytic properties remain fairly unaltered, as shown in **Table 2**. Data were analysed using the **Eq. 2** (see materials and method), and both the K_M and the k_{cat} obtained from fitting are similar to the kinetic parameters of the wild type PNPOx **(Table 1)**.

	Enzyme form	**K_M (μM)**	**k_{cat} (s^{-1})**
Crystallographic site	K145A/F177A	2.4 ± 0.4	0.12 ± 0.1
	N84A/K145A/F177A	2.7 ± 0.5	0.03 ± 0.01
	N84W/K145A/F177A	3.3 ± 0.4	0.07 ± 0.01

Table 2 Kinetic *parameters obtained from kinetics of PNP oxidation in crystallographic site mutants of E. coli PNPOx.*

Analysis of FMN and PLP binding equilibria

Dissociation constants for FMN binding to wild type and crystallographic mutants of PNPOx were analysed by FMN fluorescence quenching observed upon binding of the cofactor to the apo-enzyme,[100] under excitation at 450 nm. Emission spectra were recorded from 470 nm to 570 nm, with excitation and emission slits set at 2 nm and 4 nm, respectively. Fluorescence emission values between 520 nm and 530 nm were averaged and analysed according to a modified version of **Eq. 8**, in which F_{rel} is the measured relative fluorescence, F_0 is fluorescence in the absence of apo-PNPOx, F_{inf} is fluorescence at infinite apo-PNPOx concentration (for details see materials and methods). The experiments were performed in 50 mM Na-HEPES buffer, pH 7.6, at 25 °C, using a fixed amount of FMN (50 nM) and increasing concentrations of the apo-enzyme (from 30 nM to 1000 nM) **(Fig. 3.13)**. The dissociation constant values, obtained for all the crystallographic PNPOx mutants were similar to that of the wild type enzyme, as shown in **Table 3**. Only the triple mutant of PNPOx in which Asn84 is replaced with a tryptophan residue shows a K_D for FMN slightly higher with respect to the other enzyme forms, this may be due to the steric effect derived from the replacement of an asparagine with a tryptophan residue.

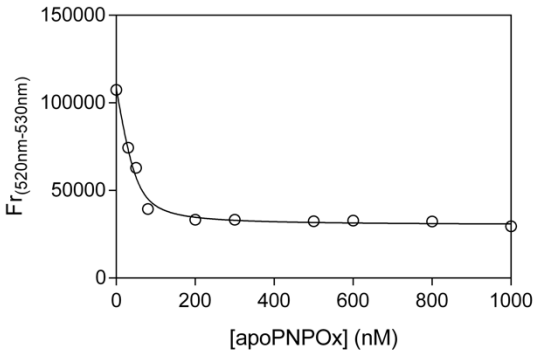

Figure 3.13 *Analysis of FMN binding properties of the wild type PNPOx.* The figure shows the FMN binding curve obtained with 50 nM FMN and increasing protein subunit concentrations (30, 50, 80, 160, 200, 300, 500, 600, 800, 1000 nM). Fluorescence emission values between 520 nm and 530 nm were averaged and analysed according to a modified version of the **Eq. 8.** Similar curves were obtained with all mutant forms.

Furthermore, PLP binding to PNPOx mutant forms was characterised using a spectrofluorimetric method and taking the advantage of the increase in FMN fluorescence upon addition of PLP (from 0.1 to 6 μM) to an enzyme solution (100 nM, protein subunit concentration). Fluorescence emission spectra were recorded from 470 nm and 570 nm upon excitation at 450 nm. Excitation and emission slits were set at 3 nm and 5 nm, respectively. Emission fluorescence values between 520 nm and 530 nm were averaged and fitted to **Eq. 8**. For all mutant forms, saturation curves similar to that shown for wild type PNPOx **(Fig. 3.10)** were obtained. The estimated dissociation constants are reported in **Table 3**. All the crystallographic site mutants of *E. coli* PNPOx are still able to bind PLP, as shown by similar K_D values.

	Enzyme form	K_D^{FMN} (nM)	K_D^{PLP} (μM)
	Wild type	10.6 ± 0.9	0.15 ± 0.04
Crystallographic site	K145A/F177A	11.5 ± 3.6	0.47 ± 0.06
	N84A/K145A/F177A	15.9 ± 2.9	0.36 ± 0.05
	N84W/K145A/F177A	24.6 ± 0.5	0.33 ± 0.07

Table 3 *Parameters obtained from equilibrium measurements on crystallographic site mutants of E. coli PNPOx.* The reported data are the mean ± the standard error of three independent experiments.

Retention of PLP by crystallographic site mutants of E. coli PNPOx

All the crystallographic site mutants (100 μM) were incubated with an equimolar amount of PLP, as described above for the wild type enzyme. Then, the proteins were passed through a size exclusion chromatography column and the stoichiometry binding of PLP to the PNPOx mutants was evaluated from the activity of the reconstituted holo-SHMT (see materials and methods for details). The percentage of PLP estimated for K145A/F177A, N84A/K145A/F177A and N84W/K145A/F177A PNPOx mutants are the following: 68 ± 9; 70 ± 11; 79 ± 12, respectively. The stoichiometry binding of PLP is quite similar to that of the wild type enzyme (66 ± 26, PLP %), thus further confirming that the crystallographic site is not the allosteric binding site of PLP.

3.2.2 Characterisation of *E. coli* PNPOx mutants identified through molecular docking

Thanks to our collaboration with professor Stefano Pascarella (Department of Biochemical Sciences "A. Rossi Fanelli", Sapienza Università di Roma), docking experiments were carried out that indicated a possible alternative binding site. This is a cleft on the protein surface that is mainly delimited by arginine residues and is located at the subunit interface **(Fig. 3.14)**.

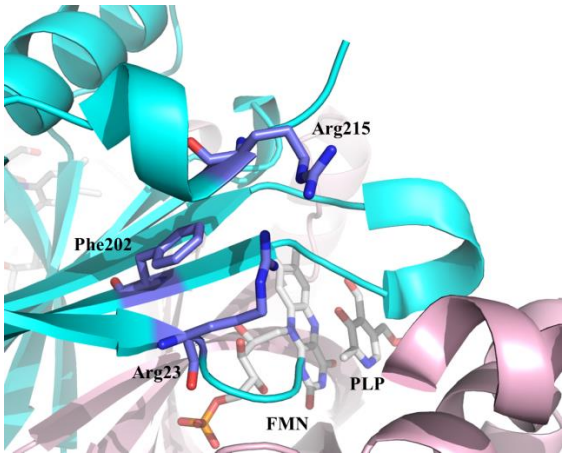

Figure 3.14 *Dimeric structure of E. coli PNPOx showing the molecular docking site*. PLP and FMN are shown as sticks in atom-based colours. The amino acid residues identified through molecular docking experiments are shown as sticks in blue and labelled. The two enzyme subunits are shown in cyan and pink, respectively.

The degree of conservation of this surface area across γ-proteobacteria suggests its functional importance. In contrast, the binding site indicated by crystallographic data shows a very poor evolutionary conservation. Thus, the single mutant forms (R23L, R215L, F202M) and also the double R23L/R215L PNPOx mutant were produced through site-directed mutagenesis. All mutant forms of *E. coli* PNPOx were purified and

characterised with respect to their catalytic activity and capability to bind PLP.

Thermal denaturation and kinetic studies on molecular docking site mutants of PNPOx

The three single (R23L, R215L and F202M) and the double (R23L/R215L) mutants of *E. coli* PNPOx were produced, expressed and purified. First of all, all these mutant forms were analysed with respect to their structural stability and their catalytic properties. Data obtained from differential scanning fluorimetry analysis showed that R23L/R215L and F202M PNPOx mutants are less stable than the other enzyme forms, displaying a lower melting temperature value (46.3 ± 0.5 °C and 44.7 ± 0.3 °C, respectively) **(Fig. 3.15)**. Instead, the other two single mutants, R23L and R215L, show T_m values of 53.6 ± 0.4 °C and 53.1 ± 0.2 °C, respectively; and those are quite similar to that of wild type PNPOx (53.1 ± 0.3 °C) **(Fig. 3.15)**. The instability of the double mutants could be due to the position of the amino acid residues at the interface between the two subunits of the dimer.

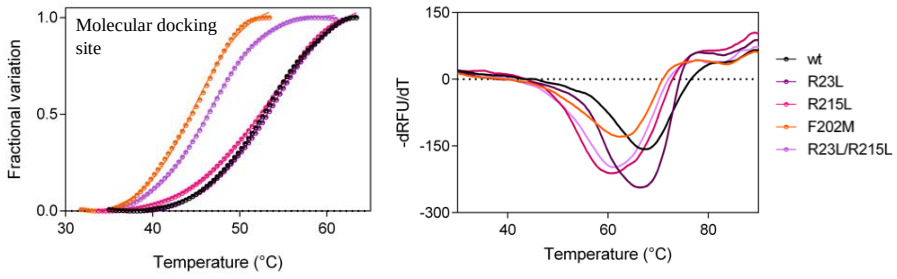

Figure 3.15 *Differential scanning fluorimetry of molecular docking site mutants of E. coli PNPOx.* The fluorescence change is illustrated in the figures on the left, and is expressed as fractional variation as a function of temperature. Graphs on the right show the first derivative

(–dRFU/dT) as a function of temperature. Thermal denaturation data were fitted to the Boltzmann equation to obtain the melting temperatures,[118] reported in the text. The curves are the result of three independent experiments but, to better understand the data, the standard error bars were not reported in the graph.

Then, enzymatic assays of molecular docking site mutants of PNPOx were carried out in 50 mM TRIS-HCl buffer, pH 7.6, at 37 °C. The progress of the reaction was followed at 414 nm, as explained before for the crystallographic site mutants. Initial velocities were determined over the first 40 s of the reaction. The values of K_M and k_{cat} obtained by fitting to **Eq. 2** are shown in **Table 4**. Both kinetic parameters are not altered by mutations in the molecular docking site, in fact the values obtained are comparable to those of the wild type **(Table 1)**.

	Enzyme form	**K_M (μM)**	**k_{cat} (s^{-1})**
Molecular docking site	R23L	1.3 ± 0.1	0.07 ± 0.01
	R215L	2.3 ± 0.9	0.07 ± 0.03
	R23L/R215L	3.9 ± 0.6	0.08 ± 0.03
	F202M	3.6 ± 0.4	0.14 ± 0.04

Table 4 *Parameters obtained from the kinetics of PNP oxidation in molecular docking site mutants of E. coli PNPOx.*

Analysis of PLP binding equilibrium and retention

To verify whether the site identified by molecular docking may be the secondary PLP binding site, the PNPOx mutant forms were analysed with respect to their ability to bind PLP. As previously described for both wild

type and crystallographic site mutants, the binding of PLP to the enzyme was characterised using a spectrofluorimetric method. Data were analysed according to the quadratic **Eq. 8** and the resulting dissociation constants are reported in **Table 5**. Interestingly, the values of the dissociation constant are 10-fold higher with respect to the wild type, thus suggesting that the replacement of the arginine and phenylalanine residues with leucine and methionine residues, respectively, impairs the binding of PLP. Furthermore, when these mutant forms of PNPOx were incubated with PLP and passed through a desalting column, a much lower percentage of PLP with respect to what observed with wild type PNPOx was retained **(Table 5)**. Thus, this molecular docking binding site appears to be a good candidate as secondary PLP binding site; however, further studies are needed to better clarify if this is actually the site of interest.

	Enzyme form	**K_D^{PLP} (μM)**	**% PLP**
	Wild type	0.15 ± 0.04	66 ± 26
Molecular docking site	R23L	1.4 ± 0.05	37 ± 16
	R215L	1.1 ± 0.04	32 ± 15
	R23L/R215L	1.6 ± 0.1	30 ± 16
	F202M	0.84 ± 0.04	35 ± 9

Table 5 *Parameters obtained from PLP binding equilibrium analysis and retention measurements on molecular docking site mutants of E. coli PNPOx.*

3.2.3 Analysis of PLP binding in active site mutants of *E. coli* PNPOx

Although, as explained above, from our kinetic experiments it is clear that PLP can bind at an allosteric site with greater affinity than at the active site, we wanted to make sure that the PLP binding observed by fluorimetric measurements takes place at the allosteric site. Therefore, we decided to produce and analyse PNPOx mutants whose ability to bind PLP at the active site is impaired. Thus, a quadruple mutant (K72I/Y129F/R133L/H199A) was produced, in which four crucial amino acid residues involved in the electrostatic binding of the substrate phosphate[38] were replaced by hydrophobic residues **(Fig. 3.16)**. Moreover, another active site single mutant was produced, in which His199 residues was replaced with an alanine residue. This residue is found in the flexible turn of the second monomer **(Fig. 3.16)**. The His199 may contribute to the stabilization of the transition state by its interaction with PNP, in fact it acts on PLP sandwiching the pyridine moiety onto the isoalloxazine ring while catalysis takes place.[38]

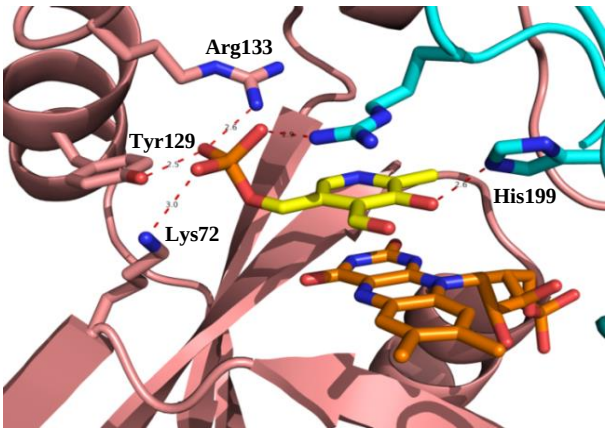

Figure 3.16 *Enlarged view of PNPOx active site structure.* Cartoon backbone representation of the *E. coli* PNPOx dimer (PDB code: IG79) with PLP bound at the active site. The two subunits are shown in cyan and pink, respectively. Active site residues involved in binding of PLP are shown as sticks and labelled. Interatomic distances indicated by red dashes are

expressed in Ångstrom. It can be assumed that the PNP substrate binds establishing the same interactions with active site amino acid residues.[38]

Studies of stability and catalytic activity on active site mutants of E. coli PNPOx

The single (H199A) and the quadruple (K72I/Y129F/R133L/H199A) mutants were produced by site-directed mutagenesis and then, expressed and purified as described in materials and methods. The thermal stability of these mutants was evaluated through the differential scanning fluorimetry, using 2 µM enzyme in 50 mM Na-HEPES buffer at pH 7.6, containing 150 mM NaCl **(Fig. 3.17)**. Data were fitted to the Boltzmann equation and the resulting T_m were the following: 49.8 ± 0.3 °C and 47.5 ± 0.1 °C for H199A and the quadruple mutant, respectively. These estimated values demonstrate that the active site mutant forms of PNPOx, as expected, are less stable than the wild type (T_m = 53.1 ± 0.3 °C).

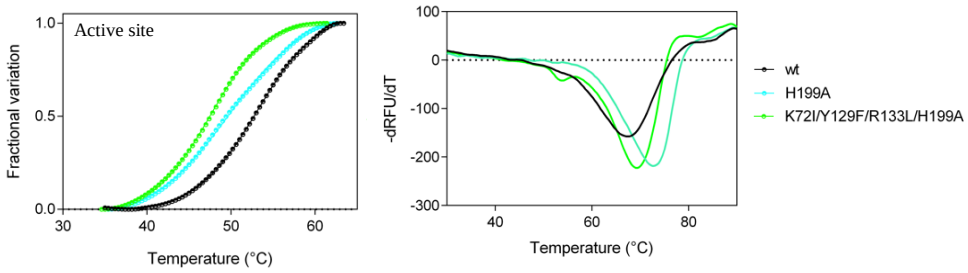

Figure 3.17 *Differential scanning fluorimetry of active site mutants of E. coli PNPOx.* Graphs on the left show fluorescence change expressed as fractional variation as a function of temperature. The first derivative (–dRFU/dT) is illustrated in the figures on the right as a function of temperature. Thermal denaturation data were fitted to the Boltzmann equation to obtain the melting temperatures, listed in the text. The curves are the result of three independent experiments but, to better show the data, the standard error bars were not reported in the graph.

Concerning the catalytic properties of the active site mutants of PNPOx, the quadruple mutant enzyme has a very small residual activity that allowed determination of kinetic parameters, which are respectively 560-fold lower (k_{cat} = $5.3 \cdot 10^{-4} \pm 0.7 \cdot 10^{-4}$ s^{-1}) and 120-fold higher (K_M = 238 ± 77 μM) than those of wild type PNPOx.[38] Di Salvo and collaborators[38] performed the catalytic characterisation of H199A PNPOx mutant, that displays a greatly decreased affinity for PNP substrate (K_M = 70 ± 5.0 μM), while the k_{cat} (0.14 ± 0.01 s^{-1}) is comparable to that of the wild type.[38]

Binding of PLP at the active site

To verify if PLP binding observed by fluorimetric measurements with PNPOx takes place at the active site or at a secondary allosteric site, also the wild type apo-enzyme was analysed. Both PNP and PLP bind at the active site of PNPOx making stacking interactions with the FMN cofactor.[56] Elimination of FMN is expected to affect PLP binding at the active site. The intrinsic fluorescence of apo-PNPOx, deprived of its FMN cofactor, was measured at increasing PLP concentrations. Emission fluorescence between 335 nm and 345 nm was averaged and fitted to a modified version of **Eq. 8**. A decrease of fluorescence was observed, which allowed determination of a dissociation constant (corresponding to K_I) of 0.28 ± 0.01 μM **(Fig. 3.18 A, black symbols)**, which is not very different from that obtained with the holo-form of the enzyme. Fluorimetric measurements of the H199A mutant demonstrate that this mutant is still capable to bind PLP with a K_D of about 0.89 ± 0.04 μM. As previously described the quadruple PNPOx mutant (K72I/Y129F/R133L/H199A) has a very reduced capacity to use PNP as

substrate, however it is still able to bind PLP, as demonstrated by fluorimetric measurements **(Fig. 3.18 A, red symbols)**, with a dissociation constant (0.45 ± 0.02 μM) that is comparable to that of the wild type enzyme. Differently from the wild type enzyme, titration of concentrated solutions of the quadruple mutant enzyme with PLP gave a binding stoichiometry of two PLP molecule per enzyme dimer **(Fig. 3.18 B)**. This suggests that a significant change of the active site could alter the stoichiometry of PLP binding at the allosteric site.

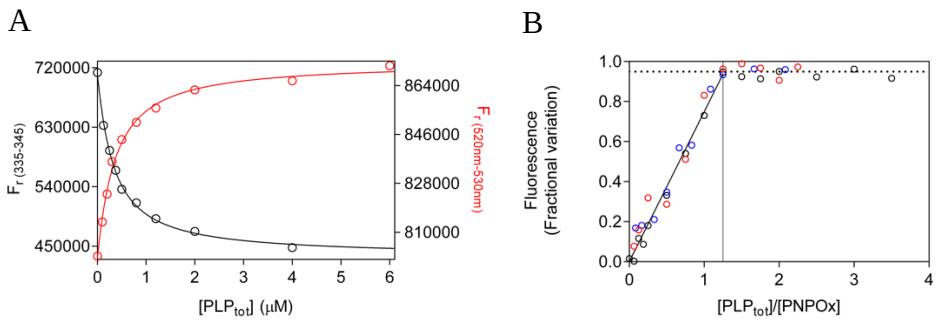

Figure 3.18 *PLP binding to enzyme forms with altered active site structure*. **A)** Fluorometric analysis of PLP binding to apo-PNPOx (100 nM) was carried out exciting at 280 nm. The average fluorescence emission between 335 and 345 nm was plotted against PLP concentration (black symbols). PLP binding to the holo-form of the quadruple mutant (red symbols) was analysed as previously described for wild type PNPOx. Both sets of data were fitted using the quadratic **Eq. 8**, obtaining K_D values listed in the text. **B)** Titration of more concentrated PNPOx quadruple mutant solutions (4 μM, black symbols; 8 μM, red symbols; and 12 μM, blue symbols; protein subunit concentrations). Fluorescence change was expressed as a function of the [PLP_{tot}]/[protein] ratio, as above mentioned for the wild type PNPOx **(Fig. 3.10)**. The vertical thin line through the stoichiometry point indicates that about two PLP molecules bind per enzyme dimer.

Analysis of PLP retention by the active site mutant forms of PNPOx showed that the amount of PLP which remains in complex with the protein is lower when comparing the mutants (PLP percentage equal to 29 ± 13 for H199A and 37 ± 9 for the quadruple mutant) with the wild type enzyme (66 ± 26, PLP %). This result is consistent with the higher dissociation constants found with the mutants and confirms that the tight PLP binding at PNPOx does not involve the active site.

Furthermore, PLP binding to the quadruple PNPOx mutant was also analysed in the presence of increasing concentrations of PNP, in order to check if the two vitamers compete to bind to the enzyme. The competition experiments in which K_D for PLP binding was fluorimetrically determined at different fixed PNP concentrations (0.1, 0.5, 1, 2 , 3, 4, 6 μM) clearly indicate that PNP and PLP do not compete for binding at the same site **(Fig. 3.19),** thus further confirming that the active site is not the site that binds PLP with high affinity.

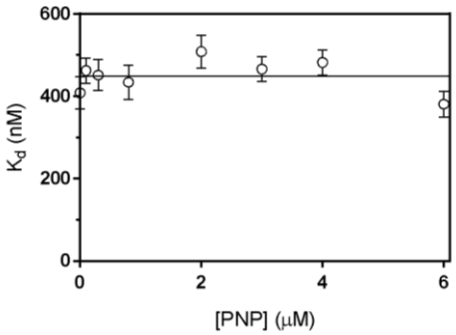

Figure 3.19 *Competition binding experiments*. PLP binding to PNPOx quadruple mutant was analysed at different fixed PNP concentrations, using the same fluorimetric method. A series of saturation curves were obtained from which K_D for PLP at different PNP concentrations was determined using **Eq. 8**. The continuous line through the experimental points results from the least square fitting of data to a linear equation with slope 0, which returned for K_D a value of 0.45 ± 0.01 μM, in agreement with the K_D value determined in the absence of PNP (0.45 ± 0.02 μM).

Part II

Studies on human PNPOx

3.3 Allosteric regulation of human PNPOx

The second part of this work focused on the characterisation of human PNPOx and some mutant forms found in patients with neonatal epileptic encephalopathy (NEE). First of all, we tested the human enzyme to determine if a secondary, allosteric PLP binding site was present. In previous studies, it has been reported that the human PNPOx, as also described for the *E. coli* enzyme,[54] can bind PLP at a tight binding site.[34] Moreover, the human enzyme is inhibited by PLP with an apparent inhibition constant of 3.2 μM.[34] The ability to retain PLP in a tight binding site can be related to the transfer of this vitamer to the apo-forms of vitamin B_6-dependent enzymes, as previously demonstrated by the formation of physical complex between human PNPOx and vitamin B_6 enzymes.[39] Considering all these observations, a possible allosteric site, as found in *E. coli,* could be present in the human PNPOx; and thus the same experiments carried out with the *E. coli* enzyme were performed with the wild type form of human PNPOx.

3.3.1 Kinetic studies of the wild type human PNPOx

Allosteric feedback inhibition

As previously described for the *E. coli* enzyme, the reaction catalysed by the wild type human PNPOx was analysed both in Na-HEPES and TRIS-HCl buffers. Also for the human enzyme a first deceleration phase, in which the initial velocity of the reaction decreases, was observed when the assay was performed in HEPES buffer. After approximately 40 s of the reaction, a decrease in the rate of PLP formation was observed **(Fig. 3.20)**. Instead, in

TRIS buffer, the first deceleration phase disappears. Data were fitted to **Eq. 1**, as mentioned above for *E. coli* PNPOx.

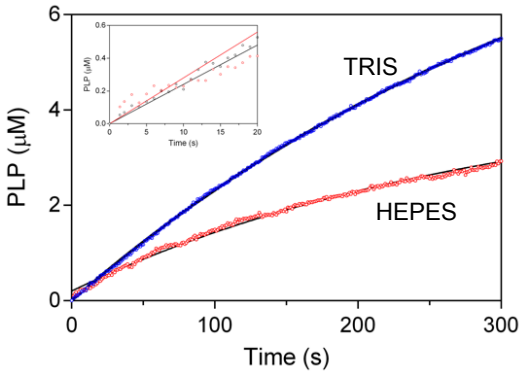

Figure 3.20 *Kinetics of PNP oxidation to PLP in TRIS and HEPES buffers catalysed by human PNPOx*. Comparison of kinetics obtained with 0.5 μM enzyme (protein subunit concentration) and 15 μM PNP, carried out in 50 mM TRIS-HCl and 50 mM Na-HEPES buffers at pH 7.6. The kinetic trace obtained in HEPES buffer was analysed as previously mentioned for the *E. coli* PNPOx (compare to **Fig. 3.2**). The inset shows the enlargement of the first 20 s of the reactions.

The time course of the reaction in the presence of increasing PNP substrate concentrations shows an exponential process, followed by a linear phase **(Fig. 3.21 A)**. Data were fitted to **Eq. 1** (as explained for the *E. coli* enzyme). In addition, as the PNP substrate concentration raises, a hyperbolic increase of the initial velocity of the reaction was observed, as shown in the inset of **Figure 3.21 A**.

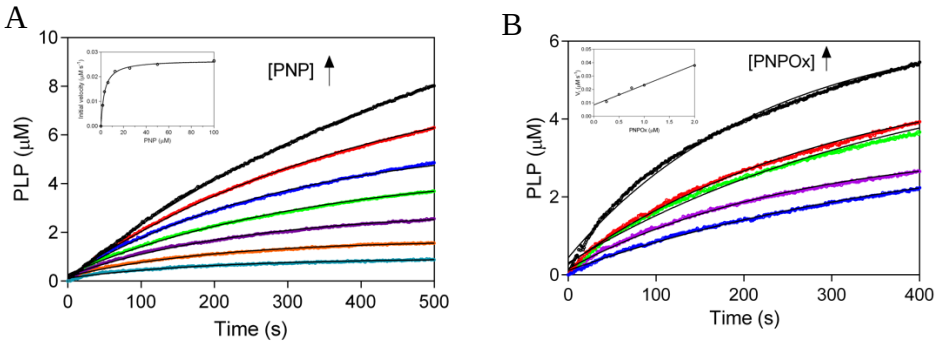

Figure 3.21 *Analysis of reactions catalysed by PNPOx in HEPES buffer*. **A)** A fixed concentration of enzyme (0.5 µM) was mixed with buffer containing different PNP concentrations (1.56, 3.13, 6.25, 12.5, 25, 50 and 100 µM). The inset shows that the initial velocity of the reaction hyperbolically increases, as the substrate concentration raises. All kinetic traces were fitted to **Eq. 1** (for details see materials and methods). **B)** Increasing enzyme concentration (0.25, 0.5, 0.75, 1 and 2 µM), while keeping PNP concentration fixed (15 µM), proportionally increased the initial velocity of the reaction, as shown in the inset and determined from fitting of kinetics to **Eq. 1.**

Furthermore, when the experiment was performed with a fixed amount of substrate (15 µM) and increasing enzyme concentrations (from 0.25 to 2 µM) **(Fig. 3.21 B)**, the amplitude of the first phase grows proportionally with respect to the enzyme concentration **(Fig. 3.21 B, inset).**

Then, to estimate the kinetic parameters of the wild type PNPOx, the catalytic measurements were carried out in TRIS-HCl buffer pH 7.6, at 37 °C. Since a high enzyme concentration (2 µM) was used, the saturation curve obtained varying the PNP substrate concentration, was fitted to the quadratic **Eq. 2**, instead of the Michaelis –Menten equation **(Fig. 3.22)**. The initial velocity was analysed fitting the first 40 s of the reaction. The values of the kinetic parameters, similar to those reported in the literature,[34,92] are the following: $K_D = 1.48 \pm 0.26$ µM and $k_{cat} = 0.06 \pm 0.01$ s^{-1}.

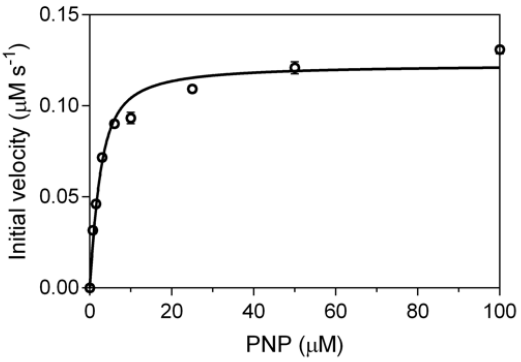

Figure 3.22 *Analysis of initial velocity of the reaction in TRIS buffer*. The saturation curve obtained by plotting the initial velocity of the reaction as a function of substrate concentration was analysed using quadratic **Eq. 2**, obtaining the kinetic parameters listed in the text. The reported data are the mean ± standard error of three independent measurements.

To check if increasing amount of PLP produced by PNPOx could influence the time course of the reaction, the same experiment, shown in **Figure 3.21**, was performed using different exogenous PLP concentrations (from 0.17 to 16 μM), 0.5 μM PNPOx (protein subunit concentration) and 15 μM PNP **(Fig. 3.23).** In this case, as the PLP amount increased, the first deceleration phase of the reaction disappeared, as displayed in the inset of **Figure 3.23.**

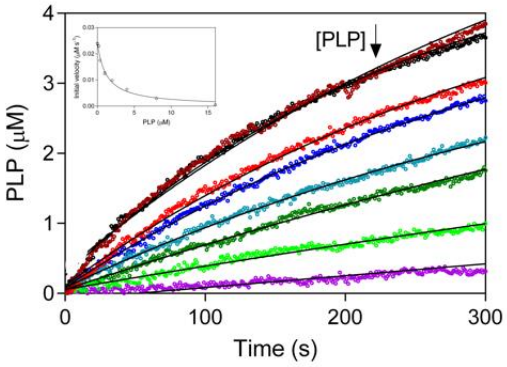

Figure 3.23 *Effect of PLP on reaction kinetics in HEPES buffer*. Kinetics obtained by the addition of increasing concentrations of exogenous PLP (0, 0.17, 0.35, 1, 2, 4, 8 and 16 μM) to reactions containing 0.5 μM enzyme and 15 μM PNP.

As for the *E. coli* PNPOx, a competitive PLP product inhibition was previously proposed for the human enzyme, with an apparent K_I equal to 3.2 μM.[34] However, a complete inhibition kinetics characterisation with human PNPOx has not been performed yet. Thus, the inhibition kinetic experiments were carried out in HEPES buffer, using the same conditions described above for the *E. coli* enzyme in **Figure 3.7**. Different concentrations of PNP substrate and exogenous PLP were included in the reaction mixture, using 2 μM enzyme **(Fig. 3.24 A).** Also in this case, analysing the obtained saturation curves, mixed-type inhibition properties were observed, since the PLP concentration influences both V_{max} and K_D **(Fig. 3.24 B).**

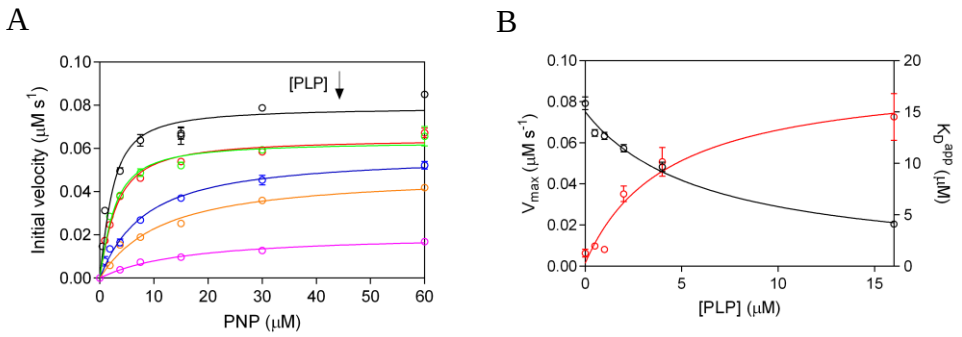

Figure 3.24 *Characterization of PLP inhibition*. **A)** The initial velocity of the reaction was measured with 2 µM enzyme (protein subunit concentration), varying PNP concentration while keeping exogenous PLP fixed and at different concentrations (0, 0.5, 1, 2, 4 and 16 µM). The resulting saturation curves were fitted to **Eq. 2. B)** Fitting of V_{max} (black symbols) and K_D (red symbols), using **Eqs. 3, 4 and 5** gave estimates of dissociation constants. The estimated K_D is 0.7 ± 0.4 µM, when PLP is absent. At infinite PLP concentration, the K_{Dp} is estimated to be 17.0 ± 1.5 µM. Error bars correspond to s.e.m. of parameter values.

The mixed-type inhibition behaviour was also confirmed by a double reciprocal plot of initial velocity data **(Fig. 3.25 A).** Moreover, the secondary plot of K_D/V_{max} and $1/V_{max}$ as a function of PLP concentration **(Fig. 3.25 B)** gave the following inhibition constants, K_I = 0.73 ± 0.02 µM and K_{Is} = 3.53 ± 0.3 µM. These constants, as shown in **Scheme 1A**, refer to PLP binding to free and substrate-bound enzymes, respectively.

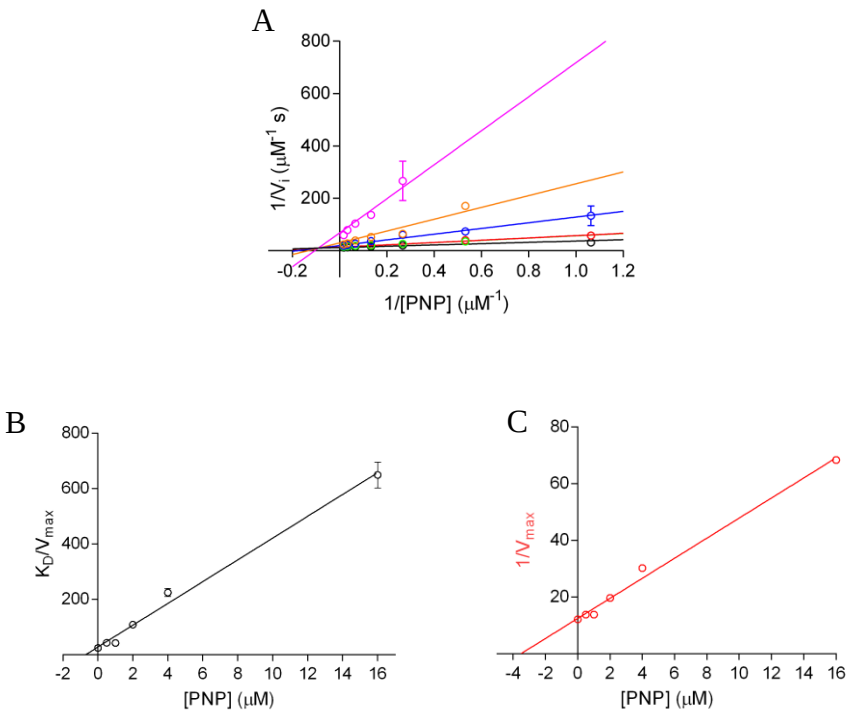

Figure 3.25 *Characterisation of PLP inhibition*. **A)** Plot of the reciprocals initial velocities ($1/V_i$) as a function of the concentration of the substrate (1/ [PNP]) and the secondary plot of **B)** K_D/V_{max} and **C)** $1/V_{max}$ as a function of PLP concentration allowed determination of K_I and K_{Is}.

Analysis of the PLP binding equilibrium using different fluorimetric methods

Fluorimetric measurements were carried out to analyse the ability of the human enzyme to bind PLP. The experiment takes advantage of changes in FMN microenvironment as a consequence of PLP binding. The experiments were performed mixing 100 nM enzyme with increasing PLP concentrations (from 30 to 4000 nM), in 50 mM Na-HEPES buffer pH 7.6, at 25 °C. The analysis of data using the quadratic **Eq. 8** allowed to estimate the dissociation

constants. Concerning the wild type PNPOx, the K_D for PLP obtained is about 0.95 ± 0.02 µM **(Fig. 3.26 A)**, which is comparable to the K_I for PLP binding to free enzyme determined by inhibition kinetics. Then, a more concentrated PNPOx solution (2 µM) was titrated with PLP and the stoichiometry of PLP binding was found to be of two molecules per PNPOx dimer **(Fig. 3.26 B)**. Even if for the PNPOx of *E. coli* the presence of two allosteric sites for the PLP is not excluded, in the human form of the enzyme the binding of the PLP at one of the two sites does not alter the affinity for the second site.

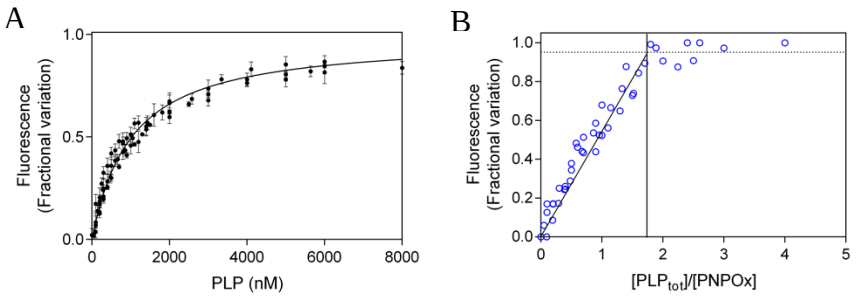

Figure 3.26 *Analysis of PLP binding equilibrium of the wild type PNPOx.* **A)** The figure shows the PLP binding curve obtained with 100 nM PNPOx (protein subunit concentration). Reported data are from five independent experiments. Data were fitted to **Eq. 8**. **B)** Binding stoichiometry analysis obtained with 2 µM protein subunit concentration (blue symbols). Fluorescence change, expressed as fractional variation as a function of the $[PLP_{tot}]$/[protein] ratio, is linear as shown by the thick continuous line, up to the stoichiometry point corresponding to the crossing with the horizontal dotted line. The vertical thin line through the stoichiometry point indicates that about two PLP molecules bind per enzyme dimer.

Subsequently, also the differential scanning fluorimetry was used to study the binding of PLP to the wild type human PNPOx. When the PNPOx (2 µM)

was heated in presence of different PLP concentrations (from 0.78 to 50 µM) the melting temperature increased **(Fig. 3.27).** The melting temperatures, resulting from fitting of data to the Boltzmann equation, were plotted as a function of PLP concentration. The observed saturation curve **(Fig. 3.27 C)** was analysed using the quadratic **Eq. 8** and gave a dissociation constant of 4.22 ± 0.25 µM.

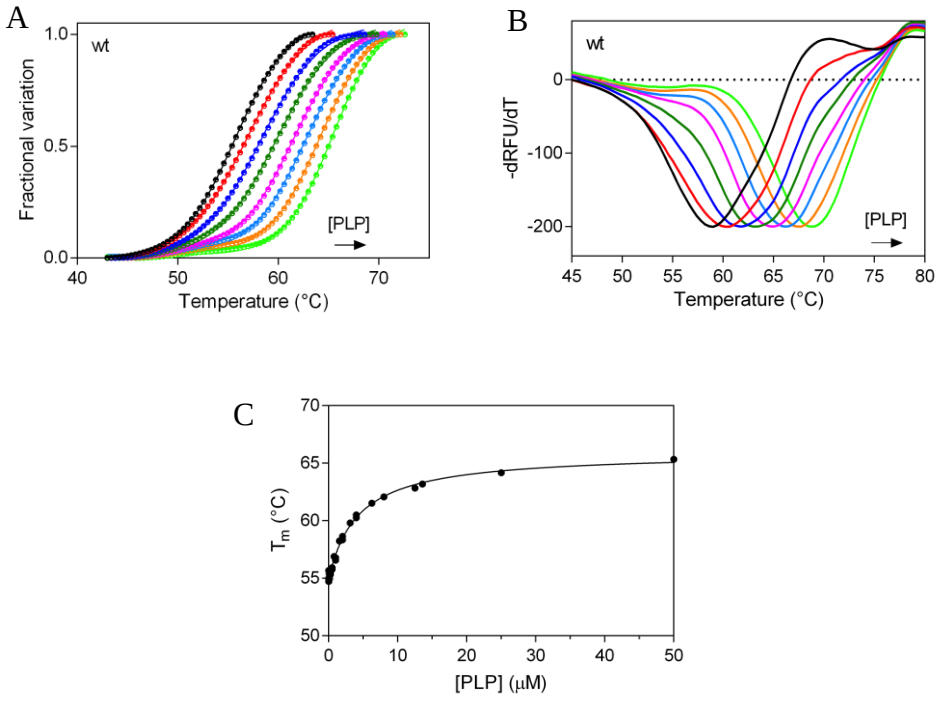

Figure 3.27 *Differential scanning fluorimetry of human wild type PNPOx in presence of different PLP concentrations.* **A)** The fluorescence change is expressed as fractional variation as a function of temperature. **B)** Graphs show first derivative (–dRFU/dT) as a function of temperature. The experiment was carried out using 2 µM enzyme and different PLP concentrations (0, 0.78, 1.56, 3.13, 6.25, 12.5, 25 and 50 µM). Thermal denaturation data were fitted to the Boltzmann equation to obtain the melting temperatures,[118] reported in graph C. The curves are the result of three independent experiments but, to easily show the data, the standard error bars were not reported in the graph. **C)** Saturation curve is obtained

plotting the melting temperatures as a function of the PLP concentrations. Data were analysed using the quadratic **Eq. 8** to estimate the dissociation constant reported in the text.

Interestingly, the K_D observed for the wild type human PNPOx indicates the binding of PLP at the active site, which is not seen with differential scanning fluorimetry assay in the *E. coli* enzyme. Then, using these two fluorimetric methods we were able to estimate a dissociation constant for each of the two binding sites for PLP, the allosteric site and the active site.

3.4 Different mutations in human PNPOx are related to the neonatal epileptic encephalopathy (NEE)

PNPOx deficiency was originally reported as a severe life-threatening neonatal encephalopathy responsive to pyridoxal-5′-phosphate (PLP) but not to pyridoxine (PN).[88] This part of the work aims to characterise the human PNPOx mutant forms most frequently found in patients affected by NEE. The known mutations of human PNPOx were analysed to check if these may influence the structure, stability and function of the enzyme, thus favoring the onset of the disease.

3.4.1 Identified mutations in human PNPOx show different outcomes

Many mutations are reported in the literature, some of which have already been characterised. The mutations found in affected children are listed in **Table 6**, where the response of patients to the treatments used and the outcome of the disease are also reported. The most frequent mutation,

R225H, was found in 10 patients, each of whom showed different phenotypic effects, from the mild[91,127] to the severe ones[70,91] in one case this mutation was not compatible with life.[91] Given the high number of patients with mutations at the R225 position, the R225H, the R225C[128] and the double mutant R116Q/R225H PNPOx were characterised. Among all known mutations, two exhibiting a mild effect, G118R[102] and R141C, were also chosen for characterisation. The latter was found in one patient who also had a deletion of three amino acid residues (Ala94_Leu97del).[91] Finally, another mutation which is characterised by the replacement of the stop codon with a glutamine residue (X262Q), was analysed. This mutation leads to the formation of a longer protein (28 amino acid are added at the C-terminal end) and the death of the patients.[88]

PNPOx mutation	**Response to PN**	**Response to PLP**	**n. of affected patients**	**Outcome**
G118R[(102)]	+	+	1	Mild
R141C[(91)]	+	Not used	1	Mild
R225H[(70, 91,127)]	+	Not used	10	6 mild 3 severe 1 death
R225C[(128)]	-	+	1	Mild
R116Q/R225H[(910, 91)]	+ (-) in 1 patient	Seizures	4	3 severe 1 death
X262Q[(88)]	-	Not used	2	Death

Table 6 *Summary of the characterised mutations of human PNPOx.* For each PNPOx mutation is reported the number of affected patients to date, the outcome of the disease, and the response to the treatment with pyridoxine (PN) or pyridoxal 5'-phosphate (PLP), that has been observed to be null (-) or positive (+). In the case of the double mutant R116Q/R225H, the treatment with PLP results in seizures.

3.4.2 Characterisation of human PNPOx mutants

Differential scanning fluorimetry analysis

All the PNPOx variants described above were constructed through site-direct mutagenesis, expressed and purified, as explained in materials and methods. All proteins were analysed using differential scanning fluorimetry **(Fig. 3.28)**, to verify if the mutations affect the stability of the protein, thus altering the function of the enzyme and contributing to the onset of the disease. The R225H mutation is the most frequent among those reported in the literature,[70,91,127] while for R225C, only one case has been described.[128] This two human PNPOx mutants are more stable than wild type PNPOx (T_m = 58 ± 0.1), in fact they show melting temperatures equal to 62.3 ± 0.1 (R225H) and 67.6 ± 1.2 (R225C). Furthermore, the already characterised R116Q mutation[91,92] was also analysed to compare it with the double R116Q/R225H PNPOx mutant. Concerning the R116Q mutant, the T_m is lower than wild type and, interestingly, this lower stability is also found in the double mutant R116Q/R225H **(Table 7)**.

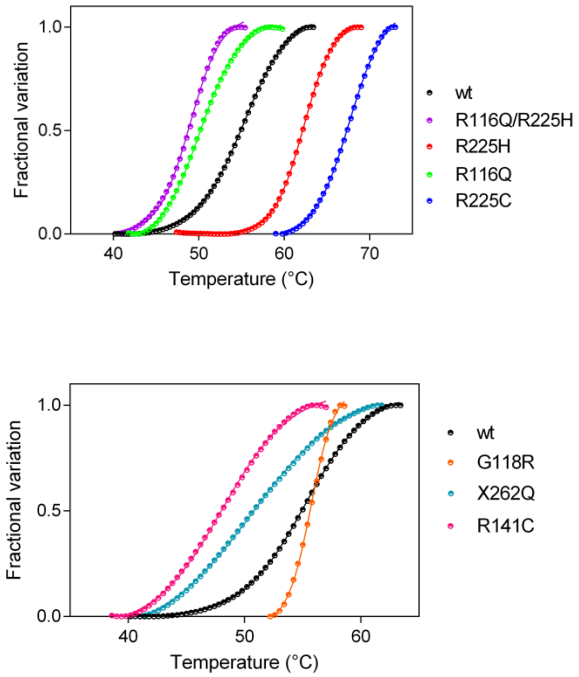

Figure 3.28 *Differential scanning fluorimetry of human PNPOx.* Fluorescence change, expressed as fractional variation as a function of temperature. Data were fitted to the Boltzmann equation to obtain the melting temperatures,[118] reported in **Table 7**. The curves are the result of three independent experiments but, to easily show the data, the standard error bars were not reported in the graph.

Among all mutations, only G118R has a T_m similar to that of the wild type enzyme, while the other two mutants, R141C and X262Q, are less stable (as displayed in **Figure 3.28** and **Table 7**).

Enzyme form	T_m (°C)
Wild type	58 ± 0.1
G118R	55.7 ± 2.9
R141C	48.1 ± 0.3
R225C	67.6 ± 1.2
R225H	62.3 ± 0.1
R116Q	50.1 ± 0.1
R116Q/R225H	51.1 ± 0.2
X262Q	50.6 ± 0.6

Table 7 *Melting temperatures of wild type and mutant forms of human PNPOx*. The values of the melting temperatures were obtained from fitting to the Boltzmann equation.

Kinetic studies on human PNPOx mutants

To precisely understand how the pathogenic mutations G118R, R141C, R225C, R225H, R225H/R116Q and X262Q affect enzymatic activity, kinetic measurements of the mutant PNPOx forms, as for the wild type, were carried out by following the formation of the aldimine complex between PLP and TRIS, which maximally absorbs at 414 nm, using 50 mM TRIS-HCl buffer pH 7.6, at 37 °C. As shown in **Figure 3.29** not all PNPOx mutants, once purified, are completely in the holo-form, thus, the FMN concentration was used to calculate the k_{cat} of the mutants, in order to compare the values obtained for the various enzymes.

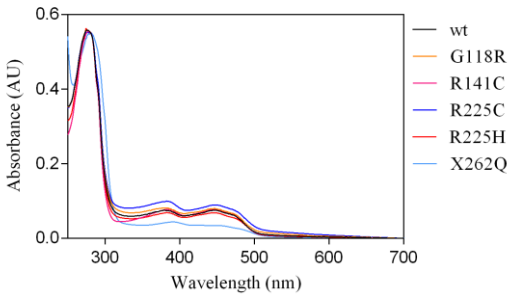

Figure 3.29 *Absorption spectra of wild type and mutants of human PNPOx*. All enzymes exhibit absorption maxima at 280 nm, 385 nm and 445 nm. These last two peaks are those typical of the flavinmononucleotide (FMN).

The K_M and k_{cat} values resulting from the kinetic measurements of both wild type and mutants are listed in **Table 8**. All mutations increased K_M values; this result could be due to the location of all mutated residues near or at the active site. The G118R mutant shows a greatly decreased affinity for substrate PNP, thus confirming the low response of the patient to the pyridoxine.[102] All mutations also altered the catalytic activity and, among these, R225 mutants showed the lowest k_{cat} values (especially when mutated to Cys), indicating that this residue is really important for the catalysis of the reaction. Kinetic studies clearly show that all mutations lead to a significant loss of catalytic efficiency (k_{cat}/K_D) of the enzymes, particularly G118R and R225H/R116Q PNPOx mutants, as compared with the wild type enzyme.

Enzyme form	K_M (µM)	k_{cat} (s^{-1})	k_{cat}/K_M (s^{-1} μM^{-1})	% k_{cat}/K_M
Wild type	1.5 ± 0.3	0.061 ± 0.002	0.041 ± 0.007	100 ± 24.8
G118R	122.4 ± 34.9	$3.9 \cdot 10^{-3} \pm 2.6 \cdot 10^{-4}$	$3.2 \cdot 10^{-5} \pm 9 \cdot 10^{-6}$	0.08 ± 0.03
R141C	20.8 ± 3.6	$8.1 \cdot 10^{-3} \pm 3.3 \cdot 10^{-4}$	$3.9 \cdot 10^{-4} \pm 7 \cdot 10^{-5}$	0.95 ± 0.24
R225C	7.8 ± 2.5	$3.8 \cdot 10^{-4} \pm 1.7 \cdot 10^{-5}$	$4.9 \cdot 10^{-5} \pm 1.6 \cdot 10^{-5}$	0.12 ± 0.04
R225H	17 ± 1.7	$0.002 \pm 2.9 \cdot 10^{-4}$	$1.2 \cdot 10^{-4} \pm 2.1 \cdot 10^{-5}$	0.79 ± 0.4
R225H/R116Q	5.6 ± 2.6	$0.002 \pm 9.2 \cdot 10^{-5}$	$3.3 \cdot 10^{-4} \pm 1.6 \cdot 10^{-4}$	0.08 ± 0.03
X262Q	10.8 ± 3.2	$0.002 \pm 6.9 \cdot 10^{-5}$	$1.6 \cdot 10^{-4} \pm 4.9 \cdot 10^{-5}$	0.39 ± 0.14

Table 8 *Kinetic parameters of human PNPOx, determined in TRIS-HCl buffer*.

Allosteric binding site in the R225H PNPOx mutant

The R225H mutation of human PNPOx was found in 10 patients with NEE[70,91,127] furthermore, in four other patients this mutation was associated with the R116Q mutation.[90,91] Since other patients have the amino acid residue R225 also mutated in cysteine or leucine,[95,128] this arginine residue seems to be particularly associated with the onset of the encephalopathy; thus, a more detailed kinetic characterisation of the R225H PNPOx mutant was performed to study its allosteric properties. As previously described for both *E. coli* and human wild type PNPOx, the experiment was carried out in 50 mM Na-HEPES and 50 mM TRIS-HCl buffers pH 7.6, at 37 °C. Although this mutant has a much higher K_D for PNP and a much lower k_{cat} than the wild type PNPOx, it has very similar allosteric properties, in fact the catalytic activity is different when measured in TRIS or in HEPES buffer **(Fig. 3.30**

A), thus suggesting that the PLP accumulation in the solvent determines the deceleration observed in HEPES buffer, as described before for the wild type enzyme. The time course of the reaction carried out in HEPES was fitted to **Eq. 1** (see materials and methods).

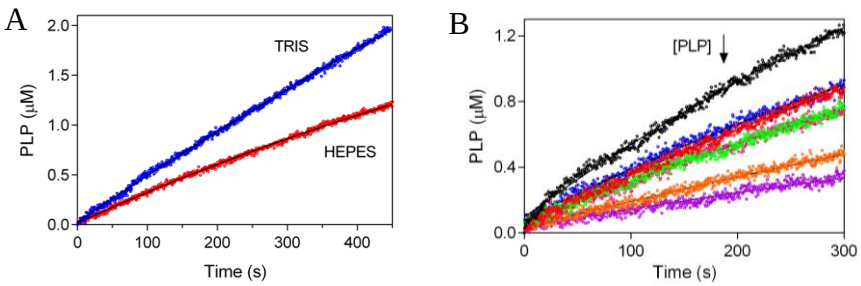

Figure 3.30 *Kinetic studies of R225H mutant*. **A)** Comparison of kinetics carried out in 50 mM TRIS-HCl and 50 mM Na-HEPES buffers at pH 7.6. **B)** Kinetics obtained by the addition of increasing concentrations of exogenous PLP (0, 0.19, 0.38, 0.75, 1.5, 3 and 6 μM) to reactions. The experiments were carried out with 1 μM enzyme (protein subunit concentration) and 60 μM PNP and the kinetics traces fitted to **Eq. 1** (continuous black lines through the experimental traces). The time course obtained in TRIS buffer was fitted to a closed form of the time-integrated Michaelis-Menten equation.[126]

Moreover, it was observed that, adding exogenous PLP (from 0.19 to 6 μM) in HEPES buffer **(Fig. 3.30 B)**, the first deceleration phase disappears as shown in **Figure 3.23** for the wild type PNPOx. This observation suggested that the deceleration phase resulted from PLP inhibition. In fact, the exogenous PLP binds to the enzyme and progressively reduces the amplitude of the first deceleration phase.

3.4.3 Analysis of FMN and PLP binding equilibria in human PNPOx mutants

Active site mutants impair the FMN binding equilibrium

To measure the dissociation constant of the FMN binding equilibrium, fluorescence titration experiments were performed with the wild type and all mutant enzymes. The apo-form of the enzymes was produced as explained in the materials and methods section. The excitation was set at 450 nm and the emission fluorescence was recorded between 470 and 570 nm. Data were analysed using the modified version of quadratic **Eq. 8**, as previously described for the *E. coli* enzyme. The G118R, R225H and R225H/R116Q mutants bind the cofactor with a dissociation constant (94 ± 19 nM; 168 ± 52 nM; 82 ± 17 nM; respectively) that is about 7-, 10-fold higher as compared with that of the wild type enzyme (13.1 ± 1.7 nM)[92] **(Fig. 3.31)**. The R225C PNPOx has a higher K_D (380 ± 129 nM) than the aforementioned mutants, while the mutations that mostly affect the FMN binding are R141C (K_D = 1360 ± 428 nM) and X262Q (K_D = 2300 ± 453 nM) **(Fig. 3.31)**. For the latter in particular, high K_D is probably due to the addition of 28 amino acid residues near the active site.

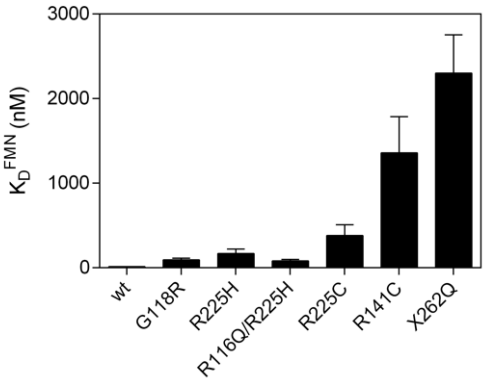

Figure 3.31 *Dissociation constants of FMN binding equilibrium*. The graph compares the K_D values of FMN binding equilibrium of the wild type and mutant PNPOx forms. The K_D values were obtained as previously described for the *E. coli* PNPOx in **Figure 3.13**. The experimental condition were the same reported in **Figure 3.13**. Reported values are the mean ± standard deviation of three independent measurements.

PLP binding analysis of R225H mutant through differential scanning fluorimetry

As abovementioned for the wild type PNPOx, the differential scanning fluorimetry analysis of PLP binding was also performed for the R225H mutant **(Fig. 3.32)**. Also in this case, adding increasing concentrations of PLP, an increase in the melting temperature was observed. In fact, the different melting temperatures reported as a function of PLP concentration showed a hyperbolic behavior **(Fig. 3.32 C)**. The analysis of data using the quadratic **Eq. 8** allowed to estimate a dissociation constant for the R225H PNPOx equal to 16.5 ± 4.1 μM, which describes the PLP binding at the active site of the enzyme. This is a higher value than that obtained with the wild type enzyme (4.22 ± 0.25 μM), and this can probably be explained by the important role of the Arg225 residue in the catalysis.

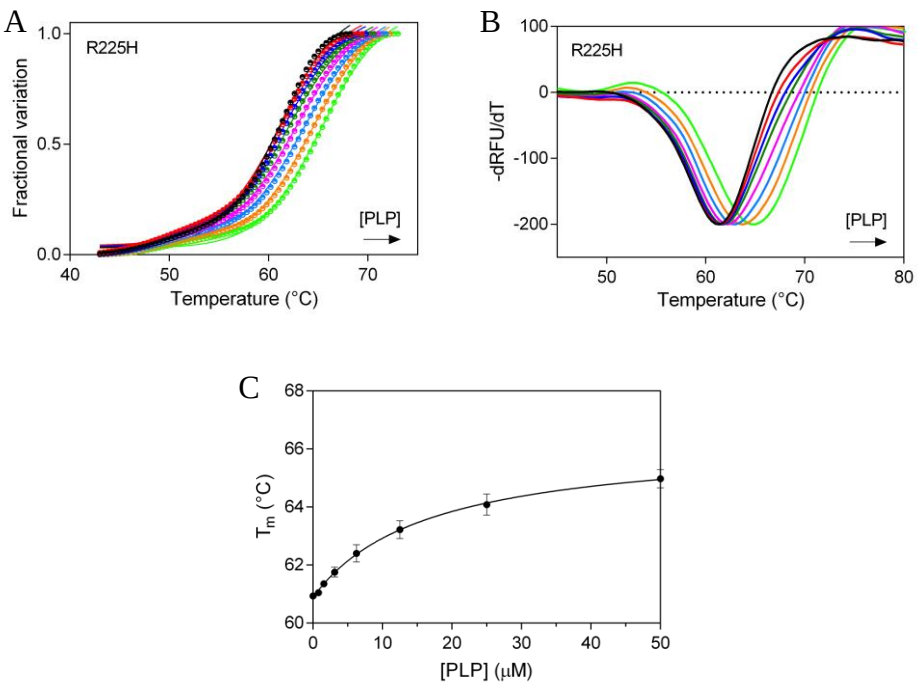

Figure 3.32 *Differential scanning fluorimetry of R225H PNPOx in presence of different PLP concentrations.* **A)** The fractional variation is plotted as a function of temperature. **B)** First derivative (–dRFU/dT) is expressed as a function of temperature. The experimental conditions were the same reported in **Fig. 3.27**. The curves are the result of three independent experiments but, to easily understand the data, the standard error bars were not reported in the graph. **C)** A saturation curve is obtained by plotting the melting temperatures as a function of the PLP concentration. Data were analysed as described before in **Fig. 3.27**.

Part III

Studies of pyridoxal kinase human variants

3.5 Pyridoxal kinase human variants are related to DNA damage and cancer

The catalytically active form of vitamin B_6, pyridoxal 5'-phosphate, is a cofactor in several enzyme reactions, such as the biosynthesis of many neurotransmitters, including dopamine, norepinephrine, histamine, serotonin, and γ-aminobutyric acid.[4] Thus, it is not surprising that PLP is beneficial for many human diseases, such as schizophrenia, epilepsy, Alzheimer's disease, Parkinson's disease, malaria, diabetes, and cancer.[46,129] In humans, the synthesis of PLP from its precursors (PN, PM and PL) requires a phosphorylation reaction that is catalysed by pyridoxal kinase, encoded by the *pdxK* gene (see **Figure 1.5** in the Introduction chapter 1.2.3). As previously described (see the Introduction chapter 1.7.1) using *Drosophila* as a model system carrying the mutation *dPdxk*^{1}, it has been observed that the resulting PLP depletion causes the formation of chromosome aberrations (CABs) and advanced glycation end products (AGEs), which in turn attack DNA throughout ROS formation.[85]

The third part of this work is focused on the biochemical characterisation of pyridoxal kinase (PDXK) human variants, to check if these mutant forms can display different affinity for the PN, PM and PL substrates. Moreover, in the laboratory of professor Fiammetta Vernì (Department of Biology and Biotechnology "Charles Darwin", Sapienza Università di Roma), the PDXK variants were tested in *Drosophila* with respect to CABs formation and glucose content.

3.5.1 Chromosome aberrations and hyperglycaemia caused by the expression of PDXK human variants in *dPdxk*^{1} flies

As above mentioned, mutations of the pyridoxal kinase gene in *Drosophila* (*dPdxk)* cause the formation of chromosome aberrations (CABs) which can be rescued by PLP supplementation.[85] Silencing the human *pdxK* gene gives the formation of CABs in fibroblasts and HeLa cells.[85] According to these findings, humans carrying mutations in the PDXK encoding gene could have an increased propensity to accumulate chromosome aberrations and a consequent increased risk to develop malignances.

Thanks to the collaboration with professor Fiammetta Vernì (Department of Biology and Biotechnology "Charles Darwin", Sapienza Università di Roma), some human PDXK loss-of-function variants were expressed in flies homozygous for the *dPdxk*^{1} mutation[85] and tested in Prof. Vernì's lab for their effects on CABs.

Four human PDXK variants were analysed: Asp87His (D87H), Val128Ile (V128I), His246Gln (H246Q) and Ala243Gly (A243G). The first three have been picked up from the Exome variant server (Exome variant server, http://evs.gs.washington.edu/EVS/), which contains numerous human PDXK variants not yet associated to any disease. The variants have been chosen considering their putative damaging effects predicted *in silico* by the PolyPhen-2 software and their evolutionarily conservation of the mutated residues in *Drosophila*. In particular D87H displays the highest damaging score (1.0) and concerns a conserved position in *Drosophila* and human PDXKs; V128I and H246Q carry mutations in invariant positions (http://www.flyrnai.org/cgi-bin/DRSC_orthologs.pl) and in addition display high damaging scores (0.99 and 0.98 respectively). These variants are very

rare in the population (their frequency ranging from 2.84e-5 to 7.97e-6; https://gnomad.broadinstitute.org/) and are carried in heterozygous state. A243G is absent in major databases and has been found in a genetic screening in patients with gestational diabetes. The rationale for the aforementioned investigation was the previously reported beneficial effect of vitamin B_6 on gestational diabetes and its possible effect on insulin secretion in a murine model.[130]

By site-directed mutagenesis, four constructs of human HA-tagged *pdxK* cDNA, each containing a variant, were produced and introduced in flies by germline mediated transformation. As reported in **Fig 3.33**, the D87H, V128I, H246Q and A243G variants were unable to completely rescue CABs unless the larvae were reared in a medium containing PLP (1 mM). Taken together, these findings suggest that all tested variants behave as loss of function alleles which impact on genome integrity.

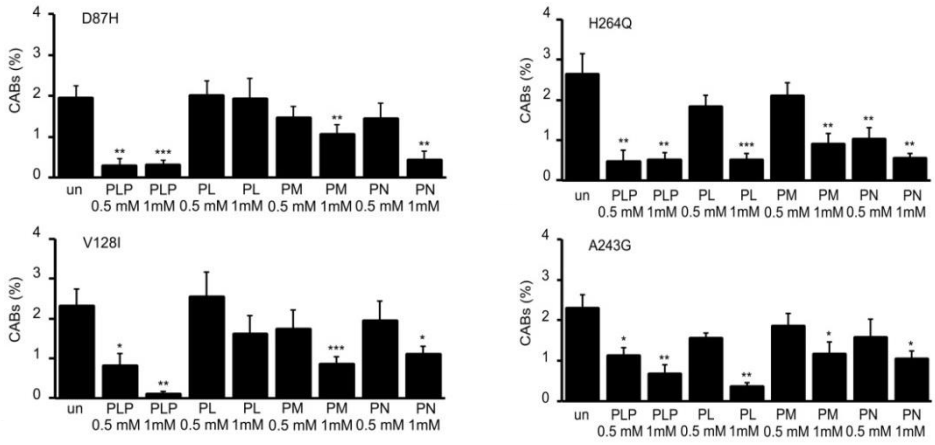

Figure 3.33 *Human PDXK variants expressed in dPdxk[1] flies do not rescue CABs.* Quantification of CABs performed on brains dissected from third instar larvae and incubated for 4 hours in 2 ml of saline supplemented with 10% foetal bovine serum (FBS, Corning) with addition of 0.5 or 1 mM PLP, PM, PL or PN. An untreated sample (un) is also

reported as a control. Each bar represents the mean value ± SD obtained by scoring at least 5 brains (~800 cells) for genotype. *,**,*** Significantly different in the Student's t test with $p < 0.05$, 0.01 and 0.001 respectively.

Mutations in the *dPdxk* gene, besides promoting CAB formation, increase glucose content in the haemolymph, generating "diabetic" flies.[85] To verify whether the expression of D87H, V128I, H246Q and A243G variants influenced glucose homeostasis, glucose levels were analysed. None of the variants was able to significantly reduce hyperglycemia caused by *dPdxk*^{1} mutation, which was instead decreased by PLP treatment **(Fig 3.34).**

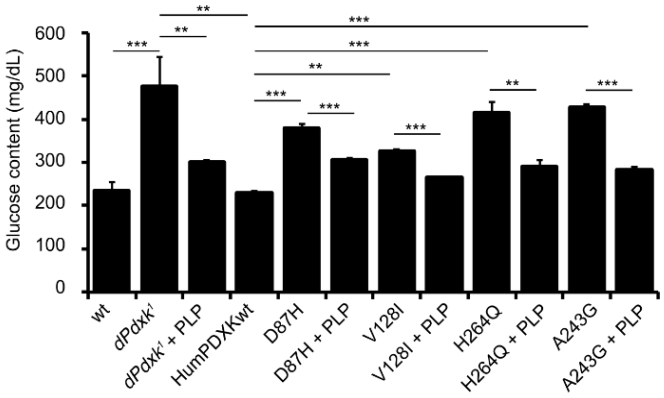

Figure 3.34 *Glucose content in human PDXK variants expressed in dPdxk*^{1} *flies.* Glucose content (mg/dL) in haemolymph from larvae expressing either wild type or PDXK variants, reared on standard medium with or without PLP (1mM) supplementation. *dPdxk*^{1} is the *Drosophila* mutant in which the gene encoding PDXK is altered. HumPDXKwt represents *dPdxk*^{1} flies where the human wild type PDXK is expressed. Columns are the means of 5 independent sample measurements ± SD (each sample = haemolymph extracted from 20 larvae). **, *** Significantly different in the Student's t test with $p < 0.01$ and <0.001 respectively.

3.5.2 Biochemical characterisation of PDXK variants

Differential scanning fluorimetry

In order to verify if the point mutations inserted into human *pdxK* gene alter the thermal stability of pyridoxal kinase, differential scanning fluorimetry measurements were carried out. The Sypro Orange dye (Thermo Scientific) was used as fluorescent dye. The procedure used in the measurements was the same previously mentioned for PNPOx. All the PDXK variants (2 μM) were analysed in 100 mM Na-BES buffer, pH 7.3, containing 150 mM NaCl. All curves **(Fig. 3.35)** were normalised and fitted to the Boltzmann equation to obtain the following melting temperatures (T_m) for wild type, A243G, H246Q, V128I and D87H PDXK variants: 50.2 ± 0.3, 49.4 ± 0.2, 48.4 ± 0.2, 49.5 ± 0.2 and 47.4 ± 0.2, respectively.

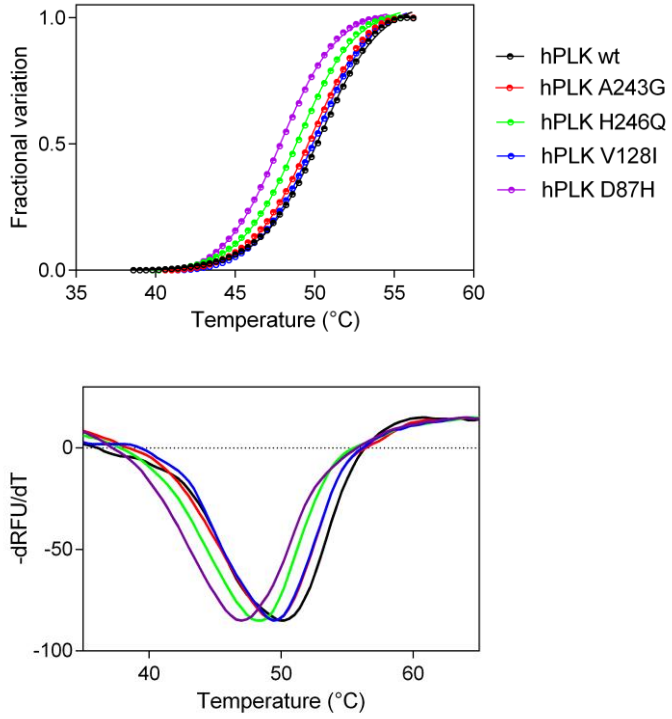

Figure 3.35 *Differential scanning fluorimetry of human PDXK variants.* The fluorescence change is illustrated in the figure above, and is expressed as fractional variation as a function of temperature. Graph below shows the first derivative (–dRFU/dT) as a function of temperature. Thermal denaturation data were fitted to the Boltzmann equation to obtain the melting temperatures,[118] listed in the text. The curves are the result of three independent experiments but, to better understand the data, the standard error bars were not reported in the graph.

Kinetic studies of the PDXK variants

To better understand why the four PDXK mutant proteins responded differently to PLP precursors, variant PDXK enzyme forms were expressed as recombinant proteins in *Escherichia coli*, purified and characterised with respect to their catalytic properties with PL, PN and PM as substrates. The

enzymatic assays were carried out in 100 mM NaBES buffer pH 7.3, containing 100 mM $MgCl_2$, at 37 °C. The conversion of PL into PLP was followed by measuring the absorbance change at 388 nm, as previously described.[108] Enzyme activity with PN and PM as substrates was measured in a spectrophotometric coupled assay, in which the phosphorylated products generated by PDXK were converted into PLP by *E. coli* PNPOx. As shown in **Table 9**, all the four mutant enzymes showed altered kinetic parameters. In particular, the D87H mutation strongly increased K_M for PL, and to a lesser extent also increased K_M for PN and PM, leaving K_M for ATP and k_{cat} almost unaltered. These observations are in agreement with the location of the Asp87 residue on an active site loop that plays a crucial role in substrate binding, and in particular with the direct interaction between the adjacent Tyr84 with the B_6 vitamer pyridine ring (**Fig. 3.36**).

PDXK		WT	D87H	V128I	H246Q	A243G
PL as substrate	$^{a}K_M^{PL}$ (μM)	189 ± 27	2090 ± 173	3839 ± 507	141 ± 10	177 ± 10
	$^{a}K_M^{ATP}$ (μM)	407 ± 65	377 ± 48	3096 ± 555	901 ± 164	1024 ± 81
	$^{b}k_{cat}$ (min^{-1})	58 ± 3	40 ± 1	67 ± 5	35 ± 1	28 ± 1
PN as substrate	$^{a}K_M^{PN}$ (μM)	7.0 ± 0.9	34.1 ± 0.4	24.8 ± 0.2	11.5 ± 2.1	9.2 ± 0.6
	$^{a}K_M^{ATP}$ (μM)	104 ± 24	125 ± 16	113 ± 6	126 ± 1	132 ± 23
	$^{b}k_{cat}$ (min^{-1})	19 ± 2	21 ± 3	20 ± 4	17 ± 4	18 ± 2
PM as substrate	$^{a}K_M^{PM}$ (μM)	5.0 ± 0.5	26.5 ± 6.3	51.5 ± 6.3	34.6 ± 7.1	31.9 ± 4.7
	$^{a}K_M^{ATP}$ (μM)	46.2 ± 8.2	55.3 ± 9.1	56.3 ± 7.2	76.8 ± 15.7	34.1 ± 7.0
	$^{b}k_{cat}$ (min^{-1})	6.9 ± 0.2	7.2 ± 0.4	8.5 ± 0.2	6.3 ± 0.3	5.0 ± 0.1

Table 9 *Kinetic parameters of human PDXK variants obtained using PN, PM and PL.* All values are the average ± standard deviation of at least three independent measurements. [a]Determined varying the concentration of the related substrate, while keeping the other fixed and saturating. [b]Determined with ATP as fixed, saturating substrate. Values of k_{cat} determined with the vitamer as fixed, saturating substrate were very similar and are not reported for simplicity.

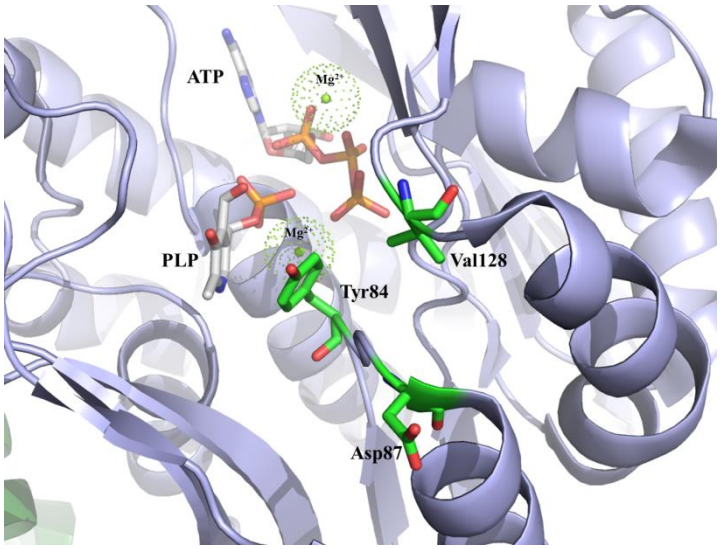

Figure 3.36 *Enlarged view of PDXK active site structure.* Cartoon backbone representation of the human PDXK dimer (PDB code: 3KEU[42]) with PLP and MgATP bound at the active site. The two subunits are shown in light blue and green, respectively. Active site residues Y84, D87 and V128 are shown as sticks in green and labelled.

The V128I mutation drastically increased K_M for PL and K_M for ATP with this vitamer, whereas it did not affect k_{cat}. This was expected, considering the role of the active site loop containing Val128 in substrate binding and specifically in the interaction with ATP (**Fig. 3.36**). K_M for PN and PM were also increased, although with these vitamers K_M for ATP and k_{cat} were unaltered. This latter observation is difficult to explain on the basis of the available results; however, it suggests that binding of B_6 vitamers different from PL may affect the modality of ATP binding by the loop containing Val128. The H246Q mutation somewhat reduced the affinity for ATP when using PL as substrate and the affinity for PM, while it did not affect K_M for PL and PN. In addition, it had the effect to halve k_{cat} with PL. Finally, A243G mutation displayed a behavior very similar to that showed by the

H246Q mutation. Given the distance of Ala243 and His246 from the active site, the observed alteration of the kinetic parameters, although relatively mild, demonstrates that the mutation of these residues is somehow transmitted to the active site of the enzyme **(Fig. 3.37)**.

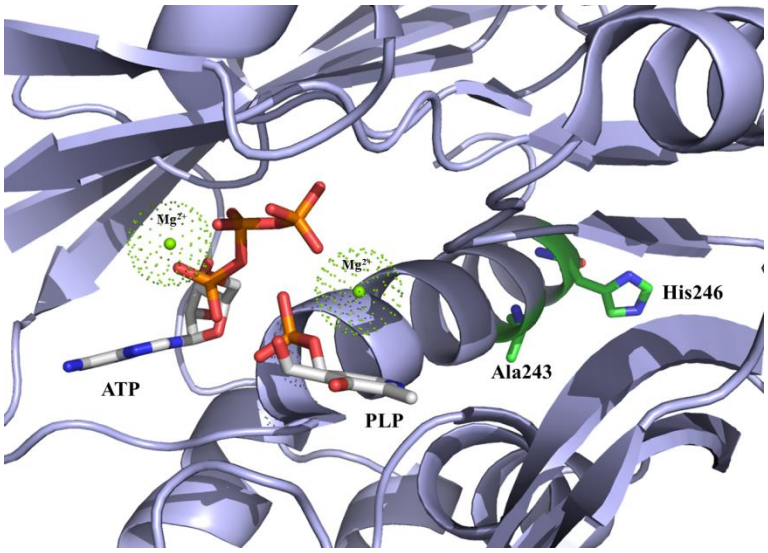

Figure 3.37 *Enlarged view of PDXK active site structure.* Cartoon backbone representation of the human PDXK dimer (PDB code: 3KEU[42]) with PLP and ATP bound at the active site. The chain is shown in light blue. Active site residues A243 and H246 are shown as sticks in green and labelled.

Taken together, these findings indicate that the specific mutations introduced in the four examined variants reduce the PDXK functionality, and thus the genome integrity can be altered and glucose homeostasis impaired.

4. Discussion

Part I
E. coli PNPOx:
a key enzyme in the regulation of vitamin B_6 biosynthesis

4.1 *E. coli* PNPOx binds PLP at an allosteric binding site

Pyridoxine 5'-phosphate oxidase (PNPOx) from *Escherichia coli* is a homodimer, of which each monomer consists of eight antiparallel β-strands and five α-helical segments.[38] This enzyme is of fundamental importance in PLP biosynthesis, in fact it catalyses the oxidation of the two substrates PNP and PMP to PLP, and this reaction is favoured by the presence of two molecules of FMN per dimer.[62] In literature, it has already reported that PNPOx knock-out mutants of *E. coli* K-12 strain are not able to grow, even in the presence of PL. This is curious, as two kinases (pdxY/K) are present in the cells that can convert the dephosphorylated vitamer into PLP.[63] In our case, the growth rates of the two knock-out strains, Δ*pdxJ* and Δ*pdxH* (lacking PNP synthase and PNPOx, respectively), were measured in M9 minimal medium, supplemented with both PN or PL **(Fig. 3.1)**. As expected, the Δ*pdxJ* strain recovers the wild type phenotype in both conditions; on the contrary, the Δ*pdxH* strain is not able to grow like the wild type strain, even when the medium is supplemented with PL. Since two PL kinases, as mentioned before, are present in bacteria, the inability of the PNPOx knock-out mutant to grow suggests that in the *E. coli* cell, PNPOx plays a role that goes beyond its catalytic function. A possible role of this enzyme could be that of PLP reservoir, as previously reported by Yang and Schirch[54], who hypothesized that PLP bound to PNPOx can be transferred to the apo-enzymes that use it as a cofactor.[54]

In prior investigations on PNPOx from *E. coli*[58] and rabbit liver[57,131] a competitive PLP inhibition was described. These observations resulted from discontinuous enzymatic assays or were carried out in TRIS buffer, which prevents accumulation of PLP in the solvent; in our case, a more sensitive continuous spectrophotometric assay in HEPES buffer allowed detection of a first deceleration phase in the kinetics of PLP formation **(Fig. 3.2)** and

showed that PLP inhibition has a mixed-type nature **(Fig. 3.7 and Fig. 3.8)**. The deceleration phase cannot result from an intrinsic feature of the reaction mechanism, such as that typical of the "ping pong" mechanism, because the amount of PLP produced in this phase is 3-fold higher than the enzyme concentration. Moreover, since the amount of PLP produced in the deceleration phase raises as substrate concentration is increased and is proportional to the enzyme concentration **(Fig. 3.3)**, this first phase cannot result from the presence of an impurity in the PNP substrate, synthesized as previously described.[54] When exogenous PLP was added to the reaction mixture the initial velocity of the reaction decreased, and therefore the deceleration phase disappeared at high PLP concentrations **(Fig. 3.5)**. These data suggest a direct link between the deceleration phase and the PLP concentration in the solvent. Furthermore, in TRIS buffer, where PLP is sequestered from the solvent, the deceleration phase is not visible **(Fig. 3.2)**. All these observations indicate that the initial deceleration phase results from PLP accumulation in the solvent that consequently favours the onset of PLP inhibition. It is possible that immediately after mixing the enzyme and PNP, when there is not yet PLP in the solvent, the maximum reaction rate is observed. As PLP is produced and accumulates in the solvent, it progressively binds to the enzyme at an allosteric site, determining a decrease of reaction rate, until this binding equilibrium reaches saturation. At this point, the enzyme is only partially inhibited and catalyses PNP oxidation at a rate that is lower than the initial rate. The concentration of PLP formed in the deceleration phase corresponds to the concentration that is sufficient to saturate the allosteric site and depends on both substrate **(Fig. 3.3 A, inset)** and enzyme **(Fig. 3.3 B, inset)** concentrations. Our experiments on the catalytic activity of the PNPOx-PLP complex, obtained after incubation of the enzyme with PLP and size exclusion chromatography, confirm this

interpretation and are not in contrast with the results obtained by other authors.[54] These authors carried out activity assays in TRIS buffer and obtained 85 ± 2% activity for the PNPOx-PLP complex, as compared to an untreated PNPOx sample. We know that TRIS buffer certainly promotes dissociation of PLP from the enzyme-PLP complex. Moreover, activity assays were carried out with a low concentration of enzyme, diluting the concentrated PNPOx-PLP complex and therefore favouring PLP dissociation. From our rapid kinetics studies, PLP dissociation is expected to be rapid enough to reach equilibrium in a few seconds (k_{OFF} = 3.24 ± 2.24 s^{-1} and k_{ON}= 11.35 ± 1.27 μM^{-1} s^{-1}). In fact, when we measured the kinetics of PNP oxidation to PLP in HEPES using 0.5 µM PNPOx-PLP complex, we could not observe any difference with respect to a control PNPOx sample, that was not incubated with PLP. However, with 8 µM PNPOx-PLP complex, a neat difference was observed, consisting in the lack of the decelerating phase and in a reduced activity **(Fig. 3.11)**, similarly to what observed when exogenous PLP was included in the reaction mixtures **(Fig. 3.5)**. A work from several years ago showed that PNPOx purified from rabbit liver followed a substituted-enzyme ("ping pong") mechanism when acting on PNP as substrate.[124] According to this mechanism, PNP is converted into PLP in the first half reaction, leaving the enzyme in the E_r reduced form. In the second half reaction, molecular oxygen binds to this form of the enzyme and is reduced to H_2O_2 **(Scheme 1B)**. According to the "ping pong" mechanism, when PNP substrate concentration is varied at a fixed, non-saturating oxygen concentration, PLP is expected to give a mixed-type inhibition.[132] This is because PLP is expected to bind at the active site of two different forms of the enzyme (E_r and E_o) with different affinity. In our case, since K_M for PNP increases as PLP is increased, the oxidised form (E_o in **Scheme 1B**) should bind PLP with higher affinity than the reduced form (E_r). If this was the case

of *E. coli* PNPOx, saturation of the higher affinity site would result in complete inactivation, since all enzyme would be in the E_o·PLP form. However, in our experiments, this hypothesis was left out, since the presence of PLP concentrations that can saturate the high affinity site gives only a partial inactivation of PNPOx. On the other hand, both K_M and k_{cat} would decrease as PLP increases if PLP binds only to E_r. Moreover, a mixed-type inhibition based on the "ping pong" mechanism implies that PLP inhibits PNPOx by binding at the active site. However, alteration of the active site (such as the elimination of FMN in the apo-enzyme and the mutations in the quadruple mutant) does not drastically affect PLP binding, as showed by fluorimetric measurements **(Fig. 3.18 A)**. A mixed-type product inhibition may also result from a compulsory-order sequential mechanism.[132] In this case, the same objections invoked for the "ping pong" mechanism can be also applied to this mechanism. As described in **Scheme 1A**, PLP can bind at an allosteric site of *E. coli* PNPOx, different from the active one. Our hypothesis is that the model is a classic linear mixed-type inhibition, in which binding equilibria of substrate and inhibitor to the enzyme are rapidly established and conversion of the substrate into product is relatively slow. Binding of PNP at the active site and binding of PLP at the allosteric site influence each other, increasing their respective dissociation constants.[133] Accordingly, two inhibition constants are measured, resulting from binding of PLP with higher affinity to the free enzyme (K_I) and with lower affinity to the enzyme-substrate complex (K_{Is}). Noticeably, K_I determined from our inhibition kinetics is similar to the dissociation constant determined in the fluorimetric (K_D = 0.15 ± 0.04 μM) and rapid kinetics experiments (k_{OFF} / k_{ON} = 0.28 ± 0.19 μM), which used the free enzyme form (E_o). Analogously, different kinetic parameters are obtained from inhibition kinetics: K_D, that is relative to substrate binding to the free enzyme, and K_{Dp}, due to substrate binding to the

enzyme-PLP complex **(Table 1)**. A comparable value of K_D was obtained from fitting of the initial velocity in HEPES buffer **(Fig. 3.4; Table 1)**. The fact that $1/V_{max}$ and K_M/V_{max} replots **(Fig. 3.8 B, C)** are linear with PLP concentration and the enzyme activity is completely abolished at infinite PLP concentration, as showed by the fitting of apparent k_{cat} as a function of PLP **(Fig. 3.7 B)**, indicate that the enzyme-PNP-PLP complex (PES in **Scheme 1A**) is completely inactive (otherwise replots would be hyperbolic) and that PLP does not compete with the PNP substrate for binding at the active site (otherwise replots would be parabolic).[133] As showed by the crystal structure obtained in the presence of PLP,[56] this vitamer is able to bind at the active site, but evidently this binding takes place with much lower affinity than binding at the allosteric site, since we could not detect it in our experiments with the *E. coli* enzyme.

The presence of an allosteric PLP binding site on *E. coli* PNPOx is also demonstrated by fluorimetric measurements on the quadruple mutant. Although in this mutant the substrate binding at the active site is heavily impaired (K_M = 238 ± 77 μM), the enzyme is still able to bind PLP with a dissociation constant (0.45 ± 0.02 μM), which is comparable to that of the wild type enzyme (K_D = 0.15 ± 0.04 μM). As expected, competition binding experiments carried out with the quadruple mutant demonstrated that the PNP substrate does not interfere with the PLP binding **(Fig. 3.19)**, thus excluding that PLP and PNP bind at the same high affinity site. However, the stoichiometry of PLP binding is affected by the significant impairment of the active site. With the wild type enzyme, the measured stoichiometry of one PLP molecule per protein dimer **(Fig. 3.10, inset)** is against the presence of two symmetric PLP binding sites, such as the secondary PLP binding site indicated by the crystallographic data.[56] It suggests that the allosteric PLP binding site may be located along one of the two symmetry axes of the dimer.

Alternatively, if two symmetric PLP binding sites are present on the PNPOx dimer, binding of PLP at one site should cause a conformational change that prevents binding at the second site. This second hypothesis may be supported by the different PLP binding stoichiometry obtained with the quadruple mutant, which is of two PLP molecules per enzyme dimer **(Fig. 3.18 B)**.

The structural and functional connection between the active site and the allosteric site is at the basis of the allosteric inhibition acted by PLP. This is evident in the revealed mixed-type inhibition mechanism, in which substrate binding and PLP binding affect each other. Therefore, it is possible that a substantial alteration of the active site, such as that present in the quadruple mutant, may have uncoupled the allosteric connections. The presence of an allosteric PLP binding site is also confirmed by the capability of the active site quadruple mutant to retain PLP upon size exclusion chromatography (37 ± 9 %). Although, in these experiments the stoichiometry of PLP binding to wild type and mutant enzymes is somewhat surprising if compared to stoichiometry obtained from equilibrium binding experiments. In analogous experiments performed by Yang and Schirch,[54] PLP binding to wild type PNPOx resulted of 100%; however, these authors used a short gravity chromatography BioGel P6-DG desalting column. In our case, the Superdex 200 10/300 GL column and the FPLC system were used to improve separation, thus favouring the dissociation of PLP from the PNPOx-PLP complex. This could explain the low PLP content of the quadruple mutant protein-PLP complex, also considering that the PLP binding at its active site is nearly abolished.

4.2 The crystallographic PLP binding site does not coincide with the PLP allosteric binding site

The actual location of the allosteric PLP binding site involved in the inhibition detected in our experiments awaits to be determined. Firstly, the PLP secondary binding site indicated by crystallographic data[56] was studied by our research group. Since in the crystal structure the plane of the pyridine ring of PLP bound at the secondary site is sandwiched between the side-chains of Phe177 and Lys145 (**Fig. 1.7**),[56] these two amino acid residues were replaced with alanine residues. Thus, the face-to-face stacking contact against Phe177 and the hydrophobic interactions with Lys145 were impaired. In addition, Asn84 which makes a close hydrogen bond interaction with the pyridine nitrogen of PLP[56] was mutated both into alanine and tryptophan residues. The double (K145A/F177A) and the two triple (N84A/K145A/F177A and N84W/K145A/F177A) PNPOx mutants of the crystallographic site did not show an altered catalytic activity when this was measured in TRIS buffer **(Table 2)**. However, as observed using the differential scanning fluorimetry, these mutant forms result less stable than the wild type enzyme **(Fig. 3.12)**, displaying lower values of the melting temperature (53.1 ± 0.3 °C, 48.5 ± 0.2 °C, 47.2 ± 0.1 °C and 47.8 ± 0.1 °C, for the wild type, K145A/F177A, N84A/K145A/F177A and N84W/K145A/F177A, respectively). The instability of the crystallographic site mutants is not considerable but could be due to the position of the amino acid residues, which are very conserved in the PNPOx family, near the active site.[56]

A further evidence that the crystallographic site is not the high affinity site is given by the estimated dissociation constants for PLP **(Table 3)**, which have values similar to the wild type; furthermore, the PNPOx mutants are able to retain PLP when are passed through the size exclusion chromatography

column (68 ± 9; 70 ± 11; 79 ± 12, PLP % for K145A/F177A, N84A/K145A/F177A and N84W/K145A/F177A PNPOx mutants, respectively).

4.3 Molecular docking experiments identified an excellent candidate for the PLP allosteric binding site

Thanks to the collaboration with professor Pascarella (Department of Biochemical Sciences "A. Rossi Fanelli", Sapienza Università di Roma), another possible PLP binding site was identified using the molecular docking method. The analysis also highlighted a high degree of conservation of this area across γ-proteobacteria that strongly suggests its functional importance compared to the crystallographic binding site, that indicates a very poor evolutionary conservation. The amino acid residues identified as important for the PLP interaction are two arginine residues, which were both mutated into leucine, and one phenylalanine residue replaced with methionine (**Fig. 3.14**). The location of these residues near the interface between the two subunits of the dimer may explain the relative thermal instability of the mutants detected by differential scanning fluorimetry **(Fig. 3.15)**. The kinetic parameters of the mutants measured in TRIS buffer are similar to the wild type enzyme, as shown in **Table 4**. Even if the mutants of the docking site still bind the PLP, the dissociation constants obtained for PLP are approximately 10-fold higher than the wild type (**Table 5**). Also the ability to retain PLP is lower than the wild type PNPOx (**Table 5**).

Moreover, thanks to our collaboration with Andrea Ilari (Institute of Molecular Biology and Pathology, National Research Council), preliminary studies on the crystal structure of the quadruple mutant show the PLP bound at the docking site. These preliminary results suggest the simultaneous involvement of three arginine residues in PLP binding, including those we

have already mutated. In future studies, we will replace these arginine residues with leucine residues to verify if the docking site is the PLP allosteric binding site.

Part II
human PNPOx:
a relevant enzyme in the onset of neonatal epileptic encephalopathy

4.4 The impairment of the human PNPOx active site is related to the NEE onset

In humans, PNPOx is a key enzyme in the salvage pathway, where, together with pyridoxal kinase (PDXK), it catalyses the conversion of the vitamers found in foods to the active form of vitamin B_6, pyridoxal 5'-phosphate (PLP). Previous studies showed the structural and functional properties of the wild type enzyme (PDB code: 1NRG).[34] The human PNPOx is a homodimer, as found with the *E. coli* enzyme; however, it differs in substrate specificity, with PMP being a slightly better substrate than PNP.[34] The vitamin B_6 metabolism is strictly related to epilepsy during the childhood, and particularly, when mutations in PNPOx gene occur, different phenotypic effects can be observed in patients, including seizures and characteristic electroencephalogram patterns.[67] In literature, several mutations in PNPOx have been reported in patients affected by neonatal epileptic encephalopathy (NEE) (**Table 6**).[90,91,102] However, only three of them have been biochemically characterised.[39,92,100] Symptoms of NEE usually appears a few minutes after birth and, if not properly treated, can lead to death. For these reasons, a better knowledge of the molecular bases of the disease is required, which might help developing more efficient treatment strategies. In 2013, Pearl and collaborators[102] identified the homozygous mutation in a highly conserved area in exon 3: c.352G>A p.G118R, predicting a substitution of arginine for glycine residue. Enzyme studies of the expressed mutant protein have not been carried out. The G118 residue is a highly conserved residue, located at the C-terminal end of an α-helix that interacts with the phosphate group of FMN **(Fig. 4.1)**. The replacement of an arginine residue with a glycine in the active site is predicted to have a negative steric effect on the interaction with FMN, as demonstrated by the 10-fold increase in both K_D for

the cofactor and K_M for the PNP substrate (**Table 8**), as compared with the wild type PNPOx.

Expression studies in Chinese hamster ovary cells were performed by Mills and collaborators,[88] to characterise a novel serious mutation found in two patients, who died in the first twenty days of life.[88] The abolition of the stop codon (X262Q) after the P261 residue (**Fig. 4.1**) causes a C-terminal 28 amino acid extension, which may perturb the structure of the enzyme, that results less stable (**Fig. 3.28**; **Table 7**). Moreover, the great alteration of kinetic parameters (**Table 8**) could be due to the perturbation of the active site structure, as shown by the high K_D for the FMN (**Fig. 3.31**). In our experiments, X262Q is the mutation that most impairs the FMN binding, showing a K_D equal to 2300 ± 453 nM. It is possible that the elongated C-terminal extends into the active site.

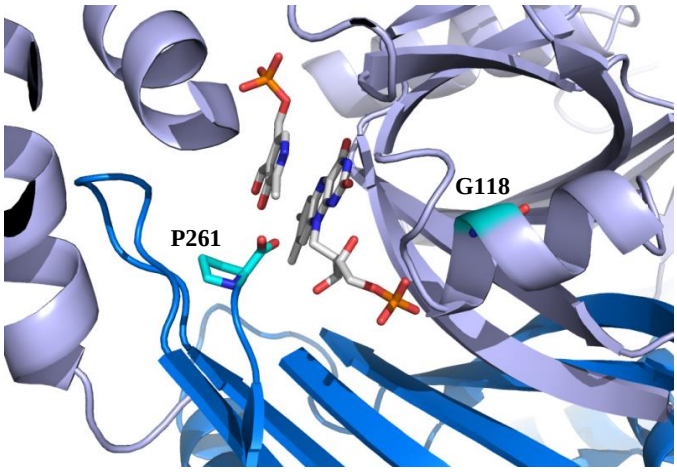

Figure 4.1 *Enlargement of human PNPOx active site.* Gly118 and Pro261 residues are shown in cyan. The two monomers of the functional PNPOx dimer (PDB code: 1NRG) are in blue and lilac; the FMN cofactor and PLP product are reported as sticks in grey.

Another mutation was found only in one patient, Arg141Cys, which is associated with the deletion c.279_290del in exon 5.[91] Arg141 is one of the 14 amino acids that are involved in the inter-subunit interactions with FMN, that is bound at the dimer interface[34,100] (**Fig. 4.2**). In fact, Arg141 is located in the highly conserved region carrying the FMN-binding site.[91] These interactions stabilize FMN binding thanks to polar contacts between the residue and the phosphate group of the coenzyme. The interactions probably ensure the correct FMN orientation for optimal substrate oxidation. As expected, the R141C mutant binds the cofactor with a dissociation constant that is approximately 100-fold higher as compared with that of the wild type enzyme (**Fig. 3.31**). The alteration of the FMN binding site also leads to a 100-fold decrease of catalytic efficiency (**Table 8**).

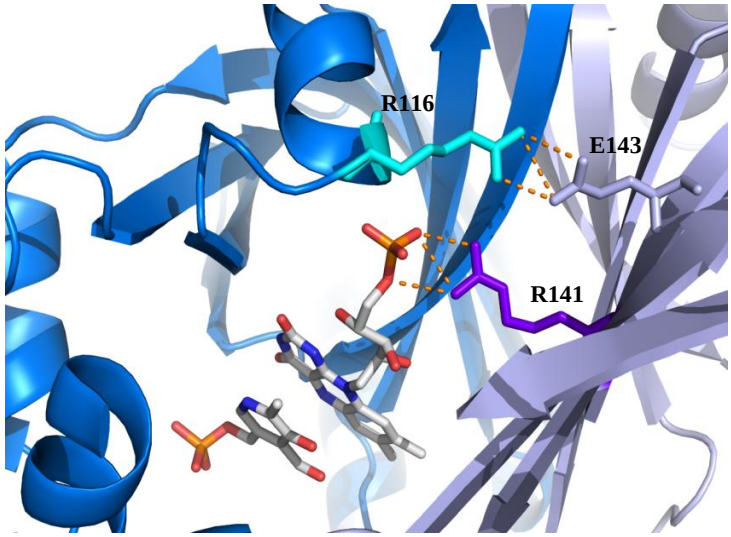

Figure 4.2 *Enlargement of human PNPOx active site.* Arg116 and Arg141 residues are shown in cyan and violet, respectively. The two monomers of the functional PNPOx dimer (PDB code: 1NRG) are in blue and lilac, and FMN cofactor and PLP product are reported as sticks in grey. The interactions of Arg116 with Glu143 and of Arg141 with the phosphate group of FMN are shown as orange dashes.

Recent studies detected and characterised a new genetic variant on PNPOx gene, Arg116Gln **(Fig. 4.2)**, which is of particular interest because of its later onset of symptoms (beyond the first months of life) and its peculiar epileptic manifestations in patients.[90,92] This protein variant was expressed as a recombinant protein in *E. coli* and characterised with respect to structural and functional properties.[92] In four new-borns the substitution of Arg116 was associated with another missense mutation in Arg225, replaced with a histidine residue.[88,91] This novel mutation in exon 7 of PNPOx gene affects arginine residues presenting codons with the potential CpG DNA methylation site.[91] Ten patients have been found to be homozygous for the R225H mutation,[91] one for the R225C mutation[128] and four for the R225L mutation.[128] In the wild type PNPOx structure, there are very close hydrophobic contacts between the substrate pyridine ring and the FMN isoalloxazine ring, as well as hydrogen bond interactions between the strictly conserved residue Arg225 and the substrate (PDB code 1NRG[100]) **(Fig. 4.3)**. Previous studies on the human enzyme showed that the R225C and R225H mutants resulted in a 91% and 92% reduction in the amount of PLP synthesized over a 40-min period by PNPOx as compared with the wild type enzyme.[90] Our results confirm these observations, in fact the two mutants have considerable lower k_{cat} and higher K_M compared to the wild-type PNPOx (**Table 8**). This is probably due to the impairment of the enzyme interaction with the PNP substrate pyridine ring, resulting in non-optimal stacking interaction between PNP and FMN. These results are further confirmed by the similar parameters obtained with the Arg229Trp PNPOx mutant already characterised and located near the Arg225.[100]

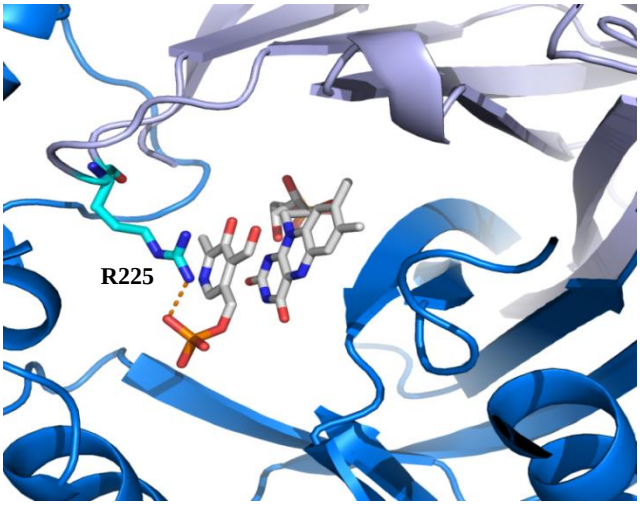

Figure 4.3 *Enlargement of human PNPOx active site.* Arg225 residue is shown in cyan and labelled. The two monomers of the functional PNPOx dimer (PDB code: 1NRG) are in blue and lilac, and FMN cofactor and PLP product are reported as sticks in grey. The interaction of Arg225 with the phosphate group of PLP is shown as orange dashes.

Furthermore, the double mutation that is characterised by the replacement of Arg116 (**Fig. 4.2**) and Arg225 (**Fig. 4.3**) with glutamine and histidine residues respectively, was found in four patients.[90,91] The affinity for FMN and kinetic parameters are quite similar to those of the single R225H mutant (**Fig. 3.31**; **Table 8**). However, it is interesting to note that the melting temperature of the double mutant is very similar to that of the single R116Q mutant (**Fig. 3.28**; **Table 7**), in fact it has been previously reported that the R116Q mutant shows heat instability.[92]

4.5 Both wild type and R225H PNPOx bind PLP at the allosteric site

The human and *E. coli* PNPOx share 39% sequence identity, but the binding sites for the FMN and the substrate are highly conserved.[34] Given the high degree of structural conservation of these binding sites, it is not surprising

that also the PLP allosteric binding site is conserved in the human PNPOx. As shown in **Figure 3.20**, the kinetic trace of the human enzyme observed in TRIS buffer is different with respect to that obtained in HEPES buffer. As described for the *E. coli* PNPOx in HEPES buffer, where PLP can accumulate in the solvent, a first deceleration phase was followed by a linear phase (**Fig. 3.20**). Furthermore, the amount of PLP produced in the deceleration phase reaches a maximum value when substrate concentration increase (**Fig. 3.21 A**) and tends to a minimum value as the enzyme concentration decreases (**Fig. 3.21 B**). The deceleration phase results from PLP accumulation as suggested by kinetic traces obtained in presence of different exogenous PLP concentrations, where the first burst phase disappears as the PLP increases (**Fig. 3.23**). All these observations suggest that the PLP produced during turnover reduces the velocity of the reaction, when it binds at an allosteric site.

As described for sheep brain and *E. coli* PNPOx,[58,59] PLP was described as a product inhibitor also of the human enzyme; in fact, in previous studies, it has been reported a value of the PLP inhibition constant equal to 3.2 μM.[34] As previously described for the *E. coli* enzyme, in our experiments, the PLP inhibition of human enzyme shows a mixed-type nature (**Fig. 3.24**). Interestingly, the inhibition constant reported in literature[34] is very similar to the constant for the substrate-bound enzyme observed in kinetic experiments (K_{Is} = 3.53 ± 0.3 μM) (**Fig. 3.25**). Moreover, our differential scanning fluorimetry assays has allowed us to estimate the K_D for the PLP binding at the active site of the wild type human PNPOx (K_D = 4.22 ± 0.25 μM; **Fig. 3.27**), that is not seen with same experiments in the *E. coli* enzyme. Moreover, the inhibition constant for the free enzyme form (K_I in **Scheme 1A**) obtained in our kinetic studies is equal to 0.73 ± 0.02 μM and, noticeably, it is comparable to the dissociation constant determined in the

fluorimetric experiments (K_D = 0.9 ± 0.02 μM) (**Fig. 3.26**). All these results strongly suggest that the PLP allosteric binding site is also present in human wild type PNPOx. The same behavior was observed also in the R225H mutant; in fact, as shown in **Figure 3.30 A**, the kinetic trace of the reaction observed in HEPES buffer differs from that obtained in TRIS buffer. Furthermore, when increasing exogenous PLP concentrations are added to the reaction mixture, the first deceleration phase lowers (**Fig. 3.30 B**). Therefore, even if the mutation of the Arg225 residue impairs the active site it does not alter the structure of the PLP allosteric binding site. In our laboratory, other experiments are in progress to better characterise the other PNPOx mutant forms with respect to the properties of the PLP allosteric binding site.

Part III
human PDXK: connection between vitamin B_6 metabolism and diabetes

4.6 Mutations in the *pdxK* gene impair vitamin B_6 metabolism

PLP deficiency has been associated to many human pathologies, including cancer and diabetes.[111] Specifically, the onset of type 2 diabetes can be due to the insulin resistance determined by an alteration of vitamin B_6 metabolism, as previously reported.[80,81] Furthermore, Merigliano and collaborators[111] observed a protective role of PLP against DNA damage, resulting from vitamin B_6 deficiency[85] in *Drosophila* models of type 2 diabetes. Due to widely conserved pathways which govern metabolism, *Drosophila* is considered a precious organism for the study of metabolic human genetic diseases, both to validate the causative nature of the genetic variants found in patients, and to obtain functional information about novel disease-linked genes.

Previously, the depletion of the pyridoxal kinase gene (*pdxK*) was analysed in *Drosophila* where it results in chromosome aberrations (CABs) as a consequence of hyperglycemia, another phenotype also elicited by *pdxK* depletion.[85] In humans, low *pdxK* expression levels have been correlated to lung cancer[84] and more recently also to insulin resistance which leads to type 2 diabetes.[80] While mutations in the human PNPOx gene, described above, are associated with epilepsy,[88] there is currently no PDXK variants associated to any specific disease, except for a recent work in which two bi-allelic mutations in *pdxk* have been associated to polyneuropathy.[134] In fact, an impairment in the PNPOx function does not entirely block PLP production, since it can be synthesized throughout the conversion of PL assumed in the diet mediated by pyridoxal kinase. On the other hand, in cells lacking PDXK, phosphorylation of B_6 vitamers does not occur and PLP is not produced at all. Thus, it is reasonable to expect, considering the wide spectrum of functions covered by PLP, that severe mutations of the *pdxK* gene seriously

compromise early developmental stages causing lethality in the homozygous condition.

4.7 PDXK variants respond differently to PLP precursors

Thanks to our collaboration with the laboratory of professor Fiammetta Vernì (Department of Biology and Biotechnology "Charles Darwin", Sapienza Università di Roma), *Drosophila* was used as a model to validate the effects of four human variants (D87H, V128I, H246Q reported in the Exome variant server and the novel A243G variant found in patients with gestational diabetes) of the *pdxK* gene on genome integrity and glucose metabolism. None of the chosen variants concern amino acid residues that are directly involved in substrate binding or catalysis; however, these residues are located in pivotal structural regions of the enzyme. Asp87 is placed on the C-terminal end of an active site loop connecting α3 helix and β4 strand, which plays a crucial role in substrate binding. Tyr84, which is part of this loop, directly interacts with the B_6 vitamer substrate stacking to its pyridine ring (**Fig. 3.36**) (PDB code: 3KEU[42]). The Val128 residue is part of another active site loop, located between strands β6 and β7 (**Fig. 3.36**), that closes on the active site as ATP binds to the enzyme. This loop, which is referred to as a flap in pyridoxal kinases, provides hydrogen bond interactions to the ATP β- and γ-phosphates (Tyr127, adjacent to Val128, binds to the γ-phosphate of ATP),[42] and is believed to sequester ATP for catalysis, preventing its unproductive hydrolysis in the absence of a bound B_6 vitamer.[104,105] Thus, variants of residues V128 and D87, which are spatially quite close to each other, are expected to affect substrate binding. On the other hand, A243 and H246, which are also close together, are located at the C-terminal end of helix α7, formed by residues 231–234, at a distance from the active site (**Fig. 3.37**). However, the N-terminus of this helix, which is positioned at the active site,

contributes with its positive charge to binding of the PLP product of the reaction catalyzed by PDXK, stabilizing its phosphate moiety.[43] A243G and H246Q variants are predicted to have milder effects than V128I and D87H on the enzyme catalytic properties.

In experiments carried out in the laboratory of professor Fiammetta Vernì (Department of Biology and Biotechnology "Charles Darwin", Sapienza Università di Roma), it was observed that human variants expressed in *dPdxk*^{1} mutant flies could not rescue CABs, differently from what obtained with the wild type copy of the *pdxK* human gene.[85] Also the expression of the A243G variant found in patients with diabetes failed to rescue CAB frequency. This finding suggests that the examined variants are loss-of-function alleles. The absence of pyridoxal kinase causes hyperglycemia and accumulation of advanced glycation end products (AGEs), thus favoring CABs formation (**Fig. 3.33**; **Fig. 3.34**). The impaired rescue of hyperglycemia displayed by the A243G variant is particularly interesting because it could be considered as a preliminary indication of the association of *pdxK* gene with diabetes that will be further investigated in future studies. The kinetic characterization of the PDXK variants showed that all mutations affected the catalytic activity of the enzyme, although with different modalities (**Table 9**). In general, the effect of D87H and V128I mutations are more drastic than those of H246Q and A243G, according to the location of the former couple of residues in a more critical region of the enzyme. Also, it is worth noting that D87H and V128I behave similarly, and also variants H246Q and A243G display similar biochemical defects, in agreement with the relative proximity of these residues. Interestingly, PLP precursors (PL, PM and PN) have different effects on CAB frequency observed upon expression of different variants (**Fig. 3.33**). The results obtained from the *in vitro* characterization of the enzymes parallel this observation, showing that

the kinetic parameters of PLP precursors are differently affected by the mutations (**Table 9**). In particular, the higher K_M for PL (about 10-fold than wild type) displayed by D87H explains why this mutant protein did not respond to PL. Differently, K_M values for PM and PN about 5 times higher than wild type explain the rescue observed only at 1 mM concentration. The very high K_M for both ATP and PL found in the V128 mutant protein explains why PL failed to rescue CABs, whereas PN and PM reduced CAB frequency but only at the higher concentration (**Fig. 3.33**). The H246Q variant, whose mutant enzyme form has normal kinetic parameters with PN, responds to both concentrations of this vitamer. The same mutant, displaying slightly altered kinetic parameters for ATP (when PL is used as substrate) and PM, responded positively to these precursors but only at the higher concentration. The A243G mutant enzyme displayed kinetic parameters very similar to those showed by H246Q (**Table 9**). Similarly to H246Q, this variant responded to PL and PM; however, 0.5 mM PN was unable to reduce CAB frequency (**Fig. 3.33**). Such different effects of PDXK mutations on the catalytic properties are very interesting, since they are related to the structure and the function of the enzyme. However, their full understanding is not possible on the basis of the available data and is postponed to future investigations.

4.8 PLP is the vitamer that best reduces glucose levels and CABs formation

PLP treatment of brains from larvae expressing each of the PDXK variants drastically reduced CABs (**Fig. 3.33),** suggesting that this molecule can enter brain cells. Moreover, the evaluation of glucose content in haemolymph from larvae expressing wild type or PDXK variants, demonstrates that the glucose levels recover the wild type phenotype when larvae were reared on standard

medium supplemented with 1 mM PLP (**Fig. 3.34**). In the literature, it has been reported that in humans only the dephosphorylated B_6 vitamers can pass the blood-brain barrier, in fact PLP needs to be dephosphorylated to PL by phosphatases before entering cells.[116,135] However, it is not known if the same mechanism occurs in flies. In *Drosophila, dPdxk*^{1} is a recessive mutation and heterozygotes do not show CABs, and we could expect that the same is also true in humans. However, if PLP levels are low and, therefore, PDXK has a reduced functionality also the heterozygous condition could be particularly critical, as for example in gestational diabetes. Analogously, PDXK variants in heterozygous condition could also impact on genome integrity either in patients treated with drugs that reduce PLP levels or in patients affected by pathologies such as celiac disease and diabetes which determine a decrease in PLP levels.[98,136,137] Thus, being able to detect PDXK mutations in such contexts could preserve genome integrity and, furthermore, the vitamin B_6 administration may be considered an important therapy.

5. Conclusions and future perspectives

In *Escherichia coli*, PNPOx plays an important regulatory role in PLP metabolism. It catalyses the synthesis of PLP and, at the same time, acts as a PLP-carrier protein, keeping the concentration of this cofactor in the free form at a low level. Our investigations demonstrated that PLP inhibition results from binding of this vitamer at an allosteric site of *E. coli* PNPOx, distinct from the active site. We also observed that the PLP binding site identified by crystallographic studies is not the actual allosteric site. However, an excellent candidate for an allosteric site is that identified through molecular docking and crystallography experiments, carried out respectively by professor Stefano Pascarella (Department of Biochemical Sciences "A. Rossi Fanelli", Sapienza Università di Roma) and Dr. Andrea Ilari (Institute of Molecular Biology and Pathology, National Research Council). In future studies, it will be interesting to test the effect of mutations of this novel allosteric PLP binding site *in vivo*. PNPOx mutant forms will be expressed in a knock out *E. coli* strain lacking the *pdxH* gene encoding PNPOx. The analysis of bacterial growth, vitamin B_6 requirements and composition of the amino acid pool will provide information on the actual role of the allosteric site in PLP metabolism and bacterial physiology.

Concerning human PNPOx, which is structurally very similar to the *E. coli* enzyme and is inhibited by PLP, our studies suggest that the same allosteric feedback inhibition, as observed in the *E. coli* PNPOx, is present in the human enzyme. Although the allosteric site has not yet been identified, the location of this PLP binding site is probably the same as observed in the *E. coli* enzyme. If this hypothesis will be confirmed in the future, we will be able to look for variants of the allosteric PLP binding site in the human population, that are already known and not yet associated with a dysregulation of vitamin B_6 metabolism. Furthermore, in our investigations of human PNPOx, we characterised the molecular basis of some of the

mutations that are related to the onset of the neonatal epileptic encephalopathy. All these mutants of human PNPOx, given their location near the active site of the enzyme, show altered kinetic parameters, thus suggesting that a reduced PLP production occurs in epileptic patients.

Finally, the experiments carried out with human PDXK using *Drosophila* as model, demonstrated that the analysed human variants affect DNA stability and glucose homeostasis. We showed that the human pyridoxal kinase variants respond differently to the three PL, PN and PM vitamers, and this observation is suggested not only by the kinetic analysis of PDXK variants, but also by the studies carried out in the laboratory of professor Fiammetta Vernì (Department of Biology and Biotechnology "Charles Darwin", Sapienza Università di Roma) on *Drosophila dPdxk*^{1} mutants, that express the chosen variants. Our studies suggest that subjects carrying PDXK variants in heterozygosity may have a propensity to DNA damage and diabetes. Thus, being able to detect PDXK mutations in these subjects could help preserving their genome integrity and, in the future, may pave the way for personalized cares based on B_6 administration. Given our successful experience, in the future it would be interesting to use *Drosophila* as a model system for the expression of human PNPOx mutants, in order to study the phenotypic effects of the mutations of the allosteric PLP binding site.

6. References

1. Percudani, R. & Peracchi, A. The B6 database: A tool for the description and classification of vitamin B6-dependent enzymatic activities and of the corresponding protein families. *BMC Bioinformatics* **10**, 273 (2009).
2. Sugimoto, R., Saito, N., Shimada, T. & Tanaka, K. Identification of YbhA as the pyridoxal 5'-phosphate (PLP) phosphatase in escherichia coli: Importance of PLP homeostasis on the bacterial growth. *J. Gen. Appl. Microbiol.* **63**, 362–368 (2017).
3. Di Salvo, M. L., Contestabile, R. & Safo, M. K. Vitamin B 6 salvage enzymes: Mechanism, structure and regulation. *Biochimica et Biophysica Acta - Proteins and Proteomics* (2011) doi:10.1016/j.bbapap.2010.12.006.
4. Allgood, V. E., Powell-Oliver, F. E. & Cidlowski, J. A. Vitamin B6 influences glucocorticoid receptor-dependent gene expression. *J. Biol. Chem.* **265**, 12424–12433 (1990).
5. Percudani, R. & Peracchi, A. A genomic overview of pyridoxal-phosphate-dependent enzymes. *EMBO Rep.* **4**, 850–854 (2003).
6. Schneider, G., Käck, H. & Lindqvist, Y. The manifold of vitamin B6 dependent enzymes. *Structure* **8**, 1–6 (2000).
7. Eliot, A. C. & Kirsch, J. F. Pyridoxal Phosphate Enzymes: Mechanistic, Structural, and Evolutionary Considerations. *Annu. Rev. Biochem.* **73**, 383–415 (2004).
8. ALEXANDER, F. W., SANDMEIER, E., MEHTA, P. K. & CHRISTEN, P. Evolutionary relationships among pyridoxal-5′-phosphate-dependent enzymes: Regio-specific α, β and γ families. *Eur. J. Biochem.* **219**, 953–960 (1994).
9. Grishin, N. V., Phillips, M. A. & Goldsmith, E. J. Modeling of the spatial structure of eukaryotic ornithine decarboxylases. *Protein Sci.* **4**,

1291–1304 (1995).

10. Giuseppe Arienti. *Biochimica degli alimenti e della nutrizione.* (2011).
11. Nardella, C. *et al.* Isolation of a complex formed between acinetobacter baumannii HemA and HemL, key enzymes of tetrapyrroles biosynthesis. *Front. Mol. Biosci.* **6**, 1–11 (2019).
12. Bilski, P., Li, M. Y., Ehrenshaft, M., Daub, M. E. & Chignell, C. F. Vitamin B6 (pyridoxine) and its derivatives are efficient singlet oxygen quenchers and potential fungal antioxidants. *Photochem. Photobiol.* **71**, 129–34 (2000).
13. Ehrenshaft, M., Bilski, P., Li, M., Chignell, C. F. & Daub, M. E. A highly conserved sequence is a novel gene involved in de novo vitamin B6 biosynthesis. *Proc. Natl. Acad. Sci. U. S. A.* **96**, 9374–9378 (1999).
14. Knöckel, J. *et al.* The antioxidative effect of de novo generated vitamin B 6 in Plasmodium falciparum validated by protein interference. *Biochem. J.* **443**, 397–405 (2012).
15. Tully, D. B., Allgood, V. E. & Cidlowski, J. A. Modulation of steroid receptor-mediated gene expression by vitamin B6. *FASEB J.* **8**, 343–9 (1994).
16. Salhany, J. M. & Schopfer, L. M. Pyridoxal 5′-phosphate binds specifically to soluble CD4 protein, the HIV-1 receptor: Implications for aids therapy. *J. Biol. Chem.* **268**, 7643–7645 (1993).
17. Tramonti, A., Nardella, C., Salvo, M. L., Pascarella, S. & Contestabile, R. The MocR-like transcription factors: pyridoxal 5′-phosphate-dependent regulators of bacterial metabolism. *FEBS J.* **285**, 3925–3944 (2018).
18. Grubman, A. *et al.* Vitamin B6 is required for full motility and virulence in Helicobacter pylori. *MBio* **1**, 1–9 (2010).

19. Dick, T., Manjunatha, U., Kappes, B. & Gengenbacher, M. Vitamin B6 biosynthesis is essential for survival and virulence of Mycobacterium tuberculosis. *Mol. Microbiol.* **78**, 980–988 (2010).
20. Klotz, K. A., Lemke, J. R., Korinthenberg, R. & Jacobs, J. Vitamin B6-Responsive Epilepsy due to a Novel KCNQ2 Mutation. *Neuropediatrics* **48**, 199–204 (2017).
21. Thériault, O. *et al.* Pyridoxal-5'-phosphate (MC-1), a vitamin B6 derivative, inhibits expressed P2X receptors. *Can. J. Physiol. Pharmacol.* **92**, 189–96 (2014).
22. Beamer, E., Kovács, G. & Sperlágh, B. ATP released from astrocytes modulates action potential threshold and spontaneous excitatory postsynaptic currents in the neonatal rat prefrontal cortex. *Brain Res. Bull.* **135**, 129–142 (2017).
23. Wang, H. S. *et al.* Pyridoxal phosphate is better than pyridoxine for controlling idiopathic intractable epilepsy. *Arch. Dis. Child.* **90**, 512–515 (2005).
24. Reid, E. S. *et al.* Seizures Due to a KCNQ2 Mutation: Treatment with Vitamin B6. in *JIMD reports* vol. 27 79–84 (2015).
25. Fitzpatrick, T. B., Moccand, C. & Roux, C. Vitamin B6 biosynthesis: charting the mechanistic landscape. *Chembiochem* **11**, 1185–93 (2010).
26. Fitzpatrick, T. B. *et al.* Two independent routes of de novo vitamin B6 biosynthesis: not that different after all. *Biochem. J.* **407**, 1–13 (2007).
27. Laber, B., Maurer, W., Scharf, S., Stepusin, K. & Schmidt, F. S. Vitamin B6 biosynthesis: Formation of pyridoxine 5'-phosphate from 4-(phosphohydroxy)-L-threonine and 1-deoxy-D-xylulose-5-phosphate by PdxA and PdxJ protein. *FEBS Lett.* **449**, 45–48 (1999).
28. Burns, K. E., Xiang, Y., Kinsland, C. L., McLafferty, F. W. & Begley,

T. P. Reconstitution and Biochemical Characterization of a New Pyridoxal-5‘-Phosphate Biosynthetic Pathway. *J. Am. Chem. Soc.* **127**, 3682–3683 (2005).

29. Raschle, T., Amrhein, N. & Fitzpatrick, T. B. On the two components of pyridoxal 5′-phosphate synthase from Bacillus subtilis. *J. Biol. Chem.* **280**, 32291–32300 (2005).
30. Mittenhuber, G. Phylogenetic analyses and comparative genomics of vitamin B6 (pyridoxine) and pyridoxal phosphate biosynthesis pathways. *Journal of Molecular Microbiology and Biotechnology* (2001).
31. Darin, N. *et al.* Mutations in PROSC Disrupt Cellular Pyridoxal Phosphate Homeostasis and Cause Vitamin-B6-Dependent Epilepsy. *Am. J. Hum. Genet.* **99**, 1325–1337 (2016).
32. Middleton, H. M. Intestinal hydrolysis of pyridoxal 5’-phosphate in vitro and in vivo in the rat. Effect of amino acids and oligopeptides. *Dig. Dis. Sci.* **35**, 113–20 (1990).
33. Albersen, M. *et al.* The Intestine Plays a Substantial Role in Human Vitamin B6 Metabolism: A Caco-2 Cell Model. *PLoS One* **8**, (2013).
34. Musayev, F. N., Di Salvo, M. L., Ko, T.-P., Schirch, V. & Safo, M. K. Structure and properties of recombinant human pyridoxine 5′-phosphate oxidase. *Protein Sci.* (2003) doi:10.1110/ps.0356203.
35. Bohney, J. P., Fonda, M. L. & Feldhoff, R. C. Identification of Lys190 as the primary binding site for pyridoxal 5′-phosphate in human serum albumin. *FEBS Lett.* **298**, 266–268 (1992).
36. Stanulović, M., Jeremić, V., Leskovac, V. & Chaykin, S. New pathway of conversion of pyridoxal to 4-pyridoxic acid. *Enzyme* **21**, 357–69 (1976).
37. Spector, R. & Johanson, C. E. Vitamin transport and homeostasis in

mammalian brain: Focus on vitamins B and E. *J. Neurochem.* **103**, 425–438 (2007).

38. Di Salvo, M. L., Safo, M. K., Musayev, F. N., Bossa, F. & Schirch, V. Structure and mechanism of Escherichia coli pyridoxine 5′-phosphate oxidase. *Biochim. Biophys. Acta - Proteins Proteomics* **1647**, 76–82 (2003).
39. Ghatge, M. S. *et al.* Inactive mutants of human pyridoxine 5′-phosphate oxidase: A possible role for a noncatalytic pyridoxal 5′-phosphate tight binding site. *FEBS Open Bio* (2016) doi:10.1002/2211-5463.12042.
40. Ghatge, M. S. *et al.* Pyridoxal 5′-phosphate is a slow tight binding inhibitor of E. coli pyridoxal kinase. *PLoS One* **7**, 16–19 (2012).
41. Di Salvo, M. L. *et al.* Active site structure and stereospecificity of Escherichia coli pyridoxine-5′-phosphate oxidase. *J. Mol. Biol.* **315**, 385–397 (2002).
42. Musayev, F. N. *et al.* Crystal Structure of human pyridoxal kinase: Structural basis of M + and M 2+ activation . *Protein Sci.* **16**, 2184–2194 (2007).
43. Gandhi, A. K. *et al.* Kinetic and structural studies of the role of the active site residue Asp235 of human pyridoxal kinase. *Biochem. Biophys. Res. Commun.* **381**, 12–5 (2009).
44. Windebank, A. J. Neurotoxicity of pyridoxine analogs is related to coenzyme structure. *Neurochem. Pathol.* **3**, 159–67 (1985).
45. Critcher, MS and Sobczyńska-Malefora, A. The prevalence of low and very high vitamin B6 (Pyridoxal 5'-phosphate) concentrations in hospital patients | Viapath. *Biomed. Sci.* (2015).
46. Merigliano, C., Mascolo, E., Burla, R., Saggio, I. & Vernì, F. The Relationship Between Vitamin B6, Diabetes and Cancer. *Front. Genet.*

9, 1–5 (2018).

47. Rippa, M., Signorini, M. & Pontremoli, S. Purification and Properties of Two Forms of 6-Phosphogluconate Dehydrogenase from Candida utilis. *Eur. J. Biochem.* **1**, 170–178 (1967).
48. Gao, G. J. & Fonda, M. L. Kinetic analysis and chemical modification of vitamin B6 phosphatase from human erythrocytes. *J. Biol. Chem.* **269**, 7163–7168 (1994).
49. Prunetti, L. *et al.* Evidence that COG0325 proteins are involved in PLP homeostasis. *Microbiol. (United Kingdom)* **162**, 694–706 (2016).
50. Eswaramoorthy, S. *et al.* Structure of a yeast hypothetical protein selected by a structural genomics approach. *Acta Crystallogr. D. Biol. Crystallogr.* **59**, 127–35 (2003).
51. Ito, T. *et al.* Conserved pyridoxal protein that regulates ile and val metabolism. *J. Bacteriol.* **195**, 5439–5449 (2013).
52. Beynon, R. J., Leyland, D. M., Evershed, R. P., Edwards, R. H. T. & Coburn, S. P. Measurement of the turnover of glycogen phosphorylase by GC/MS using stable isotope derivatives of pyridoxine (vitamin B6). *Biochem. J.* **317**, 613–619 (1996).
53. Ink, S. L. & Henderson, L. M. Effect of binding to hemoglobin and albumin on pyridoxal transport and metabolism. *J. Biol. Chem.* **259**, 5833–5837 (1984).
54. Yang, E. S. & Schirch, V. Tight binding of pyridoxal 5'-phosphate to recombinant Escherichia coli pyridoxine 5'-phosphate oxidase. *Arch. Biochem. Biophys.* **377**, 109–114 (2000).
55. Cheung, P.-Y. *et al.* Interaction between pyridoxal kinase and pyridoxal-5-phosphate-dependent enzymes. *J. Biochem.* **134**, 731–8 (2003).
56. Safo, M. K., Musayev, F. N., Di Salvo, M. L. & Schirch, V. X-ray

structure of Escherichia coli pyridoxine 5′-phosphate oxidase complexed with pyridoxal 5′-phosphate at 2.0 Å resolution. *J. Mol. Biol.* (2001) doi:10.1006/jmbi.2001.4734.

57. WADA, H. & SNELL, E. E. The enzymatic oxidation of pyridoxine and pyridoxamine phosphates. *J. Biol. Chem.* **236**, 2089–2095 (1961).
58. Zhao, G. & Winkler, M. E. Kinetic limitation and cellular amount of pyridoxine (pyridoxamine) 5'- phosphate oxidase of Escherichia coli K-12. *J. Bacteriol.* (1995) doi:10.1128/jb.177.4.883-891.1995.
59. Choi, S. Y., Churchich, J. E., Zaiden, E. & Kwok, F. Brain pyridoxine-5-phosphate oxidase. Modulation of its catalytic activity by reaction with pyridoxal 5-phosphate and analogs. *J. Biol. Chem.* (1987).
60. Yang, Y., Tsui, H. C. T., Man, T. K. & Winkler, M. E. Identification and function of the pdxY gene, which encodes a novel pyridoxal kinase involved in the salvage pathway of pyridoxal 5'-phosphate biosynthesis in Escherichia coli K-12. *J. Bacteriol.* **180**, 1814–1821 (1998).
61. Bowers-Komro, D. M. & McCormick, D. B. Pyridoxamine-5'-phosphate oxidase exhibits no specificity in prochiral hydrogen abstraction from substrate. *J. Biol. Chem.* **260**, 9580–9582 (1985).
62. Di Salvo, M., Yang, E., Zhao, G., Winkler, M. E. & Schirch, V. Expression, purification, and characterization of recombinant Escherichia coil pyridoxine 5'-phosphate oxidase. *Protein Expr. Purif.* (1998) doi:10.1006/prep.1998.0904.
63. Lam, H. M. & Winkler, M. E. Characterization of the complex pdxH-tyrS operon of Escherichia coli K-12 and pleiotropic phenotypes caused by pdxH insertion mutations. *J. Bacteriol.* **174**, 6033–6045 (1992).
64. Nelson, D. L. (David L., Nelson, D. L. (David L., Lehninger, A. L. &

Cox, M. M. *Lehninger principles of biochemistry*. (W.H. Freeman, 2008).

65. Safo, M. K. *et al.* X-ray structure of Escherichia coli pyridoxine 5′-phosphate oxidase complexed with FMN at 1.8 Å resolution. *Structure* **8**, 751–762 (2000).
66. Hatch, J. *et al.* Normal Neurodevelopmental Outcomes in PNPO Deficiency: A Case Series and Literature Review. *JIMD Rep.* **26**, 91–7 (2016).
67. Wang, H. S. & Kuo, M. F. Vitamin B6 related epilepsy during childhood. *Chang Gung Med. J.* **30**, 396–401 (2007).
68. Albersen, M. *et al.* Vitamin B6 in plasma and cerebrospinal fluid of children. *PLoS One* **10**, 1–11 (2015).
69. Baumgartner-Sigl, S. *et al.* Pyridoxine-responsive seizures as the first symptom of infantile hypophosphatasia caused by two novel missense mutations (c.677T>C, p.M226T; c.1112C>T, p.T371I) of the tissue-nonspecific alkaline phosphatase gene. *Bone* **40**, 1655–1661 (2007).
70. Ware, T. L. *et al.* Typical and atypical phenotypes of PNPO deficiency with elevated CSF and plasma pyridoxamine on treatment. *Dev. Med. Child Neurol.* (2014) doi:10.1111/dmcn.12346.
71. Wilson, M. P., Plecko, B., Mills, P. B. & Clayton, P. T. Disorders affecting vitamin B6 metabolism. *J. Inherit. Metab. Dis.* **42**, jimd.12060 (2019).
72. Surtees, R., Mills, P. & Clayton, P. Inborn errors affecting vitamin B 6 metabolism . *Future Neurol.* (2006) doi:10.2217/14796708.1.5.615.
73. Farrant, R. D., Walker, V., Mills, G. A., Mellor, J. M. & Langley, G. J. Pyridoxal phosphate de-activation by pyrroline-5-carboxylic acid. Increased risk of vitamin B6 deficiency and seizures in

hyperprolinemia type II. *J. Biol. Chem.* **276**, 15107–15116 (2001).

74. Turgeon, M. O., Perry, N. J. S. & Poulogiannis, G. DNA damage, repair, and cancer metabolism. *Front. Oncol.* **8**, (2018).
75. Booth, A. A., Khalifah, R. G., Todd, P. & Hudson, B. G. In vitro kinetic studies of formation of antigenic advanced glycation end products (AGEs). Novel inhibition of post-Amadori glycation pathways. *J. Biol. Chem.* **272**, 5430–5437 (1997).
76. Toyota, T. *et al.* The Endocrine Pancreas in Pyridoxine Deficient Rats. *Tohoku J. Exp. Med.* **134**, 331–336 (1981).
77. Dranoff, J. A. *et al.* Prevention of liver fibrosis by the purinoceptor antagonist pyridoxal-phosphate-6-azophenyl-2′,4′-disulfonate (PPDAS). *In Vivo (Brooklyn).* **21**, 957–966 (2007).
78. Rubí, B. Pyridoxal 5'-phosphate (PLP) deficiency might contribute to the onset of type I diabetes. *Med. Hypotheses* **78**, 179–82 (2012).
79. Kotake, Y., Ueda, T., Mori, T., Igaki, S. & Hattori, M. Abnormal tryptophan metabolism and experimental diabetes by xanthurenic acid (XA). *Acta Vitaminol. Enzymol.* **29**, 236–9 (1975).
80. Moreno-Navarrete, J. M. *et al.* Metabolomics uncovers the role of adipose tissue PDXK in adipogenesis and systemic insulin sensitivity. *Diabetologia* **59**, 822–32 (2016).
81. Liu, Z. *et al.* Vitamin B6 prevents endothelial dysfunction, insulin resistance, and hepatic lipid accumulation in Apoe -/- mice fed with high-fat diet. *J. Diabetes Res.* **2016**, (2016).
82. Rorsman, F. *et al.* Aromatic-L-amino-acid decarboxylase, a pyridoxal phosphate-dependent enzyme, is a β-cell autoantigen. *Proc. Natl. Acad. Sci. U. S. A.* **92**, 8626–8629 (1995).
83. Atkinson, M. A. *et al.* Cellular immunity to a determinant common to glutamate decarboxylase and Coxsackie virus in insulin-dependent

diabetes. *J. Clin. Invest.* **94**, 2125–2129 (1994).

84. Galluzzi, L. *et al.* Prognostic Impact of Vitamin B6 Metabolism in Lung Cancer. *Cell Rep.* **2**, 257–269 (2012).
85. Marzio, A., Merigliano, C., Gatti, M. & Vernì, F. Sugar and Chromosome Stability: Clastogenic Effects of Sugars in Vitamin B6-Deficient Cells. *PLoS Genet.* **10**, (2014).
86. Kuo, M.-F. & Wang, H.-S. Pyridoxal phosphate-responsive epilepsy with resistance to pyridoxine. *Pediatr. Neurol.* **26**, 146–7 (2002).
87. Clayton, P. T. Case report Neonatal epileptic encephalopathy. *Lancet* **361**, 7741–7741 (2003).
88. Mills, P. B. *et al.* Neonatal epileptic encephalopathy caused by mutations in the PNPO gene encoding pyridox(am)ine 5′-phosphate oxidase. *Hum. Mol. Genet.* **14**, 1077–1086 (2005).
89. Porri, S. *et al.* Positive outcome following early diagnosis and treatment of pyridoxal-5′-phosphate oxidase deficiency: A case report. *Neuropediatrics* (2014) doi:10.1055/s-0033-1353489.
90. Mills, P. B. *et al.* Epilepsy due to PNPO mutations: Genotype, environment and treatment affect presentation and outcome. *Brain* **137**, 1350–1360 (2014).
91. Plecko, B. *et al.* Pyridoxine responsiveness in novel mutations of the PNPO gene. *Neurology* (2014) doi:10.1212/WNL.0000000000000344.
92. di Salvo, M. L. *et al.* Biochemical data from the characterization of a new pathogenic mutation of human pyridoxine-5′-phosphate oxidase (PNPO). *Data Br.* **15**, 868–875 (2017).
93. Veeravigrom, M. *et al.* Pyridoxal 5'-phosphate-responsive epilepsy with novel mutations in the PNPO gene: A case report. *Genet. Mol. Res.* **14**, 14131–14135 (2015).
94. Jaeger, B. *et al.* Pyridoxine responsive epilepsy caused by a novel

homozygous PNPO mutation. *Mol. Genet. Metab. Reports* **6**, 60–63 (2016).

95. Guerriero, R. M. *et al.* Systemic Manifestations in Pyridox(am)ine 5′-Phosphate Oxidase Deficiency. *Pediatr. Neurol.* (2017) doi:10.1016/j.pediatrneurol.2017.05.024.
96. Xue, J., Chang, X., Zhang, Y. & Yang, Z. Novel phenotypes of pyridox(am)ine-5'-phosphate oxidase deficiency and high prevalence of c.445_448del mutation in Chinese patients. *Metab. Brain Dis.* **32**, 1081–1087 (2017).
97. Levtova, A. *et al.* Normal Cerebrospinal Fluid Pyridoxal 5'-Phosphate Level in a PNPO-Deficient Patient with Neonatal-Onset Epileptic Encephalopathy. *JIMD Rep.* **22**, 67–75 (2015).
98. Clayton, P. T. B6-responsive disorders: A model of vitamin dependency. *J. Inherit. Metab. Dis.* **29**, 317–326 (2006).
99. Khayat, M. *et al.* PNPO deficiency: An under diagnosed inborn error of pyridoxine metabolism. *Mol. Genet. Metab.* (2008) doi:10.1016/j.ymgme.2008.04.008.
100. Musayev, F. N. *et al.* Molecular basis of reduced pyridoxine 5′-phosphate oxidase catalytic activity in neonatal epileptic encephalopathy disorder. *J. Biol. Chem.* (2009) doi:10.1074/jbc.M109.038372.
101. Ruiz, A. *et al.* A new fatal case of pyridox(am)ine 5′-phosphate oxidase (PNPO) deficiency. *Mol. Genet. Metab.* **93**, 216–218 (2008).
102. Pearl, P. L. *et al.* Partial Pyridoxine Responsiveness in PNPO Deficiency. *JIMD Rep.* **9**, 139–142 (2013).
103. Cao, P., Gong, Y., Tang, L., Leung, Y.-C. & Jiang, T. Crystal structure of human pyridoxal kinase. *J. Struct. Biol.* **154**, 327–332 (2006).
104. Li, M. H. *et al.* Conformational Changes in the Reaction of Pyridoxal

Kinase. *J. Biol. Chem.* **279**, 17459–17465 (2004).

105. Safo, M. K. *et al.* Crystal structure of pyridoxal kinase from the Escherichia coli pdxK gene: Implications for the classification of pyridoxal kinases. *J. Bacteriol.* **188**, 4542–4552 (2006).
106. Zhang, Y., Dougherty, M., Downs, D. M. & Ealick, S. E. Crystal structure of an aminoimidazole riboside kinase from Salmonella enterica: Implications for the evolution of the ribokinase superfamily. *Structure* **12**, 1809–1821 (2004).
107. Di Cera, E. A structural perspective on enzymes activated by monovalent cations. *J. Biol. Chem.* **281**, 1305–1308 (2006).
108. di Salvo, M. L., Hunt, S. & Schirch, V. Expression, purification, and kinetic constants for human and Escherichia coli pyridoxal kinases. *Protein Expr. Purif.* **36**, 300–306 (2004).
109. , MCCORMICK, Donald B.; GREGORY, Margaret E; SNELL, E. E. Pyridoxal phosphokinases. I. Assay, distribution, I. Assay, distribution, purification, and properties. **236**, (1961).
110. Gandhi, A. K. *et al.* Crystal structures of human pyridoxal kinase in complex with the neurotoxins, ginkgotoxin and theophylline: Insights into pyridoxal kinase inhibition. *PLoS One* **7**, 1–11 (2012).
111. Merigliano, C., Mascolo, E., La Torre, M., Saggio, I. & Vernì, F. Protective role of vitamin B6 (PLP) against DNA damage in Drosophila models of type 2 diabetes. *Sci. Rep.* **8**, 1–12 (2018).
112. Gylling, B. *et al.* Vitamin B-6 and colorectal cancer risk: a prospective population-based study using 3 distinct plasma markers of vitamin B-6 status. *Am. J. Clin. Nutr.* **105**, 897–904 (2017).
113. Bunting,Samuel F and Nussenzweig, A. END-JOINING, TRANSLOCATIONS AND CANCER. *Nat. Rev. Cancer* (2013) doi:10.1038/nrc3537.

114. Ames, B. N. & Wakimoto, P. Are vitamin and mineral deficiencies a major cancer risk? *Nat. Rev. Cancer* **2**, 694–704 (2002).
115. Hellmann, H. & Mooney, S. Vitamin B6: A Molecule for Human Health? *Molecules* **15**, 442–459 (2010).
116. Bowling, F. G. Pyridoxine supply in human development. *Semin. Cell Dev. Biol.* **22**, 611–8 (2011).
117. Kanellis, P. *et al.* A screen for suppressors of gross chromosomal rearrangements identifies a conserved role for PLP in preventing DNA lesions. *PLoS Genet.* **3**, 1438–1453 (2007).
118. Vivoli, M., Novak, H. R., Littlechild, J. A. & Harmer, N. J. Determination of protein-ligand interactions using differential scanning fluorimetry. *J. Vis. Exp.* 1–13 (2014) doi:10.3791/51809.
119. Peterson, E. A. & Sober, H. A. Preparation of Crystalline Phosphorylated Derivatives of Vitamin B6. *J. Am. Chem. Soc.* **76**, 169–175 (1954).
120. Malatesta, F. The study of bimolecular reactions under non-pseudo-first order conditions. *Biophys. Chem.* **116**, 251–256 (2005).
121. Contestabile, R., Angelaccio, S., Maytum, R., Bossa, F. & John, R. A. The contribution of a conformationally mobile, active site loop to the reaction catalyzed by glutamate semialdehyde aminomutase. *J. Biol. Chem.* **275**, 3879–3886 (2000).
122. Florio, R. *et al.* Structural stability of the cofactor binding site in Escherichia coli serine hydroxymethyltransferase - The role of evolutionarily conserved hydrophobic contacts. *FEBS J.* **276**, 7319–7328 (2009).
123. Neidhardt, F. C. What the bacteriologists have learned about heat shock. *Genes Dev.* **1**, 109–110 (1987).
124. Choi, J. D., Bowers-Komro, M., Davis, M. D., Edmondson, D. E. &

McCormick, D. B. Kinetic properties of pyridoxamine (pyridoxine)-5'-phosphate oxidase from rabbit liver. *J. Biol. Chem.* **258**, 840–845 (1983).

125. Kwon, O., Kwok, F. & Churchich, J. E. Catalytic and regulatory properties of native and chymotrypsin-treated pyridoxine-5-phosphate oxidase. *J. Biol. Chem.* **266**, 22136–22140 (1991).
126. Schnell, S. & Mendoza, C. Enzymological Considerations for the Theoretical Description of the Quantitative Competitive Polymerase Chain Reaction (QC-PCR). *J. Theor. Biol.* **184**, 433–440 (1997).
127. Accorsi, P. *et al.* Pyridoxine responsiveness in pyridox(am)ine-5-phosphate oxidase deficiency: The importance of early treatment. *Clin. Neurol. Neurosurg.* **163**, 90–93 (2017).
128. Veerapandiyan, A. *et al.* Electroencephalographic and seizure manifestations of pyridoxal 5'-phosphate-dependent epilepsy. *Epilepsy Behav.* (2011) doi:10.1016/j.yebeh.2010.12.046.
129. Di Salvo, M. L., Safo, M. K. & Contestabile, R. Biomedical aspects of pyridoxal 5'-phosphate availability. *Front. Biosci. - Elit.* (2012) doi:10.2741/e428.
130. Spellacy, W. N., Buhi, W. C. & Birk, S. A. Vitamin B6 treatment of gestational diabetes mellitus. *Am. J. Obstet. Gynecol.* **127**, 599–602 (1977).
131. Merrill, A. H., Horiike, K. & McCormick, D. B. Evidence for the regulation of pyridoxal 5′-phosphate formation in liver by pyridoxamine (pyridoxine) 5′-phosphate oxidase. *Biochem. Biophys. Res. Commun.* **83**, 984–990 (1978).
132. Cornish-Bowden, A. J. *Fundamentals of Enzyme Kinetics*. (2012).
133. Segel, I. H. *Enzyme Kinetics: Behavior and Analysis of Rapid Equilibrium and Steady-State Enzyme Systems*. (1975).

134. Chelban, V. *et al.* PDXK mutations cause polyneuropathy responsive to pyridoxal 5′-phosphate supplementation. *Ann. Neurol.* **86**, 225–240 (2019).
135. Di Salvo, M. L., Contestabile, R. & Safo, M. K. Vitamin B 6 salvage enzymes: Mechanism, structure and regulation. *Biochim. Biophys. Acta - Proteins Proteomics* **1814**, 1597–1608 (2011).
136. Okada, M., Shibuya, M., Yamamoto, E. & Murakami, Y. Effect of diabetes on vitamin B6 requirement in experimental animals. *Diabetes. Obes. Metab.* **1**, 221–5 (1999).
137. Nix, W. A. *et al.* Vitamin B status in patients with type 2 diabetes mellitus with and without incipient nephropathy. *Diabetes Res. Clin. Pract.* **107**, 157–65 (2015).

Collaborations

Prof. Stefano Pascarella

Department of Biochemical Sciences “A. Rossi Fanelli”

Sapienza Università di Roma

Prof. Francesco Malatesta

Department of Biochemical Sciences “A. Rossi Fanelli”

Sapienza Università di Roma

Prof. Fiammetta Vernì

Department of Biology and Biotechnology "Charles Darwin"

Sapienza Università di Roma

Dr. Andrea Ilari

Institute of Molecular Biology and Pathology

National Research Council

Publications

1. "Human cytosolic and mitochondrial serine hydroxymethyltransferase isoforms in comparison: full kinetic characterisation and substrate inhibition properties".

   Angela Tramonti, Caterina Nardella, Martino L. di Salvo, Anna Barile, Francesca Cutruzzolà and Roberto Contestabile.

   Biochemistry 2018, 57(51):6984-6996

2. "Isolation of a comple formed beteween *Acinetobacter baumannii* HemA and HemL, key enzymes of tetrapyrroles biosynthesis".

   Caterina Nardella, Dalila Boi, Martino L. di Salvo, Anna Barile, Jörg Stetefeld, Angela Tramonti and Roberto Contestabile.

   Frontiers in Molecular Biosciences 2019, 26;6:6

3. "Copper homeostasis as target of both consolidated and innovative strategies of anti-tumor therapy".

   Anastasia De Luca, Anna Barile, Mario Arciello, Luisa Rossi. *Journal of Trace Elements in Medicine and Biology* 2019, 55:204-213

4. "Allosteric feedback inhibition of pyridoxine 5'-phosphate oxidase from *Escherichia coli*".

   Anna Barile, Angela Tramonti, Martino L. di Salvo, Isabel Nogués, Caterina Nardella, Francesco Malatesta and Roberto Contestabile. *Journal of Biological Chemistry* 2019, 294(43):15593-15603

5. "The expression of four pyridoxal kinase (PDXK) human variants in *Drosophila* impacts on genome integrity".

Elisa Mascolo* and Anna Barile*, Lorenzo Stufera Mecarelli, Noemi Amoroso, Chiara Merigliano, Arianna Massimi, Isabella Saggio, Torben Hansen, Angela Tramonti, Martino L. Di Salvo, Fabrizio Barbetti, Roberto Contestabile and Fiammetta Vernì.

Scientific Reports 2019, 9(1):14188

*these authors contributed equally to this work

Acknowledgements

My most sincere thanks goes to Prof. Roberto Contestabile, who accompanied me patiently during these three years of PhD. I also thank Prof. Di Salvo and Dr. Angela Tramonti, who helped me along this path. I thank all my laboratory mates, who have made the work environment fantastic every day, or almost.

A special thanks goes to my family that has supported me for years and always encourages me to do my best.

And finally, I want to thank all the people who have been close to me in the past, those who still support me today and those who will accompany me in the days ahead.